Influence of Temperature and Moisture Content on Thermal Performance of Green Roof Media

by

Bohan Shao
B.ASc, Harbin Institute of Technology, 2013

A Thesis Submitted in Partial Fulfillment
of the Requirements for the Degree of

MASTER OF APPLIED SCIENCE

in the Department of Mechanical Engineering

Supervisory Committee

Influence of Temperature and Moisture Content on Thermal Performance of Green Roof Media

by

Bohan Shao
B.ASc, Harbin Institute of Technology, 2013

Supervisory Committee

Dr. Caterina Valeo, (Department of Mechanical Engineering)
Co-Supervisor

Dr. Phalguni Mukhopadhyaya, (Department of Civil Engineering)
Co-Supervisor

Abstract

Supervisory Committee

Dr. Caterina Valeo, (Department of Mechanical Engineering)
Co-Supervisor

Dr. Phalguni Mukhopadhyaya, (Department of Civil Engineering)
Co-Supervisor

Numerical estimates of the ability of a green roof to reduce energy consumption in buildings are plagued by a lack of accuracy in thermal properties that are input to the model. An experimental study into the thermal conductivity at different temperatures and moisture contents was performed using four different commercially available substrates for green roofs. In the unfrozen state, as moisture content increased, thermal conductivity increased linearly. In the phase transition zone between +5 ºC and -10ºC, as temperature decreased, thermal conductivity increased sharply during the transition from water to ice. When the substrate was frozen, thermal conductivity varied exponentially with substrate moisture content prior to freezing. Power functions were found between thermal conductivity and temperature (when shifted up by +10.001ºC). Two equally sized, green roof test cells were constructed and tested to compare various roof configurations including a bare roof, varying media thickness for a green roof, and vegetation. The results show that compared with the bare roof, there is a 75% reduction in the interior temperature amplitude for the green roof with 150mm thick substrate. When a sedum mat was added, there's a 20% reduction in the amplitude of the inner temperature as compared with the cell without sedum mat.

Table of Contents

Supervisory Committee ii
Abstract iii
Table of Contents iv
List of Tables vi
List of Figures vii
Nomenclature viii
Acknowledgments x
Chapter 1 Introduction 1
1.1 Research Background 1
1.2 Research Objectives 3
1.3 Thesis Outline 4
Chapter 2 Literature Review 5
2.1 Green Roof Benefits and Components 5
2.2 Energy Balance of Green Roof 6
2.3 Experimental Study of Green Roof Thermal Properties 8
2.4 Experimental Study of Substrate Layer Thermal Performance 10
Chapter 3 Research Objectives 14
3.1 Gaps in Knowledge 14
3.1.1 Accuracy in substrate thermal properties that are input to the model 14
3.1.2 Substrate thermal properties in the frozen state 14
3.1.3 Outdoor experimental study on substrate layer thermal performance 15
3.2 Thesis Objectives 15
Chapter 4 Influence of Temperature and Moisture Content on Thermal Performance of Green Roof Media 17
4.1 Introduction 17
4.2 Materials and Methods 19
4.2.1 Thermal Conductivity Experimental Study 19
4.2.2 Thermal Performance Experimental Study 24
4.3 Results and Discussions 29
4.3.1 Results of Thermal Conductivity Experimental Study 29
4.3.2 Results of Thermal Performance Experimental Study 39
4.4 Conclusions 57
4.4.1 Laboratory Experimental Study of Substrate Thermal Conductivity 57
4.4.2 Outdoor Experimental Study of Substrate Layer Thermal Performance 58
Chapter 5 Conclusions and Future Study 60
5.1 Conclusions 60
5.1.1 Laboratory Experimental Study of Substrate Thermal Conductivity 60
5.1.2 Outdoor Experimental Study of Substrate Layer Thermal Performance 61
5.2 Future Study 62
Bibliography 63
Appendix A Detailed Preparation and Measurement of Substrate Thermal Conductivity Using Heat Flow Meter 68
Appendix B Thermal Conductivity Results of Four Substrates 76

Appendix C Mann-Kendall Trend Test Results..... 78
Appendix D Two-factor ANOVA Analysis of Substrate Thermal Conductivity..... 92

List of Tables

Table 1 Components of four substrates 20
Table 2 Test schedule..... 28
Table 3 Test results of 4 substrates Physical properties 29
Table 4 Thermal conductivity y (W/m·K) as a function of moisture content by mass x in the unfrozen state 32
Table 5 Thermal conductivity y (W/m·K) as a function of moisture content by mass x in the frozen state 32
Table 6 Thermal conductivity y (W/m·K) as a function of $x = T + 10.001$ 38
Table 7 Fitting functions of temperature inputs and outputs 45
Table 8 Time constant results of two sensors 45
Table 9 Two test cells fitting function parameters..... 47
Table 10 Two test cells fitting function parameters..... 50
Table 11 Fitting functions of surface and indoor air T of test cell E and F 52
Table 12 Two test cells fitting function parameters..... 56

List of Figures

Figure 1 Population, CO_2 emissions, and primary energy. Taken from [1] 1
Figure 2 Green Roof Energy Balance. Taken from[30] 7
Figure 3 (a) Dimensions (mm) of holding frame; (b) holding frame; (c) substrate with holding frame; and (d) an example final test sample. 21
Figure 4 Test Sample and reference sample arrangement (dimensions in mm) 23
Figure 5 Experimental test cell with 150mm thickness Sopraflor X (dimensions in mm)25
Figure 6 Experimental test cell. 26
Figure 7 (a) Test cell access door; (b) test cell interior; (c) cable routing from inside; (d) data logger box. 27
Figure 8 (a) Bare roof test cell surface; (b) roof with 150mm thick substrate test cell surface; (c) green roof test cell surface. 28
Figure 9 Thermal conductivity vs. average temperature for (a) dry substrates; (b) substrates with 10% moisture content by mass; (c) substrates with 20% moisture content by mass; and (d) substrates with 30% moisture content by mass thermal conductivity vs. average temperature. 31
Figure 10 Substrates thermal conductivity vs. moisture content by mass at average temperature of (a) 5ºC; (b) 20ºC; (c) 35ºC; (d) -10ºC. 34
Figure 11 Thermal conductivity vs. average temperature at different moisture content for (a) Sopraflor I; (b) Zinco Blend; (c) Sopraflor X; (d) Eagle Lake. 37
Figure 12 Thermal conductivity vs. average temperature (+10.001) at different moisture contents for (a) Sopraflor I; (b) Zinco Blend; (c) Sopraflor X; (d) Eagle Lake. 38
Figure 13 Weather Data (July 09 – July 14, 2019) 40
Figure 14 Temperature and insolation results of test cell A and B 43
Figure 15 Fitting function plots of temperature inputs and outputs 44
Figure 16 Attenuation and phase angle vs. the product of frequency and the time constant 45
Figure 17 Test cell inner ceiling temperature results of test cell A and B 46
Figure 18 Weather Data (May 30 – June 02, 2019) 48
Figure 19 Temperature results of test cell C and D 50
Figure 20 Temperature and moisture content results of test cell E and F before irrigation 52
Figure 21 Temperature and moisture content results of test cell E and F after irrigation 53
Figure 22 Weather Data (Aug 07 – Aug 13, 2019) (a) Wind speed, humidity, ait temperature, and precipitation data (b) Insolation and evaporation data 54
Figure 23 Temperature results of test cell G and H 55

Nomenclature

r''	Surface wetness factor	q_{af}	Mixing ratio for air within foliage canopy
$C_{e,g}$	Latent heat flux bulk transfer coefficient at ground layer	$q_{f,sat}$	Saturation mixing ratio at foliage temperature
C_{hg}	sensible heat flux bulk transfer coefficient at ground layer	q_g	Mixing ratio at ground surface
C_f	Bulk heat transfer coefficient	T_{af}	Air temperature with in the canopy (K)
$C_{p,a}$	specific heat of air at constant pressure	T_f	Foliage temperature (K)
Ff	Net heat flux to foliage layer (W/m2)	T_g	Ground surface temperature (K)
Fg	Net heat flux to ground surface (W/m2)	W_{af}	Wind speed with in the canopy (m/s)
H_f	Foliage sensible heat flux (W/m^2)	a_g	Albedo (short-wave reflectivity) of ground surface
H_g	Ground sensible heat flux (W/m^2)	a_f	Albedo (short-wave reflectivity) of the canopy
I_s	Incoming short-wave radiation (W/m^2)	ε_f	Emissivity of canopy
I_{ir}	Incoming long-wave radiation (W/m^2)	ε_g	Emissivity of the ground surface
l_f	Latent heat of vaporization at foliage temperature (J/kg)	ε_1	$\varepsilon_g + \varepsilon_f - \varepsilon_f \varepsilon_g$
l_g	Latent heat of vaporization at ground temperature (J/kg)	ρ_{af}	Density of air at foliage temperature (kg/m^3)
L_f	Foliage latent heat flux (W/m^2)	ρ_{ag}	Density of air at ground surface temperature
L_g	Ground latent heat flux (W/m^2)	σ	Stefan- Boltzmann constant (W/m^2K^4)
LAI	Leaf area index (m^2/m^2)	σ_f	Fractional vegetation coverage

R_t^1	Total test sample thermal resistance (m^2K/W)	EL	Eagle Lake
R_{b1}	Upper buffer sheet thermal resistance m^2K/W)	SX	Sopraflor X
$R_{b1\text{-}s}$	Interface thermal resistance between the upper buffer sheet and the substrate (m^2K/W)	ZB	ZinCo Blend
R_s	Substrate thermal resistance (m^2K/W)	SI	Sopraflor X
$R_{s\text{-}f}$	Interface thermal resistance between substrate and base frame (m^2K/W)		
R_f	Base frame thermal resistance (m^2K/W)		
$R_{f\text{-}b2}$	Interface thermal resistance between base frame and lower buffer sheet (m^2K/W)		
R_{b2}	Lower buffer sheet thermal resistance (m^2K/W)		
$R_{b1\text{-}f}$	Interface thermal resistance between the upper buffer sheet and the base frame (m^2K/W)		
$R_{s\text{-}f}$	Interface thermal resistance between substrate bottom surface and base frame top surface (m^2K/W)		
k_s	Substrate thermal conductivity (W/m·K)		
d_s	Substrate thickness (m)		

Acknowledgments

First and foremost, I would like to thank my supervisor, Dr. Caterina Valeo, for guidance, patience, giving me such a nice research project, providing a clear direction when I was stuck, giving me the freedom to pursue any new ideas, and being such a great mentor for this research project.

To my co-supervisor Dr. Phalguni Mukhopadhyaya, for support, suggestions, and help for my experimental study. I would like to thank him for sharing his experience and knowledge.

To Dr. Jianxun (Jennifer) He from the University of Calgary for her support on my experimental study. Thanks for sharing the helpful information, and providing the suggestions on my research when needed.

To Armando, Geoff, Mitch, and Aaron for helping me during the construction of the experimental test cell; to Vivian for educating me on the Heat Flow Meter; and to Mian Huang for allowing me to borrow the compaction tools and helping me on my test.

Finally, always be thankful to my parents for all kinds of supports, and thanks to my boyfriend for always being there whenever I need help.

Chapter 1 Introduction

1.1 Research Background

There is growing concern about world energy consumption due to environmental pollution, insufficient energy resources, difficulties in supply, and economic growth[1]. A significant increase in developing countries' energy consumption has been observed and it is estimated that energy consumption will continue to increase in the near future. China's total PER (primary energy requirement) increased with annual growth of 5.6% from 570 million tonnes of coal equivalent to 3200 million tonnes of coal equivalent[2]. According to the International Energy Agency (IEA), from the year 1984 to 2004, as shown in Figure 1, energy consumption increased by 49% with an annual growth of 2%, and CO_2 emissions increased by 43% with an annual growth of 1.8%. The improvement of human living places and the development of urban cities will result in high fossil fuel consumption and have a negative impact on the environment.

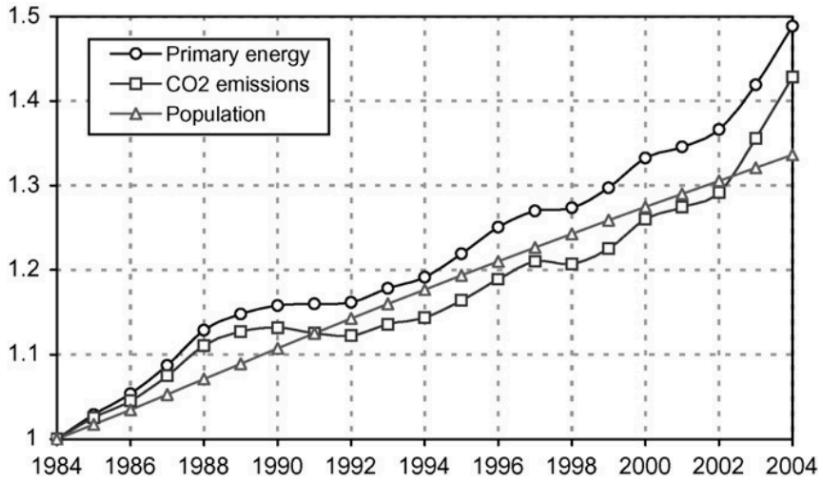

Figure 1 Population, CO_2 emissions, and primary energy. Taken from [1]

Among all the energy consumption sectors, buildings are one of the largest sectors which contributed to 32% of the energy used in the world in 2010 and contributed to 1/3 of the greenhouse gas[3][4]. In many developed countries, the building sector takes a larger part

of energy consumption compared with transportation and industry sectors. In 2004, in both the USA, and the European Union, buildings contributed to 40% of the PER in USA, and 37% of the total PER in the European Union[5]. Globally, the building sector contributes to 40% of the total PER and accounts for 30% of the CO_2 emissions[6]. Overall, to decrease global warming and to reduce the impacts on climate, energy savings in the building sector plays an important role. Therefore, many studies focused on improving building energy efficiency, especially in the study of thermal performance of building envelopes based on different designs and components.

A green roof is a roof that is covered with a vegetation layer, a substrate layer, as well as other functional layers (e.g., drainage layer and filter layer)[11], and is considered a sustainable solution to decrease the building indoor cooling and heating loads. It was first developed and mostly used in Germany[12], and became famous in other neighbouring countries in Europe. Right now many countries like Canada, USA, Japan, and Australia are making a contribution to the green roof industry by either retrofitting old buildings with green roofs or installing green roofs on new buildings[13]. Green roofs are believed to decrease the heat flux through the top of the building envelope by vegetation evapotranspiration, substrate layer evaporation and thermal resistance, and shading of the roof surface by the canopy[7]. Other than the thermal benefit, a green roof can also reduce storm water runoff, reduce the urban heat island effect, absorb sound, improve water quality, and also has ecological, social, and economic benefits.

To further study the effect of green roofs on building energy savings, several numerical studies were performed and analyzed using the modelling software EnergyPlus. EnergyPlus was developed by the U.S. DOE (Department of Energy) which combines BLAST and DOZ-2 modeling programs[8] and is a program for energy analysis and thermal load simulation. By entering the physical makeup of the building and related HVAC system, EnergyPlus will compute the cooling and heating load. Vera et al.[9] studied the influence of extensive green roof substrate, plants, and insulation on the retail stores' thermal performance using EnergyPlus version 8.6.0. The parameter inputs that varied were LAI, substrate physical properties, and roof insulation levels. Mahmoodzadeh

et al.[4] studied the effects of green roofs on school buildings (the module was developed by Portland State University) energy performance using EnergyPlus version 8.8. In their study the parameter inputs that varied were substrate moisture content, thickness, LAI, plant height, and leaf albedo. Both of these studies mentioned the limitations of the EnergyPlus program for green roof modelling, which include the fact that although the substrate moisture content varies over time, the substrate thermal properties are constant all the time. This results in a lack of accuracy in substrate thermal properties that are input to the model. Substrate thermal properties such as thermal conductivity, specific heat capacity, and albedo, play important roles in soil energy balance. Soil thermal performance varies as moisture content changes because water replaces the air amongst soil particles and connects the gaps between them. Temperature also plays an important role in thermal performance, especially in the phase transition zone. Therefore, to move forward on the numerical study of green roof energy performance, it is necessary to study the substrate thermal performance as a function of temperature and moisture content.

1.2 Research Objectives

The objectives of this research are to: i). provide guidance and insight into improving estimates of the parameters used to model energy and moisture budgets in green roof systems; and ii). analyze the thermal performance of the substrate in isolation. According to the energy balance study of green roofs (discussed in Chapter 2), substrate parameters that are critical to green roof energy budgets are density, thermal conductivity, specific heat capacity, emissivity, and albedo. Among all of these parameters, emissivity is insensitive to substrate moisture content and its composition[10], specific heat capacity can be computed based on thermal conductivity and thermal diffusivity. Therefore, this study mainly focuses on substrate thermal conductivity as a function of temperature and moisture content. To achieve the first objective, laboratory experimental studies into thermal conductivity at different temperatures and moisture contents was performed using four different commercially available substrates for green roofs. To achieve the second objective, outdoor experiments on two equally sized, experimental test cells constructed in

Victoria, BC were used to investigate the thermal performance of substrate related design parameters.

1.3 Thesis Outline

Chapter 2 contains an overview of green roof components and benefits, green roof energy balance, an experimental study of green roof substrate thermal properties, and substrate thermal performance. Chapter 3 contains a summary of gaps based on the literature review and detailed research objectives. Chapter 4 contains the methodology and results of the lab experimental study of substrate thermal conductivity as a function of temperature and moisture content, and the methodology and results of the outdoor experimental study of substrate layer thermal performance. An edited version of this chapter is to be submitted to the Journal of Energy and Buildings. Chapter 5 summarises the conclusions and future work recommendations.

Chapter 2 Literature Review

2.1 Green Roof Benefits and Components

In Japan, they require all public buildings to exceed 250m^2 or private buildings exceeding 1000m^2, must either green 20% of the roof or pay 2000 USD per year instead[14]. In various provinces of Canada, relevant by-laws require new buildings larger than 2000m^2 to green 20-60% of the building's rooftop. Green roofs can also enhance water quality by retaining pollution. Seters et al.[15] tested the chemical components and pH value for green roof run-off and found that compared with a traditional roof runoff, the water from the green roof had lower pollutant concentrations.

Green roofs are increasing in popularity in recent years due to the numerous environmental, social, and economic benefits. Research has shown that green roofs can reduce stormwater runoff as part of the rain water will be absorbed and held in the substrate layer. Speak et al.[16] found that compared with a paved roof, the intensive green roof had an average of 65.7% retention of storm water runoff. By improving the building's thermal performance, green roofs also play an important role in energy savings because it adds thermal resistance to the buildings, and absorbs less solar radiation compared with a traditional roof[17][18]. Sha et al.[19] studied the power consumption of a green roof and found that power savings of around 20.9% at day time and 15.3% at night can be seen for the green roof. Morakinyo et al.[20] studied green roof thermal effects by using a co-simulation parameter study and found that a green roof plays an important role in reducing surface temperature and energy consumption. Research has also shown that green roofs can also reduce the urban heat island effect, provide habitat for wildlife, enhance air quality, and reduce noise pollution[19], [21], [22].

Among all the layers of a green roof, the vegetation layer and the substrate layer are the most important layers; thus, they need to be strategically selected to maximize the many benefits of the green roof. The substrate layer plays an important role in water runoff reduction, peak flow reduction, water quality improvement, and thermal benefits. Based on the thickness of the substrate, a green roof can be divided into 3 categories: intensive

(above 12in or 30cm), semi-intensive (6-12in or 15-30cm), and extensive green roof (3-6 inch or 8-15cm)[19][23]. The intensive green roof has a higher water holding capacity and more plant options including small trees and shrubs; however, this requires more maintenance, irrigation, fertilization, as well as more considerations in building structure support. Compared with the intensive green roof, the extensive green roof is more common globally because of its low maintenance, nutrients, and irrigation requirements.

The vegetation layer plays an important role in improving runoff water quality[24], reducing heating effects[25], and providing animal habitat. In the selection of vegetation, geographic location, wind, humidity, temperature, rainfall, and sun exposure should be considered, noting that the choice of plant species is also influenced by the designed soil thickness. Many studies have focused on the selection of suitable plants[26][27], with most agreeing that sedum species are good options for extensive green roofs all over the world since they can survive under a variety of conditions. Teeri et al.[28] indicated that *Sedum rubrotinctum* R. T. Clausen can survive for 2 years without water, while Durhman et al.[29] indicated that Sedum can survive and also maintained active photosynthetic metabolism after 4 months without water. Succulents can also survive through droughts because they store water in their stems and leaves.

2.2 Energy Balance of Green Roof

The energy balance of a green roof, similarly for a traditional bare roof, is determined by solar radiation. Substrate and vegetation surface sensible and latent heat flux (convection and evaporative heat flux), longwave radiation from and to substrate and plant surfaces, together with heat conduction into the substrate layer is balanced with the solar radiation. Figure 2 shows the energy balance of a green roof.

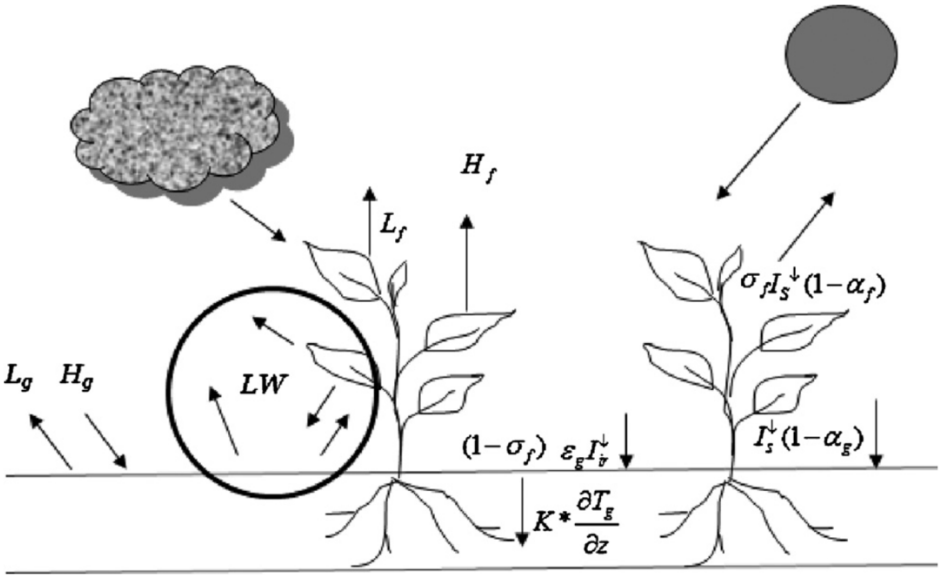

Figure 2 Green Roof Energy Balance. Taken from[30]

Foliage energy balance and soil energy budget are:

$$F_f = \sigma_f[\mathrm{I_s}\,(1-\alpha_f) + \varepsilon_f I_{ir} - \varepsilon_f \sigma T_f^4\,] + \frac{\sigma_f\,\varepsilon_g\varepsilon_f\sigma}{\varepsilon_1}\,(T_g^4 - T_f^4) + \mathrm{H_f} + \mathrm{L_f} \quad (1)$$

$$F_g = (1-\sigma_f)[\,\mathrm{I_s}\,(1-\alpha_g) + \varepsilon_g I_{ir} - \varepsilon_f T_g^4\,] - \frac{\sigma_f\,\varepsilon_g\varepsilon_f\sigma}{\varepsilon_1}\,(T_g^4 - T_f^4) + K\frac{\partial T_g}{\partial Z} + \mathrm{H_g} + \mathrm{L_g} \quad (2)$$

where $\mathrm{F_f}$ is the net heat flux to foliage layer ($\mathrm{W/m^2}$); $\mathrm{F_g}$ is the net heat flux to ground surface ($\mathrm{W/m^2}$); σ_f is the fractional vegetation coverage (calculated as a function of Leaf-Area-Index); $\mathrm{I_s}$ is the total incoming short-wave radiation ($\mathrm{W/m^2}$); α_f is the albedo (short-wave reflectivity) of the canopy; α_g is the albedo (short-wave reflectivity) of the ground surface; $\mathrm{I_{ir}}$ is the total incoming long-wave radiation ($\mathrm{W/m^2}$); ε_f is the emissivity of the canopy; σ is the Stefan-Boltzmann constant ($5.67 \times 10^{-8} W/m^2K^4$); ε_g is the emissivity of the ground surface; ε_1 is equal to $\varepsilon_\mathrm{g} + \varepsilon_\mathrm{f} - \varepsilon_\mathrm{g}\varepsilon_\mathrm{f}$; $\mathrm{T_f}$ is the foliage temperature (Kelvin); $\mathrm{T_g}$ is the ground surface temperature (Kelvin); z is the height or depth (m); $\mathrm{H_f}$ is the foliage sensible heat flux ($\mathrm{W/m^2}$); H_g is the ground sensible heat flux ($\mathrm{W/m^2}$); $\mathrm{L_f}$ is the foliage latent heat flux ($\mathrm{W/m^2}$); and $\mathrm{L_g}$ is the ground latent heat flux ($\mathrm{W/m^2}$).

Sensible heat flux in the foliage layer is:

$$H_f = (1.1LAI\rho_{af}C_{p,a}C_fW_{af})(T_{af} - T_f) \quad (3)$$

where H_f is the foliage sensible heat flux (W/m^2); LAI is the leaf area heat flux (W/m^2); ρ_{af} is the density of air at foliage temperature (kg/m^3); $C_{p,a}$is the specific heat of air at constant pressure (1005.6J/kg·K); C_f is the Bulk heat transfer coefficient; W_{af} is the Wind speed with in the canopy (m/s); and T_{af} is the Air temperature with in the canopy (Kelvin).

Latent heat flux in the foliage layer is:

$$L_f = l_fLAI\rho_{af}C_fW_{af}r''(q_{af} - q_{f,sat}) \quad (4)$$

where L_f is the foliage latent heat flux (W/m^2); l_f is the latent heat of vaporization at foliage temperature (J/kg); r'' is the Surface wetness factor; q_{af} is the mixing ratio for air within the foliage canopy; and $q_{f,sat}$ is the saturation mixing ratio at foliage temperature.

Sensible heat flux in the soil layer is:

$$H_g = \rho_{ag}C_{p,a}C_{hg}W_{af}(T_{af} - T_g) \quad (5)$$

where H_g is the ground sensible heat flux (W/m^2); ρ_{ag} is the density of air at ground surface temperature (kg/m^3); C_{hg} is the sensible heat flux bulk transfer coefficient at ground layer; and T_g is the ground surface temperature (Kelvin).

Latent heat flux in the soil layer is:

$$L_g = C_{e,g}l_gW_{af}\rho_{ag}(q_{af} - q_g) \quad (6)$$

where L_g is the ground latent heat flux (W/m^2); $C_{e,g}$ is the latent heat flux bulk transfer coefficient at ground layer; l_g is the latent heat of vaporization at ground temperature (J/kg); and q_g is the mixing ratio at the ground surface.

2.3 Experimental Study of Green Roof Thermal Properties

Sailor et al.[10] tested thermal properties of 8 substrates with different volumetric composition ratios of aggregate (expanded shale or pumice), sand, and organic matter by changing moisture content. The research divided moisture content (tested according to

ASTM D2216-05 standard) into 4 levels that are: very dry, dry (add 42g water per liter dry soil), moist (add 85g water per liter dry soil) and wet (add 225g water per liter dry soil) followed by testing thermal conductivity and specific heat capacity using dual needle probe system, thermal emissivity using contact thermometer method and albedo by putting the sample in an isolation shade ring. Results showed using pumice as aggregate has lower thermal conductivity but higher specific heat capacity and could hold more moisture than using shale. The thermal conductivity changed at a rate of 0.038 W/m·K per 0.1 increase in substrate saturation, and varied from 0.25 to 0.34W/m·K for dry substrates and from 0.31 to 0.62 W/m·K for wet substrates. Thermal conductivity can be decreased by increasing the ratio of aggregate and organic matter to sand. The albedo of dry pumice-based soils is twice as large as dry shale-based soil and the albedo of pumice is significantly larger than that of compost.

Ouldboukhitine et al.[31] measured thermal conductivity of five substrates (Siplat, Sopraflor X061, Sopraflor M, Critt aquiland, Normal aquiland) with dimensions of $3m^2$ in surface area and 15cm thickness using a TP08 Hukselfux probe and found thermal conductivity kept increasing from 0.05 to 0.7W/m·K as maximum water content increased from 0% to 100%. They also measured heat flux to calculate thermal resistance with/without plants and found it is $0.8m^2k/W$ of the sample without plants; however, thermal resistance is $0.92m^2k/W$ with ryegrass and $1.27m^2k/W$ with periwinkle.

Issa et al.[32] measured thermal conductivity, thermal diffusivity, and specific heat of sand and silt clay at different moisture content by mass with a dual-needle heat-pulse sensor, KD2 Pro. Results showed that sand thermal conductivity kept increasing until moisture content (by mass) was 19% (saturation condition). As for thermal conductivity of silt clay, unlike sand, thermal conductivity is highest at 25% moisture content and decreased as more water was added because of surface flooding. The authors also measured the thermal properties of construction materials.

Barozzi et al.[33] studied substrate thermal resistance as a function of density and moisture content using a Heat Flow Meter. Four commonly used Italian factories for growing media

were chosen and each factory was divided into extensive and intensive; thus, in total eight different samples were tested. Results showed that for extensive growing media, thermal conductivity varies from 0.118 to 0.17W/m·K for extensive growing media with density between 800 and 1000kg/m^3. Thermal conductivity varied from 0.102 to 0.128W/m·K for intensive growing media with density between 750 and 950kg/m^3. Thermal resistance increases linearly as growing media thickness increases. Thermal conductivity increased by 0.05W/m·K for Factory 1 and 4 (denser extensive substrate), 0.021W/m·K for Factory 3, and 0.006W/m·K for Factory 3 (lightest substrate sample) individually as water content increased by 10%.

Pianella et al.[22] compared transient and steady-state measurements of growing media. Thermal conductivity of three growing media was tested using a KD2 Pro thermal needle set (transient measurement) and k-Matic apparatus (steady-state measurement). Results showed that in every test, steady-state measurement always has the smallest deviation and showed more consistency compared with transient measurements. Steady-state measurements showed higher thermal conductivity than transient measurements for wet substrates. In conclusion, steady-state measurement provides more stable and accurate results for green roof numerical models.

Clarke et al.[34] studied three substrates based on scoria, terracotta, and furnace-ash thermal properties under different moisture contents (dry, moist, and saturated). A steady-state measurement (k-Matic) was applied and used in this study, to measure the loos fill substrates; a holding frame was used in the test. Results showed that thermal conductivity varied from 0.13W/m·K to 0.80W/m·K, and it increased linearly as moisture content increase.

2.4 Experimental Study of Substrate Layer Thermal Performance

Ouldboukhitine et al.[31] built a low speed wind tunnel to simulate outdoor and indoor conditions. The top side simulates outside conditions, the heating element was set to maintain a hot air temperature. The bottom tunnel simulates inside conditions, the cooling

element was set to maintain a cool air temperature indoor. The size of green roof trays is 61cm x 61cm. By exposing the green roof to constant temperature, wind speed, humidity, and sunlight, the author calculated thermal resistance using $R = \Delta T/Q$. The author also evaluated the effect of transpiration and evaporation by saturating the trays with/without vegetation and recording the weight using a balance. Since the water was evapotranspiring from the trays with vegetation but only evaporating from the trays without vegetation, the effect of transpiration and evaporation can be analyzed. Periwinkle and ryegrass were the two studied plants. Results showed the tray with vegetation always has more water loss than without ryegrass and the difference was more pronounced for periwinkle as compared with ryegrass. Periwinkle showed a higher evapotranspiration rate. As for thermal resistance, R of the tray without vegetation, was 0.8 m^2k/W, while it was 0.92m^2k/W for tray with ryegrass and 1.27m^2k/W for tray with periwinkle.

Ouldboukhitine et al.[35] built a green roof (scale 1:10) platform on the site of the University of La Rochelle and vegetated it with Tundra (sedum type) and Pampa (grass type). A weather station collected data on experimental temperature and air humidity, short and long-wave radiation, precipitation, speed and wind direction. Other sensors included thermocouples for temperature, water content sensors, heat flux sensors and, rain gauges to measure the amount of water drained. Results showed that foliage density influences thermal behavior - the denser the vegetation, the less radiation reached the surface of the soil so that it is cooler.

Lin et al.[36] performed an experiment on the roof of a four-floor building at Foo-Yin University in the Southern part of Taiwan to determine vegetation type for optimal thermal performance and the best drought endurance in tropical climates. Four types of substrates were used: sand, sand with white charcoal debris, a mixture of decomposing organic matter (i.e., peat moss, vermiculite, and burned clay with a mixture of 1:1:1) and burned reservoir sludge mixed with rice hull. The three irrigation conditions were no irrigation, once a week (2L water each time), and twice a week (2L water each time). The height of the substrate was 100mm. The authors prepared three samples for each condition, giving 144 samples in 12 measurement units overall. The author collected data on air temperature, relative humidity, solar radiation, and precipitation using a measuring station. Five thermocouple

points were set on the rooftop surface and five under the roof slab surface of each substrate. The leaf coverage ratio was also calculated to observe plant performance. Results showed that the burned sludge had the best thermal reduction percentage due to its highest porosity and water holding capacity. Human-mixed samples had good thermal reduction, but the organic matter content increased the management and maintenance. When temperature was reduced by 1ºC, electricity was reduced by 6%.

Isss et al.[32] performed a green roof test model on the West A&M University Campus with a base dimension of 1.22m x 1.22m. Airflow was prevented by injecting spray foam into polystyrene panel seams. Sand and silt clay with a height of 10cm were used as substrates. Glass (sod) with a thickness of 5cm was used as vegetation. Eight thermocouples were set in different positions to monitor the temperature. T/C #1 was shielded to prevent radiation error, moisture content was achieved by measuring mass, and wind speed and relative humidity of air were obtained from a weather station. Heat transfer in lateral directions was neglected because the thickness dimension was much smaller than other dimensions. A barren roof with only substrate, and a roof with substrate with vegetation irrigated with different amounts (0mm, 10mm or 20mm watering/day), were tested. Results showed that as soil moisture content increases, inner temperatures decreased for the sand and silt clay roof. However, as saturation conditions were reached, increasing moisture did not help to decrease the temperature. Heat flux calculations showed that without grass and watering, heat transfer improved significantly with 10mm water/day. To achieve similar heat transfer rates to sand, silt clay soil needs more than twice the amount of soil moisture. The roof with silt clay had the lowest inner temperature in the daytime and the lowest temperature fluctuation between day and night.

Huang et al.[37] explored temperature reduction and heat amplitude reduction in four types of green roofs also to investigate the impacts of air temperature, relative humidity and solar radiation on green roofs. Four types of plants were chosen: groundcover, perennial herb, vine, and shrub. The substrate was peaty soil/vermiculite/ perlite/sandy loam soil of ratio 1:1:1:1. The size of each bed was 50cm (L) x 50cm (W) x 19cm (H). Data on air temperature, relative humidity, and solar radiation was collected at 160cm above the

rooftop, and temperature sensors were located on the surface of the bare roof and on the bottom of the green roof. Results showed that temperature reduction by vegetation type was found in the following order herb > shrub > vine > groundcover. The vegetation resulted in a maximum of 3.98ºC temperature reduction and a maximum 16.45% reduction in heat amplitude. Air temperature and solar radiation were positively related to temperature reduction, while relative humidity was negatively related with temperature reduction.

Eksi et al.[38] studied green roof thermal properties under different growing media depths (50mm vs. 200mm), plant types (a mixture of sedum mat, and a mixture of seventeen grasses and herbs), and seasons (spring, summer, autumn, and winter) by monitoring a 232m^2 green roof located at Michigan State University in East Lansing. Data were collected for a year using moisture sensors, heat flux sensors, and thermocouples. Results showed that during the summer, the green roof with 50mm thickness substrate and the sedum mat had larger temperature fluctuations, which resulted in indoor air to be warmer in the daytime and cooler at night compared with the green roof with 200mm thickness substrate and herbaceous mat. In the winter, the herbaceous roof was more stable and less affected by ambient conditions. The herbaceous roof had less heat transfer to the outside in the winter but had more heat transferring to the interior.

Jiang et al.[39] combined a green roof together with indoor night ventilation and studied the total thermal performance and energy performance. The green roof test cell was constructed and located on the roof at Chongqing University. Three test measurements were performed (natural night ventilation, no night ventilation, and mechanical night ventilation) and compared with a traditional roof (no substrate and vegetation layer). Results showed that on sunny days an obvious indoor temperature reduction can be seen for the green roof test cell with night ventilation compared with no night ventilation in the daytime. It also had a 75% to 79% reduction on peak indoor air temperature. On rainy days there was no significant influence. An equation of ventilation airflow rate together with the green roof was also proposed based on climate.

Chapter 3 Research Objectives

3.1 Gaps in Knowledge

3.1.1 Accuracy in substrate thermal properties that are input to the model

Many studies have investigated the energy performance of vegetated green roofs. Sailor performed an energy simulation of a vegetated rooftop using EnergyPlus[30], Tabares-Velasco et al. performed a heat transfer model for green roofs that can be used in different energy simulation software[40]. However, these approaches are plagued by an inaccuracy in substrate thermal properties that are input to the model. Substrate thermal properties such as thermal conductivity, specific heat capacity, albedo play important roles in soil energy balance. Those parameters are influenced by substrate density, porosity, temperature, and moisture content. Low porosity makes heat transfer through substrate easier because the particles are compressed tighter, which has more interior contact points that aid conduction heat transfer[41][42]. Soil thermal performance varies as moisture content changes because water will replace the air among soil particles and connects the gaps between them[32]. Temperature also plays an important role in thermal performance, especially in the phase transition zone[43]. Substrate thermal conductivity is an important parameter when analyzing green roof energy performance. Many studies have analyzed variations in thermal conductivity; however, most of these used transient measurements. Pianella et al.[22] compared transient vs steady-state measurements and found that steady-state measurements are more consistent within replicates and provides more accurate results as compared with transient measurements.

3.1.2 Substrate thermal properties in the frozen state

Green roofs are commonly used in the USA, Japan, and Canada, but in winter, the temperatures of many cities in these countries fall below zero. Therefore, it is necessary to study substrate thermal performance under different temperatures, especially in the frozen state. Right now for the study on substrate thermal performance, most studies focused on thermal performance under different moisture contents: from dry, moist, to wet. However, temperature also plays an important role in thermal performance, especially in the phase

transition zone from the unfrozen state to the frozen state. Due to the phase changes, structure, and thermal performance from water to ice, moist substrate thermal performances between unfrozen and frozen states are completely different.

3.1.3 Outdoor experimental study on substrate layer thermal performance

Although many researchers have studied the thermal and energy performance of green roofs, very few have focused on the performance of the substrate only. This requires isolating the influence between the vegetation layer and the substrate layer and necessary for providing a better understanding of substrate layer energy performance by studying the influence of substrate properties such as dry density, physical components, moisture content, temperature, and porosity. Because many locations have a season in which there is no active vegetation, the role of the substrate may take on a more important role than the vegetation in winter seasons.

3.2 Thesis Objectives

The objectives of this research are to

(1) *Advance knowledge leading to better estimates of the parameters used to model energy and moisture budgets in green roof systems*. According to the energy balance study of green roof in Chapter 2, substrate parameters that are critical to green roof energy budget are density, thermal conductivity, specific heat capacity, emissivity, and albedo. Among all these parameters, emissivity is insensitive to substrate moisture content and its composition[10], and specific heat capacity can be computed based on thermal conductivity and thermal diffusivity. Therefore, this study mainly focuses on substrate thermal conductivity as a function of temperature and moisture content. To achieve this objective, laboratory experimental studies into the thermal conductivity at different temperatures and moisture contents was performed using four different commercially available substrates for green roofs.

(2) *Analyze the thermal performance of the substrate in isolation from vegetation.* To achieve this objective, outdoor experiments on two equally sized, experimental test cells constructed in Victoria, BC were used to investigate the thermal performance of substrate related design parameters.

Chapter 4 Influence of Temperature and Moisture Content on Thermal Performance of Green Roof Media

This chapter is a modified form (without abstract and keywords) of a journal paper in preparation for submission to the Journal *Energy and Buildings*.

4.1 Introduction

There's growing concern for global energy consumption due to the adverse environmental impacts, insufficient energy resources, difficulties in supply, and economic growth[1]. Among all the energy consumption sectors, the building sector is one of the largest sectors and contributed to 32% of energy consumption used globally in 2010 and contributed to one third of greenhouse gases[3][4]. Green roofs are becoming a prevalent development option for buildings and is considered to have good potential for decreasing the building indoor cooling and heating loads. Green roofs also have numerous environmental, social, and economic benefits as well. Research has shown that green roofs can reduce stormwater runoff and the urban heat island effect, provide habitat for wildlife, enhance air and water quality, reduce the energy consumption of buildings, and reduce noise pollution[19], [21], [22]. A green roof is a roof that is covered with a growing medium (the substrate layer), vegetation, as well as other functional layers (e.g., drainage layer and filter layer)[11]. Among all the layers of a green roof, the vegetation layer and the substrate layer are the most important layers; thus, they need to be strategically selected to maximize the many benefits of a green roof.

The substrate layer plays an important role in water runoff reduction, peak flow reduction, water quality improvement, and thermal benefits. Base on the thickness of the substrate, a green roof can be divided into three categories: intensive (above 12 in or 30cm), semi-intensive (6-12 in or 15-30cm), and extensive (3-6 inch or 8-15cm)[19][23]. The intensive green roof has a higher water holding capacity and more plant options including small trees and shrubs; however, this requires more maintenance, irrigation, fertilization, as well as more consideration to building structural support. Compared with the intensive green roof,

the extensive green roof is more common globally because of its low maintenance, nutrient, and irrigation requirements.

The vegetation layer plays an important role in improving runoff water quality[24], reducing heating effects[25], and providing animal habitat. In the selection of vegetation, geographic location, wind, humidity, temperature, rainfall, and sun exposure should all be considered while noting that the choice of plant species is also influenced by the designed soil thickness. Many studies have focused on the selection of suitable plants[26][27], with most agreeing that sedum species are good options for extensive green roofs all over the world, since they can survive under a variety of conditions. Terri et al.[28] indicated that *Sedum rubrotinctum* R. T. Clausen can survive for 2 years without water, while Durhman et al.[29] indicated that Sedum can survive and maintain active photosynthetic metabolism for as long as four months without water. Succulents can also survive through droughts because they store water in their stems and leaves[13].

Vera et al.[9] studied the influence of an extensive green roof on the retail stores' thermal performance using EnergyPlus 8.6.0. Mahmoodzadeh et al.[4] studied the effects of green roofs on school buildings energy performance using EnergyPlus 8.8. Both studies note limitations in the EnergyPlus program, such as the fact that substrate moisture content varies over time but substrate thermal properties are held constant over time. This results in a lack of accuracy in substrate thermal properties that are input to the model. In general, these approaches are plagued by a variety of problems including inaccuracy in model inputs of substrate thermal properties and lack of knowledge of the role of the substrate separate from the vegetation in the energy balance of the green roof.

With regard to the lack of accuracy in substrate thermal properties that are input to the models, it is well known that substrate thermal properties such as thermal conductivity, specific heat capacity, albedo play important roles in soil energy balance. Those parameters are influenced by substrate density, porosity, temperature, and moisture content. Low porosity makes heat transfer through substrate easier because the particles are compressed tighter, which has more interior contact points that aid conduction heat transfer[41][42].

Soil thermal performance varies as moisture content changes because water will replace the air among soil particles and connects the gaps between them[32]. Temperature also plays an important role in thermal performance, especially in the phase transition zone[43]. Substrate thermal conductivity is an important parameter when analyzing green roof energy performance. Many studies have analyzed variations in thermal conductivity; however, most of these used transient measurements. Pianella et. al.[22] compared transient vs steady-state measurement and found that steady-state measurements were more consistent within replicates and provides more accurate results as compared with transient measurements.

As noted, another problem is the lack of study on the energy performance of the substrate only. Although many researchers have studied the thermal and energy performance of green roofs, very few have focused on the performance of the substrate alone. This requires isolating the influence between the vegetation layer and the substrate layer and necessary for providing a better understanding of substrate layer energy performance. This is particularly important in seasons where the vegetation is inactive or absent.

The objectives of this study are to (i) provide insight into improving estimates of the parameters used to model energy and moisture budgets in green roof systems; and (ii) to analyze the thermal performance of the substrate in isolation from vegetation. An experimental study into the thermal conductivity at different temperatures and moisture contents was performed using four different commercially available substrates for green roofs to achieve the first objective, and experiments on two equally sized, experimental test cells constructed in Victoria, BC were used to investigate the thermal performance of substrate related design parameters to achieve the second objective.

4.2 Materials and Methods

4.2.1 Thermal Conductivity Experimental Study

Four different commercially available substrates for green roofs (Sopraflor I, Sopraflor X, ZinCo Blend and Eagle Lake) were used in this study. Table 1 shows the soil components of the four substrates.

Table 1 Components of four substrates

Substrate	Components
Sopraflor I	Mineral aggregates, blond peat, perlite, sand and compost from vegetable matter
Sopraflor X	
ZincoBlend-SI	High-quality recycled materials and minerals, enhanced with high-quality compost
Eagle Lake	Peat moss, fir bark fines, compost, sand, pumice and perlite

4.2.1.1 Sample Preparation

To study substrate thermal conductivity as a function of temperature and moisture content, the four substrates were tested under different temperatures and moisture contents. Temperature varied from -10℃ to 35℃ with an interval of 15℃. This variation is based on Calgary's outdoor air temperature. Calgary is a semi-arid, prairie city in southern Alberta, Canada. Moisture content was varied from dry substrate up to saturation with an interval of 10% moisture content by mass. Substrates were dried in an oven at 104 ºC for 48-72h as in the ASTM E2399-05 Standard[44]. Once the mass difference between the last two measurements divided by the mass of the final substrate is less than 1%, the substrate is assumed to be dry. Wet substrate was prepared at each wetness interval by adding water with a mass of 10% dry substrate. The sample was mixed well and allowed to settle down overnight before being tested.

To determine the thermal conductivity of substrates using a heat flow meter, a sample frame of appropriate dimensions using ASTM C687 and the Heat Flow Meter NETZSCH HFM 436/3/1E was constructed from pinewood[45] (thermal conductivity of 0.106W/m·K) with a paper-based phenolic board with a thickness of 1.6mm and thermal

conductivity of 0.12W/m·K for the base. ASTM C687 standard specifies thermal conductivity of the frame four edges should be lower than 0.12W/m·K to decrease the effect of edge heat flow and the bottom ,which supports the loose-fill materials, should be a thin, thermally insignificant membrane. The overall dimensions were 293mm x 293mm x 45.6mm and these dimensions are determined based on HFM Operating Instruction[46]. The base board was attached by screws and the whole frame was coated with two layers of epoxy to waterproof the frame. Joint edges between the frame edge and the base board were coated with silicone derivative to prevent water from leaking. The final structure and dimension of the holding frame are shown in Figure 3 (a) and (b).

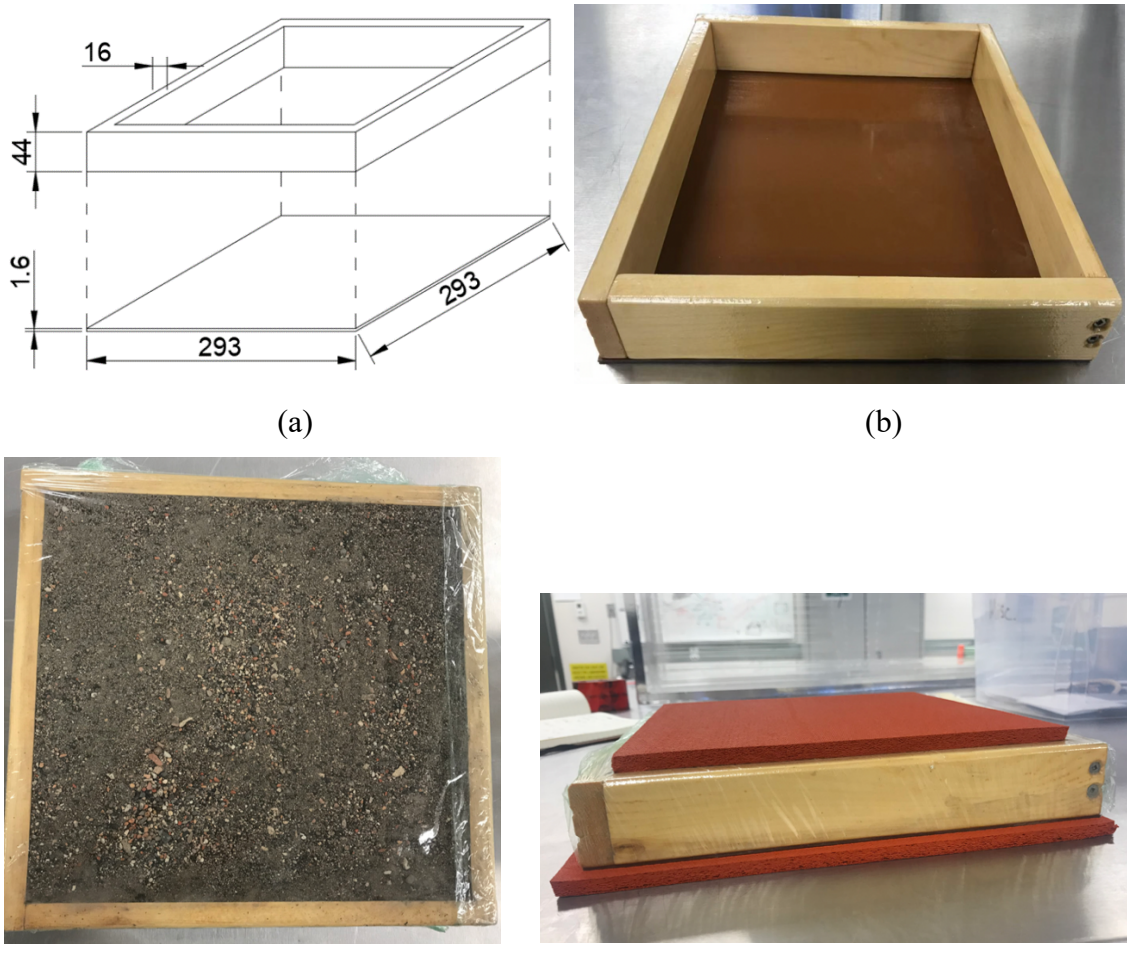

(a) (b)

(c) (d)

Figure 3 (a) Dimensions (mm) of holding frame; (b) holding frame; (c) substrate with holding frame; and (d) an example final test sample.

The dry/wet substrate was then poured into the holding frame. A 14kg cylindrical mold with a diameter of 150mm was applied at different positions of the substrate top surface. Each position was applied for 2 minutes and a 2.5kg manual rammer was dropped from a height of 150mm five times at each position for greater compression. This compaction method was based on the Standard ASTM D698-07[47]. A metal ruler was then used to level-off the substrate to the top of the holding frame. To prevent the change of the substrate moisture content, cling wrap was used to seal the substrate sample together with the holding frame. As shown in Figure 3(c).

According to Clarke[48], for samples with thermal resistance lower than 1.0m^2K/W, the most significant error may come from interface resistance. Standard ASTM C518 also suggests for the sample in which it is hard to obtain good surface contact between the sample and the testing plate, a thin sheet of suitable homogeneous material could be used between the sample and the plate surfaces. Since the surface of substrates used in this test is uneven, which may result in a high interface resistance, a buffer sheet was used to minimize the influence of interface resistance. Clarke used four different buffer sheet materials to perform the test and found silicone sponge provided the most uniform results. In this experiment, a silicone sponge with the thickness of 9mm was used as a buffer and one was placed on the top surface of the substrate and a second one on the bottom. The buffer sheets were slightly compressed during the test to perform good contact with the substrate surface as well as the bottom frame. The final test sample was then completed, as shown in Figure 3(d) (please see Appendix A for the detailed substrate preparation).

4.2.1.2 Steady-state measurements

In this study, HFM 436/3/1E was used to test the thermal conductivity of four substrates. A Heat Flow Meter is an apparatus to determine thermal conductivity through a process of steady-state measurements[46]. The test sample is in contact with hot and cold plates that have two different stable temperatures. Heat flows vertically from the upper, hot plate to the lower, cold plate through the test sample and sensors on the plates measure temperature and heat flux once per minute until all readings are stabilized. The thermal conductivity of

the test sample under steady-state conditions is then calculated (please see Appendix A for the detailed thermal conductivity measurement).

The test sample is the loose-fill substrate, together with the buffer sheet and the holding frame. The test results are thermal conductivity and thermal resistance of the whole test sample. To achieve substrate thermal conductivity, a reference sample also needs to be measured. The test sample and the reference sample arrangement are shown in Figure 4. Cling wrap was also included in both test and reference samples. It is very thin, and thermal resistance can be neglected.

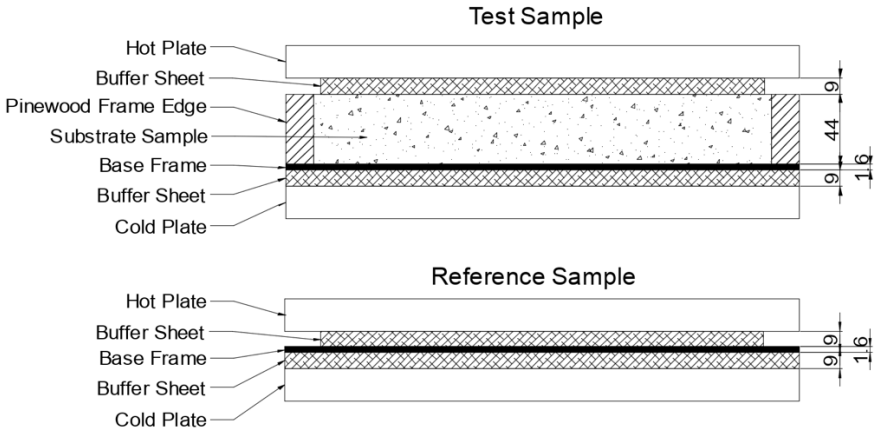

Figure 4 Test Sample and reference sample arrangement (dimensions in mm)

According to Clarke[34], the total test sample thermal resistance is :

$$R_t{}^1 = R_{b1} + R_{b1-s} + R_s + R_{s-f} + R_f + R_{f-b2} + R_{b2} \tag{7}$$

where $R_t{}^1$ is the total test sample thermal resistance; R_{b1} is the upper buffer sheet thermal resistance; $R_{b1\text{-}s}$ is the interface thermal resistance between the upper buffer sheet and the substrate; R_s is the substrate thermal resistance; $R_{s\text{-}f}$ is the interface thermal resistance between substrate and base frame; R_f is the base frame thermal resistance; $R_{f\text{-}b2}$ is the interface thermal resistance between base frame and lower buffer sheet; and R_{b2} is the lower buffer sheet thermal resistance.

The total reference sample thermal resistance is:

$$R_t{}^2 = R_{b1} + R_{b1-f} + R_f + R_{f-b2} + R_{b2} \quad (8)$$

where $R_{b1\text{-}f}$ is the interface thermal resistance between the upper buffer sheet and the base frame.

By subtracting those two thermal resistances, the resistance difference is:

$$R_{diff} = R_t{}^1 - R_t{}^2 = R_{b1-s} + R_s + R_{s-f} - R_{b1-f} \quad (9)$$

Both $R_{b1\text{-}s}$ and $R_{b1\text{-}f}$ are mediated by layers of cling wrap and these two resistances should cancel. $R_{s\text{-}f}$ is the interface thermal resistance between the substrate's bottom surface and the base frame top surface. Because the substrate and holding frame were prepared and allowed to settle overnight, this should lead to uniform contact between the substrate and holding frame and therefore, this resistance should be very small. Thus, $R_{diff}=R_s$, and the substrate thermal conductivity k_s (W/m·K) is calculated as:

$$k_s = \frac{d_s}{R_s} \quad (10)$$

where k_s is the substrate thermal conductivity, W/m·K; d_s is the substrate thickness, m; R_s is substrate thermal resistance, m^2K/W.

4.2.2 Thermal Performance Experimental Study

To further analyze the thermal performance of the substrate layer in an uncontrolled environment, two equally sized experimental test cells were constructed for testing outdoors in Victoria, BC, Canada. Victoria is located on the southern tip of Vancouver Island which has a warm-summer Mediterranean climate[49]. Figure 5 shows the experimental test cell setup. The test cell consists of a six-wall enclosure with inner dimensions of 1m x 1m x 0.6m (height), constructed using 0.016m thick plywood. Except for the top surface, the inner side of other five surfaces were insulated by 0.05m thick XPS foam, with $10m^2K/W$ thermal resistance. Four SPF solid wood vertical supports were used on the inner side of the top surface to provide support for the substrate. To prevent water from entering into the test cell, a layer of EPDM pond liner was used above the test cell top surface. The Sopraflor X substrate was then poured on the EPDM pond liner until it reached the pre-determined thickness of 150mm (extensive), and 200mm (intensive) for the experiment. As shown in Figure 5, for each test cell, four thermocouples HOBO E348-TMC50-HD with accuracy of ±0.25ºC were located at the surface of the substrate (T.C.1),

under the substrate layer, on the surface of EPDM pond liner (T.C.2), at the roof's inner plywood ceiling surface (T.C.3), and in the center of test cell (T.C.4). All are programmed to read temperature every minute at each location. For each test cell, a moisture sensor Delta ML3 Theta Probe was located inside the substrate to read the substrate moisture content every 2 minutes. Data loggers HOBO E348-U12-008 and Delta E312-GP1 were used to record data.

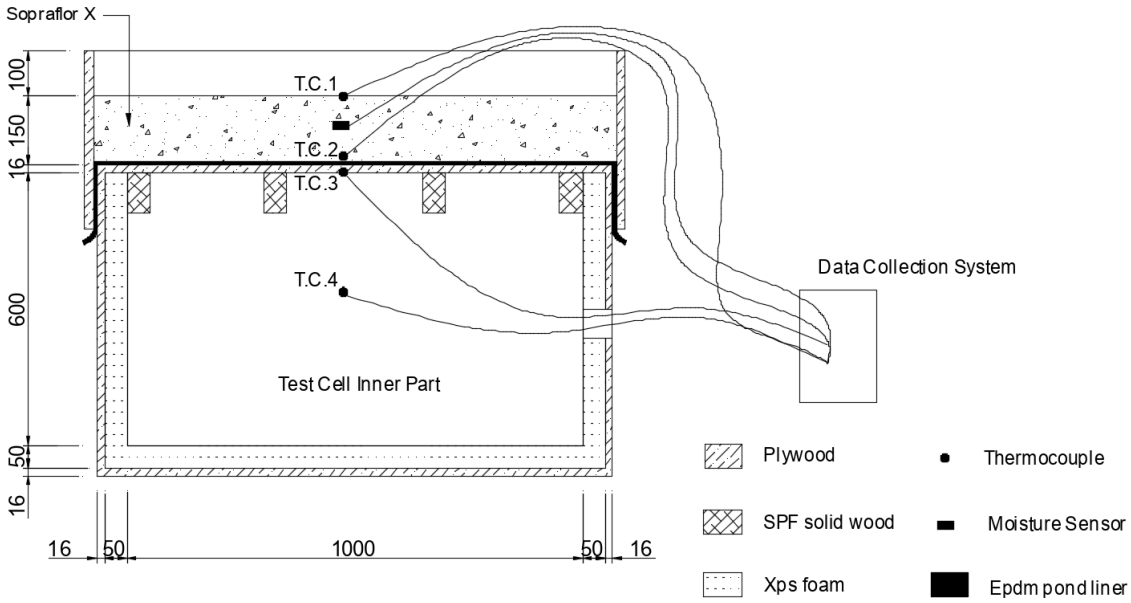

Figure 5 Experimental test cell with 150mm thickness Sopraflor X (dimensions in mm)

Images of the two experimental test cells located at the University of Victoria campus are shown in Figure 6. The test cells surfaces were painted white to reflect solar radiation that could enter through the side walls. Two cells were set up with a mild slope to avoid water accumulation on the roof. To avoid the influence of test cell and shed shadow, and to ensure they experienced the same weather conditions, the distance between them and the distance between the test cells and the shed were determined by shadow length simulation results on the Suncalc (https://www.suncalc.org/) website on March 01, 2019.

There is an access door on one side of the test cell to allow access to the interior, as shown in Figure 7 (a). The door was also insulated with XPS foam, sealed with rubber weatherseal,

and screwed tightly to minimize the heat transfer through the door. The access door was covered by the EPDM pond liner to prevent water from entering but the pond liner is not attached to the access door very tightly: an air gap between them was created so that the solar energy absorbed by the pond liner would not transfer effectively to the access door. Holes permitting cables were also insulated very well and waterproofed, as shown in Figure 7 (c). The temperature and moisture data were collected to the data logger located in a box hanging on the wood fence of the yard, as shown in Figure 7 (d). Several tests were performed from May, 2019 to August, 2019. Table 2 shows the schedule and model for each test. To analyze the impact of the substrate layer, substrate thickness and vegetation layer on green roof thermal performance, comparisons were made for the bare roof (no vegetation and substrate layer, as shown in Figure 8 (a)), vs. Roof with 150mm thick substrate (as shown in Figure 8 (b)); Roof with 150mm thick substrate vs. Roof with 200mm thick substrate; Roof with 150mm thick substrate vs. Roof with 150mm thick substrate and vegetation layer (as shown in in Figure 8 (c)).

Figure 6 Experimental test cell.

(a) (b)

(c) (d)

Figure 7 (a) Test cell access door; (b) test cell interior; (c) cable routing from inside; (d) data logger box.

Table 2 Test schedule

Test number	Date (2019)	Description	Test Cell A	Test Cell B
1	July 09 – July 15	Influence of substrate layer	Bare roof	Roof +150mm thick Sopraflor X
2	May 30 – June 02	Influence of substrate layer thickness	Roof + 150mm thick Sopraflor X	Roof + 200mm thick Sopraflor X
3	July 02 – July 08	Influence of moisture content	Roof + 150mm soil No irrigation	Roof + 150mm soil With irrigation
4	Aug 07 – Aug 13	Influence of vegetation layer	Roof + 150mm thick Sopraflor X	Roof + 150mm thick Sopraflor X + Sedum pad

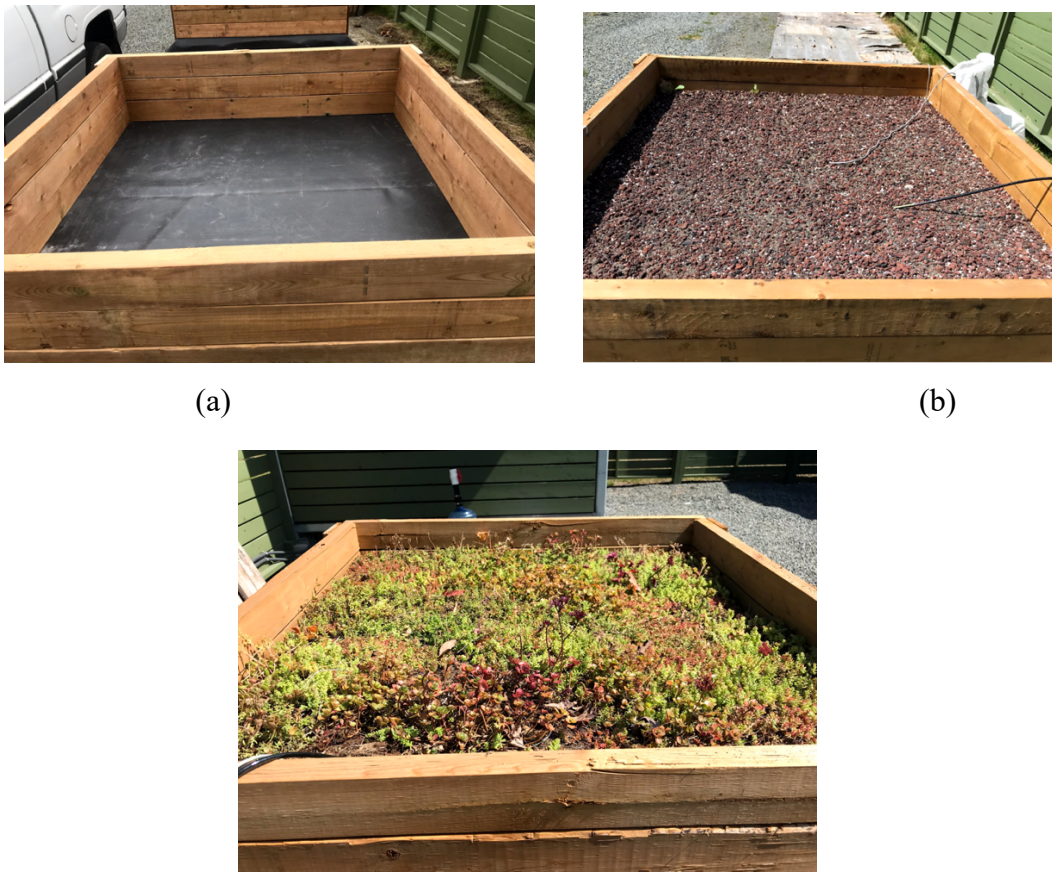

(a) (b)

(c)

Figure 8 (a) Bare roof test cell surface; (b) roof with 150mm thick substrate test cell surface; (c) green roof test cell surface.

4.3 Results and Discussions

4.3.1 Results of Thermal Conductivity Experimental Study

4.3.1.1 Thermal Conductivity vs. Dry Substrate Density

The physical properties of four substrates are shown in Table 3. Sopraflor I has the lowest dry density, which is 865.1kg/m^3 due to the high percentage of high porous mineral aggregate, with 1.75mm D_{50} average particle size [50]. Eagle Lake has the highest dry density, which is 1184.1 kg/m^3 due in part to high percentage of sand, with 0.8575mm D_{50} average particle size. These characteristics contribute to the reasons why Sopraflor I has the highest moisture holding capacity by mass and Eagle Lake has the lowest.

Table 3 Test results of 4 substrates Physical properties

Substrate	Sopraflor I	ZincoBlend	Sopraflor X	Eagle Lake
Dry Density (kg/m^3)	856.1	921.9	1022.8	1184.1
Moisture Holding Capacity	50~60%	40~50%	30~40%	30~40%

Figure 9 shows the substrates thermal conductivities at different temperatures and moisture contents (please see Appendix B for the detailed substrate thermal conductivity results). From the figure we can see that no matter the temperature or moisture content, Eagle Lake always has the highest thermal conductivity, while Sopraflor I always has the lowest. It appears, based on the results available from this study, irrespective of temperature or moisture content, the substrate with the higher dry density exhibits the higher thermal conductivity. With average particle size D_{50} of 0.8575mm, Eagle Lake particles are compressed tighter as compared with Sopraflor I (D_{50} of 1.75mm) which makes it easier for heat to transfer through the substrate. Figure 9 indicates that dry density has a significant influence on the substrate thermal conductivity.

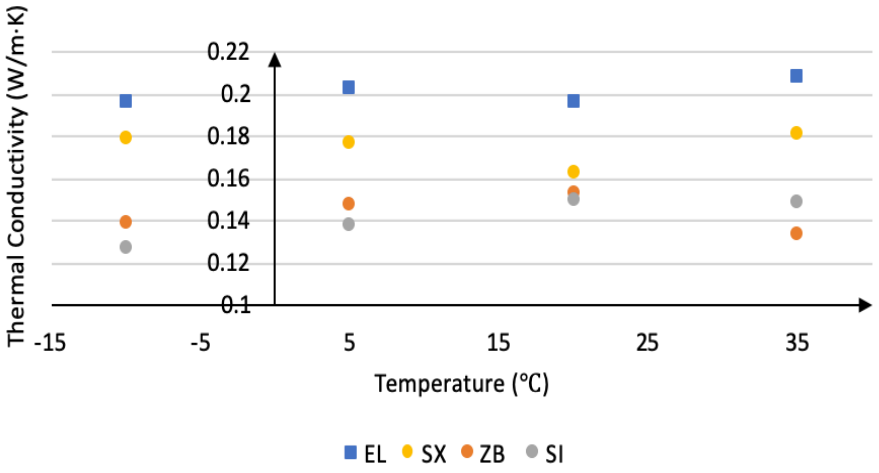
Thermal Conductivity (W/m·K)
0.22
0.2
0.18
0.16
0.14
0.12
0.1
-15
-5
5
15
25
35
Temperature (°C)
EL SX ZB SI

(a)

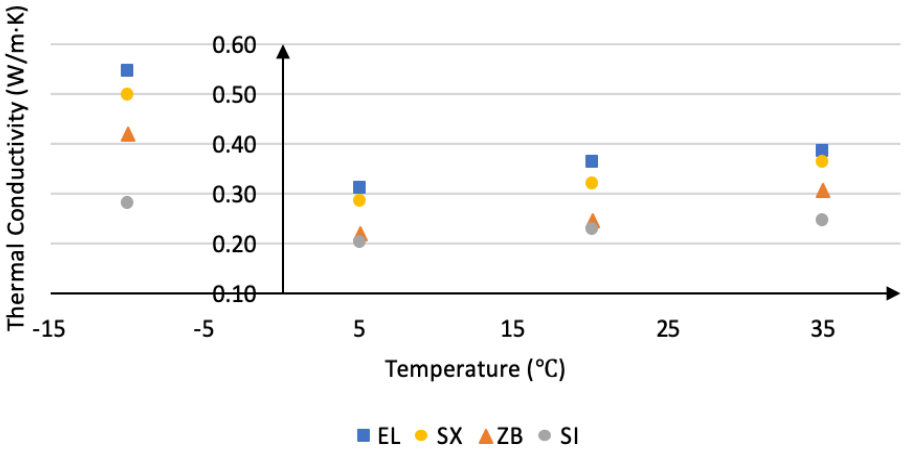
Thermal Conductivity (W/m·K)
0.60
0.50
0.40
0.30
0.20
0.10
-15
-5
5
15
25
35
Temperature (°C)
EL SX ZB SI

(b)

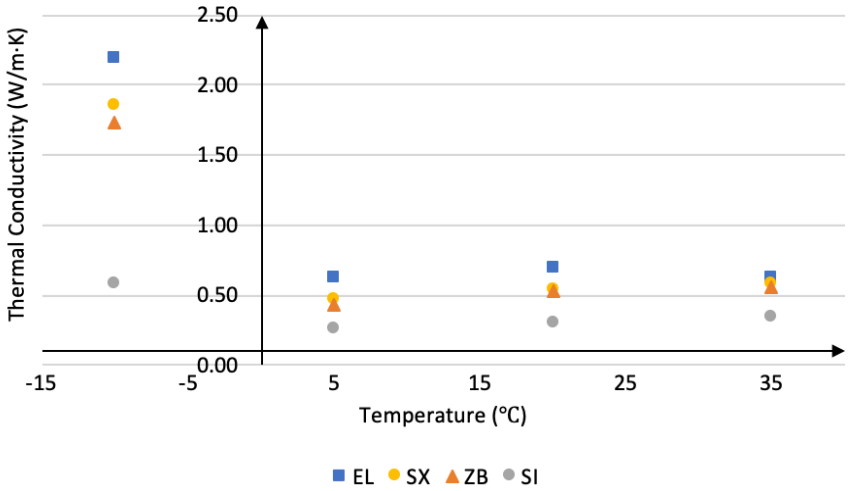
Thermal Conductivity (W/m·K)
2.50
2.00
1.50
1.00
0.50
0.00
-15
-5
5
15
25
35
Temperature (°C)
EL SX ZB SI

(c)

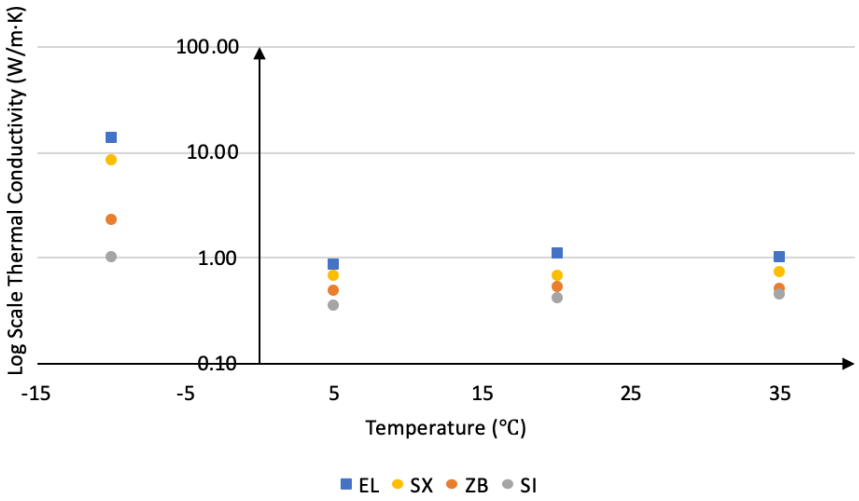

(d)

Figure 9 Thermal conductivity vs. average temperature for (a) dry substrates; (b) substrates with 10% moisture content by mass; (c) substrates with 20% moisture content by mass; and (d) substrates with 30% moisture content by mass thermal conductivity vs. average temperature.

4.3.1.2 Thermal Conductivity vs. Moisture Content

Figure 10 shows the variation of 4 substrates' thermal conductivities with moisture content under different average temperatures. Fitting function of thermal conductivity verses moisture content by mass in unfrozen and frozen state are shown in Table 4 and Table 5. It can be seen from the figure and tables that:

- Moist soil is more conductive compared with dry soil. This is because water replaced the air among soil particles and connects the gaps between them, which increased the contact area.
- In the unfrozen state (5ºC, 20ºC, and 35ºC), as shown in Figure 10 (a, b, and c), thermal conductivity increase linearly as moisture content increases. Fitting functions and coefficients of determination R^2 values are shown in Table 4. As substrate density increases, the slope of the fitting function increases. Eagle Lake (dry density 1184.1 kg/m^3) thermal conductivity shows the most significant increase (with a linear slope of 2.33-3.04) as moisture increases whereas Sopraflor I (dry density 856.1kg/m^3) thermal

conductivity shows the smallest increase (with a linear slope of 1.09-1.15). This is because a larger amount of water is added to the Eagle Lake substrate.

- In the frozen state (-10ºC) as shown in Figure 10 (d), an exponential function exists between thermal conductivity and moisture content. Fitting functions and coefficients of determination R^2 values are shown in Table 5. Thermal conductivity increases more sharply as substrate moisture content prior to freezing increases in the frozen state than in the unfrozen state. This is because the thermal conductivity of ice is much larger than that of water. As substrate dry density increases, the slope and index of the fitting function increases.

Table 4 Thermal conductivity *y* (W/m·K) as a function of moisture content by mass *x* in the unfrozen state

	5℃	20℃	35℃
Sopraflor I (SI)	$y = 1.09x + 0.08$	$y = 1.15x + 0.11$	$y = 1.15x + 0.12$
	$R^2 = 0.91$	$R^2 = 0.95$	$R^2 = 0.93$
Zinco Blend (ZB)	$y = 1.27x + 0.12$	$y = 1.30x + 0.14$	$y = 1.39x + 0.16$
	$R^2 = 0.98$	$R^2 = 0.99$	$R^2 = 0.96$
Sopraflor X (SX)	$y = 1.64x + 0.15$	$y = 1.74x + 0.16$	$y = 1.82x + 0.19$
	$R^2 = 0.98$	$R^2 = 0.99$	$R^2 = 0.99$
Eagle Lake (EL)	$y = 2.33x + 0.16$	$y = 3.04x + 0.13$	$y = 2.66x + 0.16$
	$R^2 = 0.98$	$R^2 = 0.97$	$R^2 = 0.96$

Table 5 Thermal conductivity *y* (W/m·K) as a function of moisture content by mass *x* in the frozen state

	Substrate	Fitting function	R^2
-10℃	Sopraflor I (SI)	$y = 0.12e^{8.03x}$	0.98
	Zinco Blend (ZB)	$y = 0.13e^{10.25x}$	0.98
	Sopraflor X (SX)	$y = 0.16e^{12.86x}$	0.99

Eagle Lake (EL)	$y = 0.16e^{14.08x}$	0.98

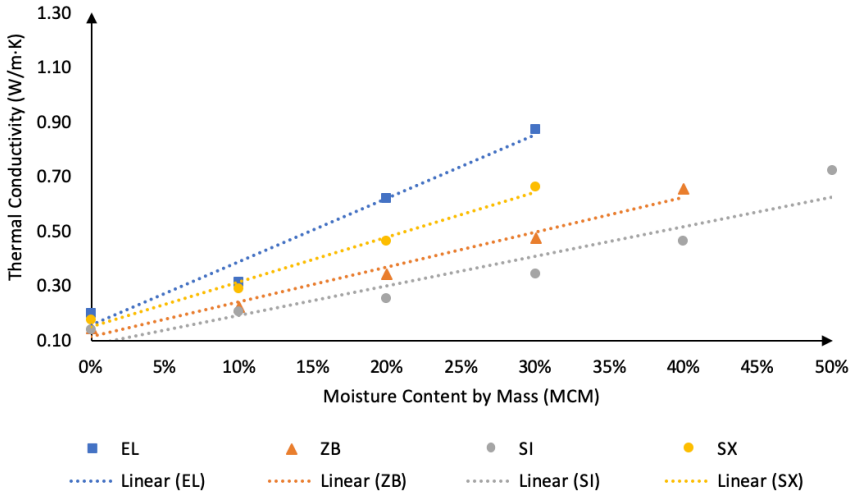

(a)

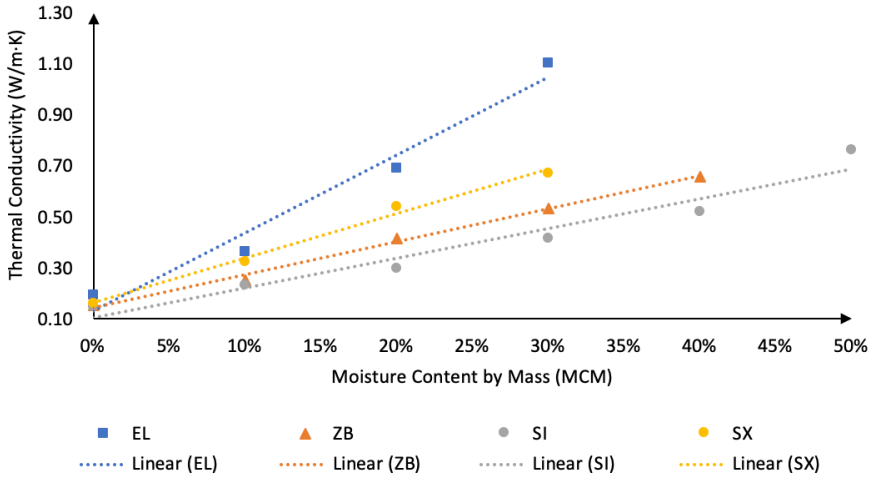

(b)

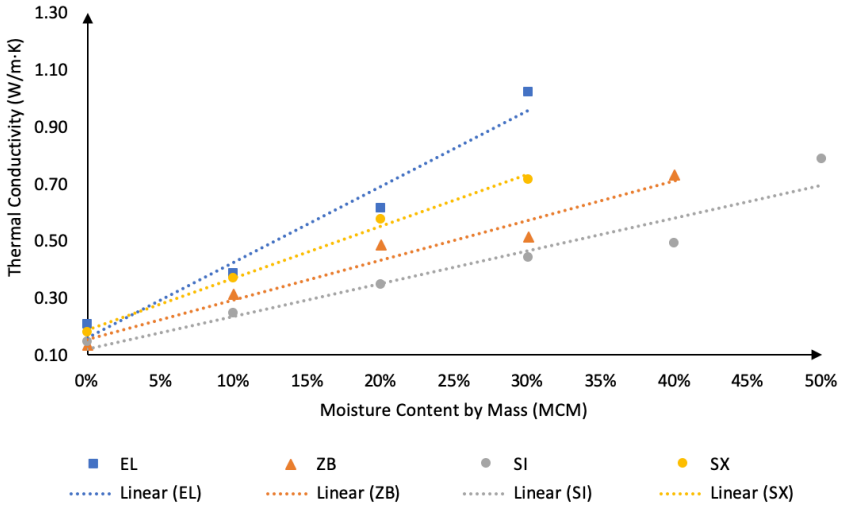

(c)

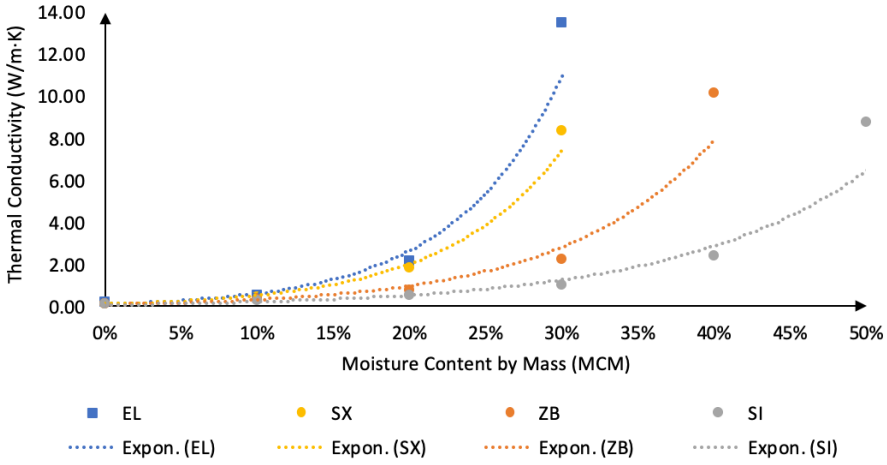

(d)

Figure 10 Substrates thermal conductivity vs. moisture content by mass at average temperature of (a) 5ºC; (b) 20ºC; (c) 35ºC; (d) -10ºC.

4.3.1.3 Thermal Conductivity vs. Average Temperature

Figure 11 shows the variation of 4 substrates thermal conductivities with average temperature under different moisture content. From the figure we can see:

In the unfrozen state (5ºC, 20ºC, and 35ºC), it is difficult to see a relationship between thermal conductivity and average temperature. To further analyze the relationship between them, the Mann-Kendall Trend Test was used to analysis the relationship between thermal conductivity and average temperature in the unfrozen state (please see Appendix C for the

detailed Mann-Kendall trend test results). Results showed all four substrates under different moisture content: p-value (0.148-0.500) is always much larger than α (0.05), which means there is no significant relationship between thermal conductivity and average temperature in the unfrozen state.

- In the phase transition zone (between -10ºC and 5ºC), as average temperature decreases, thermal conductivity increases sharply during the transition from water to ice. This is because the thermal conductivity of ice is much larger than that of water. Also during the phase transition zone, soil structure changed because of the sharp transformation from water to ice.
- To find the relationship between thermal conductivity and average temperature in both the frozen and unfrozen state, the x axis were shifted by a temperature of +10.00ºC to artificially move all the x values to be greater than zero. Figure 12 shows the variation of four substrates thermal conductivity with (temperature+10.001ºC) under different moisture content. A power function of the form of $y=A(T+10.001)^B$ is found for wet samples. Fitting functions and coefficients of determination R^2 values are shown in Table 6, and these indicate that as moisture content increases, R^2 becomes more closer to 1; when the substrate reaches its maximum moisture content, R^2=0.99.

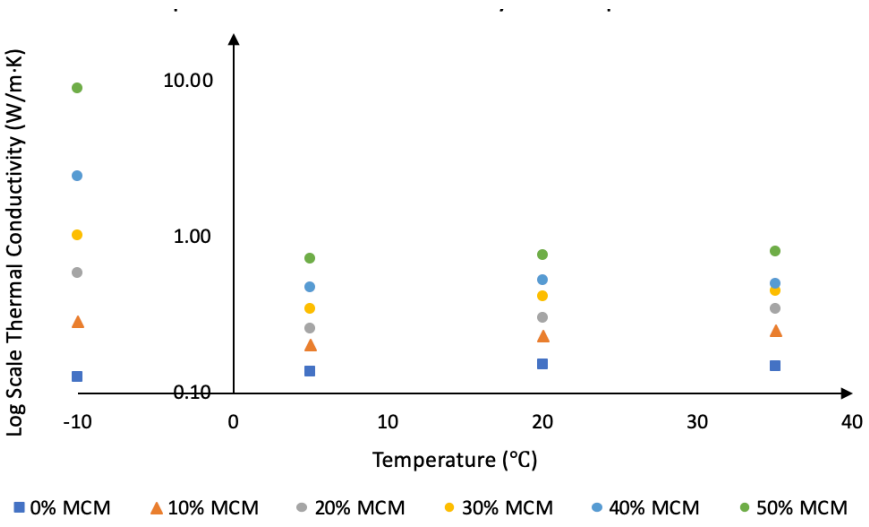

(a)

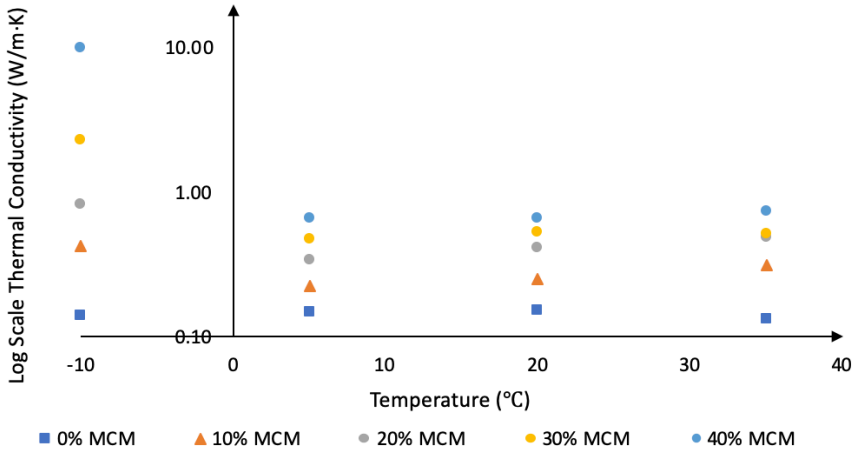
Log Scale Thermal Conductivity (W/m·K)
10.00
1.00
0.10
-10
0
10
20
30
40
Temperature (°C)
0% MCM
10% MCM
20% MCM
30% MCM
40% MCM

(b)

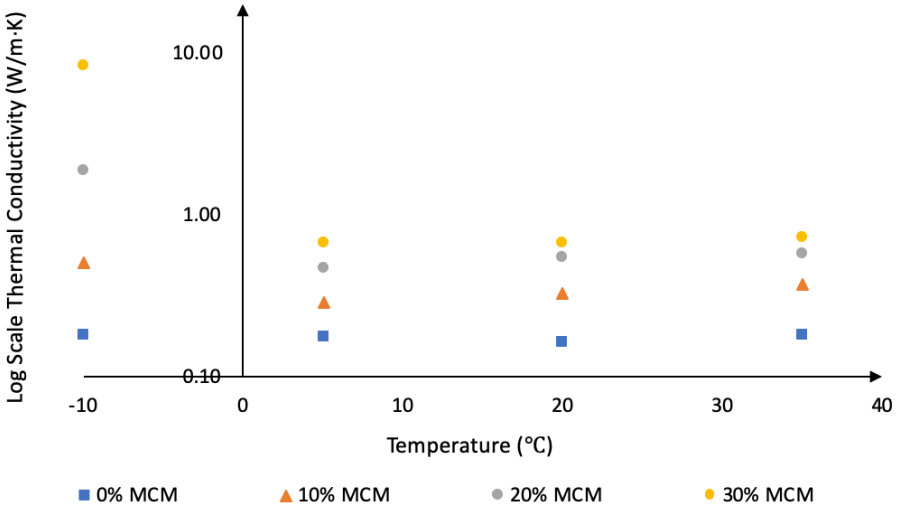
Log Scale Thermal Conductivity (W/m·K)
10.00
1.00
0.10
-10
0
10
20
30
40
Temperature (°C)
0% MCM
10% MCM
20% MCM
30% MCM

(c)

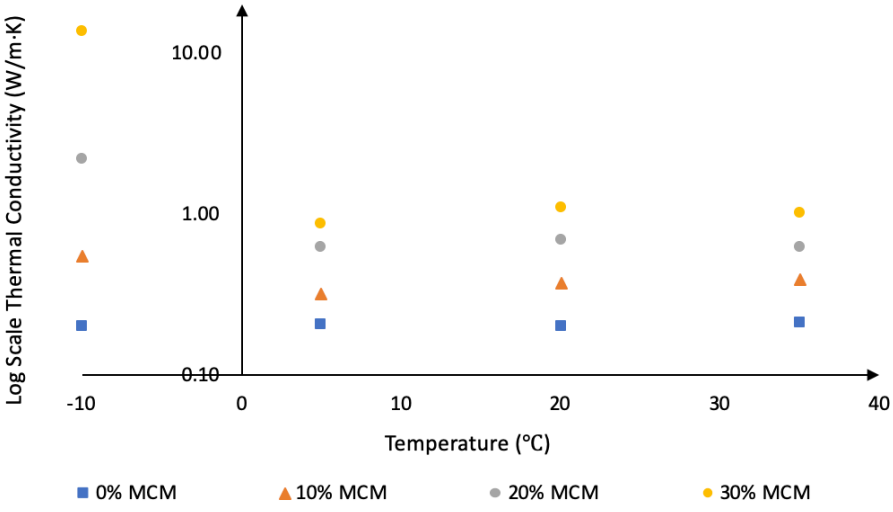
Log Scale Thermal Conductivity (W/m·K)
10.00
1.00
0.10
-10
0
10
20
30
40
Temperature (°C)
0% MCM
10% MCM
20% MCM
30% MCM

(d)

Figure 11 Thermal conductivity vs. average temperature at different moisture content for (a) Sopraflor I; (b) Zinco Blend; (c) Sopraflor X; (d) Eagle Lake.

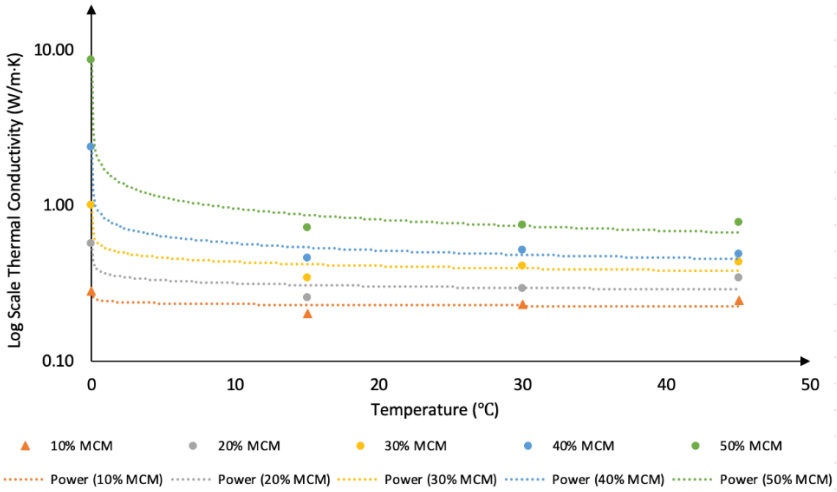

(a)

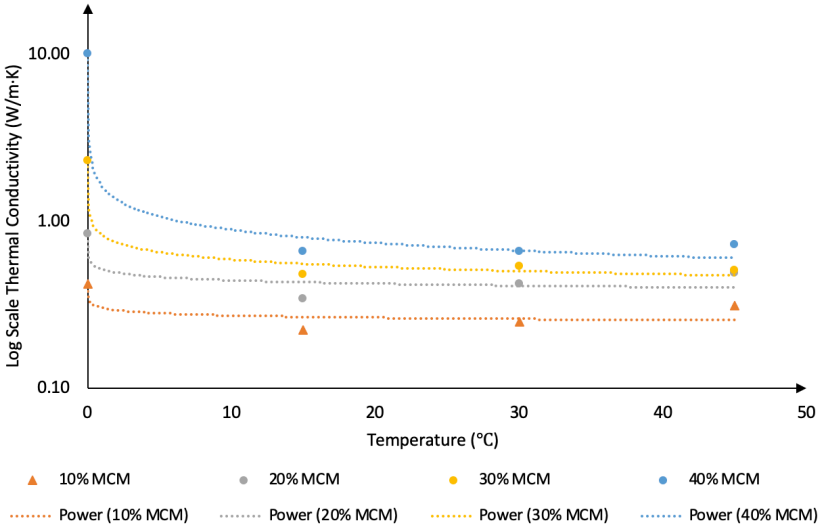

(b)

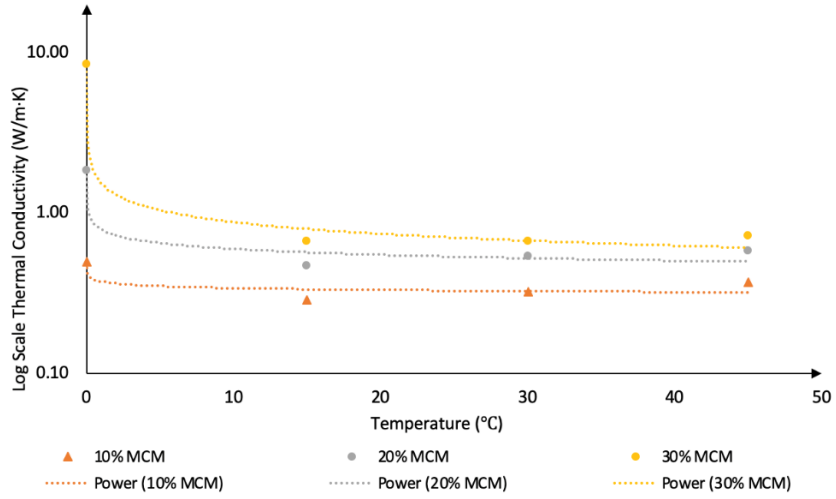

(c)

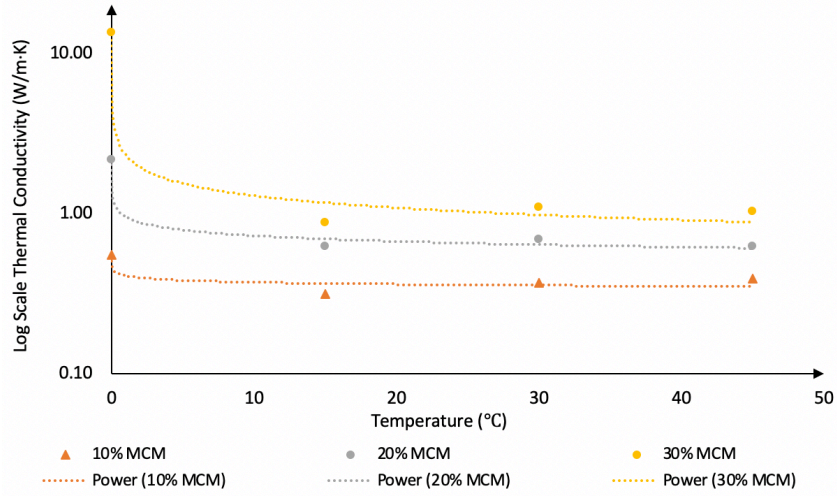

(d)

Figure 12 Thermal conductivity vs. average temperature (+10.001) at different moisture contents for (a) Sopraflor I; (b) Zinco Blend; (c) Sopraflor X; (d) Eagle Lake.

Table 6 Thermal conductivity y (W/m·K) as a function of $x = T + 10.001$

	Sopraflor I	Zinco Blend	Sopraflor X	Eagle Lake
10%	$y = 0.25x^{-0.02}$	$y = 0.30x^{-0.05}$	$y = 0.37x^{-0.04}$	$y = 0.42x^{-0.41}$
	$R^2 = 0.56$	$R^2 = 0.68$	$R^2 = 0.75$	$R^2 = 0.78$
20%	$y = 0.37x^{-0.06}$	$y = 0.52x^{-0.07}$	$y = 0.79x^{-0.12}$	$y = 0.95x^{-0.12}$

	$R^2 = 0.82$	$R^2 = 0.79$	$R^2 = 0.95$	$R^2 = 0.98$
30%	$y = 0.54x^{-0.09}$	$y = 0.83x^{-0.15}$	$y = 1.54x^{-0.24}$	$y = 2.31x^{-0.25}$
	$R^2 = 0.91$	$R^2 = 0.98$	$R^2 = 0.99$	$R^2 = 0.98$
40%	$y = 0.82x^{-0.15}$	$y = 1.63x^{-0.26}$	-	-
	$R^2 = 0.98$	$R^2 = 0.99$	-	-
50%	$y = 1.67x^{-0.24}$	-	-	-
	$R^2 = 0.99$	-	-	-

4.3.2 Results of Thermal Performance Experimental Study

4.3.2.1 Roof (Test cell A) vs. Roof with 150mm thick Substrate (Test cell B)

Data from the bare roof test cell and the roof with 150mm thickness Sopraflor X test cell were collected in Victoria from July 09, 2019 to July 15, 2019. Figure 13 shows the weather data, including air temperature, wind speed, humidity, and precipitation collecting from the weather station located on the roof of UVIC David Turpin Building. Insolation data are shown in Figure 14. Rainfall occurred from late July 09 to July 11, with peak precipitation of 5.33mm at 23:00 on July 09. Air temperature varied from 11.3 ℃ to 24.2 ℃. Daily peak insolation occurred between 11:00 to 14:30.

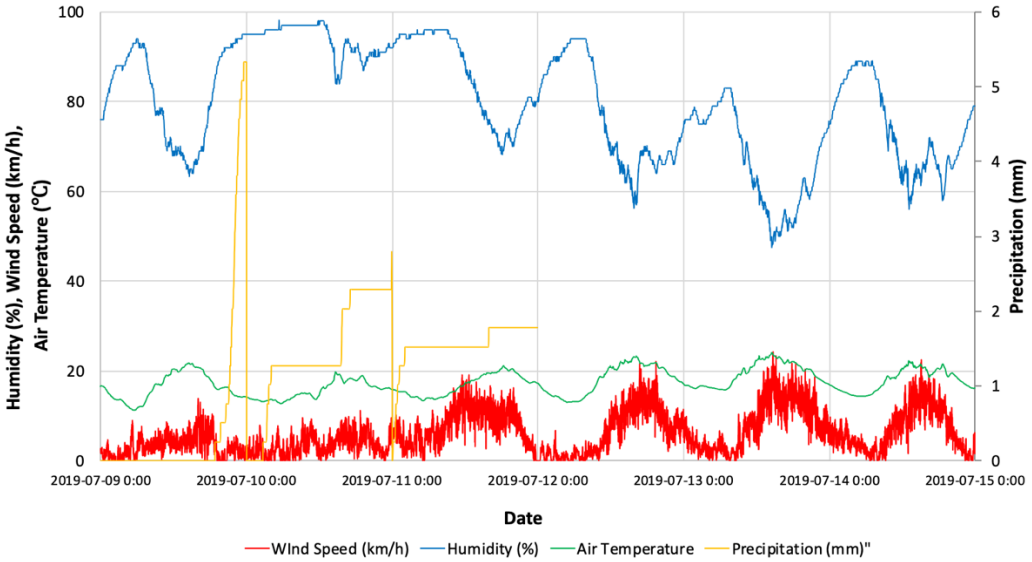

Figure 13 Weather Data (July 09 – July 14, 2019)

Figure 14 shows the surface and indoor air temperature results of test cells A and B. It can be seen that the bare roof has a large temperature fluctuation between the daytime and the nighttime. At daytime, with its roof surface black, bare roof surface temperature in the daytime is strongly influenced by solar radiation. The daily maximum bare roof surface temperature is 1.95 to 2.87 times larger than the daily maximum ambient air temperature. At night, bare roof surface temperature is similar, and sometimes even lower than the outdoor air temperature, this is because of the heat convection with cool air that flows above the roof surface, and the sky longwave radiation[39]. As for the test cell B with 150mm Substrate, a significant temperature reduction, and a time delay in reaching peak temperatures can be seen for the indoor air temperature compared with test cell A, this is because the substrate layer acted as a thermal mass which stored heat in the daytime and released this heat to ambient environment at night, this is also the reason why roof surface temperatures of cell B are higher than the outdoor air temperature at night.

To further analyze the thermal properties of the substrate layer, transient conduction, and a lumped capacitance time constant[51] were analyzed. The lumped capacitance time constant is the amount of time for the sensor to respond to the thermal environment changes, it is the product of thermal capacitance of the sensor and the thermal resistance to heat transfer from the surface of the sensor. In this study, bare roof plywood ceiling

together with EPDM pond liner were considered as sensor A, the 150mm thick substrate layer, plywood ceiling, and EPDM pond liner were considered as sensor B. Surface temperatures of two test cells were considered as input. The indoor air temperature was considered as the output of two sensors. From Figure 14 we can see, both roof surface (input), and indoor air temperature (output) are following an oscillating function. The fitting functions of temperature (ºC) inputs and outputs for both sensors versus time (hours) were obtained using the excel solver method. Fitting functions and R^2 values are shown in

Table 7 and plots of fitting functions are shown in Figure 15. Since the inputs of the sensor followed an oscillating function, the attenuation of the amplitude of the oscillation (*Att*) and the phase lag (φ) can be calculated as follows:

$$Att = \frac{1}{\sqrt{1+(2\pi f\tau)^2}} \tag{11}$$

$$\varphi = tan^{-1}(2\pi f\tau) \tag{12}$$

The frequency (f) and phase lag (φ) value can be achieved from

Table 7, so the value of τ and attenuation were calculated based on equations above, results are shown in Table 8. The results of phase angle and attenuation are also highlighted in Figure 16. The lumped time constant for sensor A is 1.87 hours, whereas the time constant for sensor B is 7.11 hours. As discussed before, the time constant is the product of thermal capacitance and the thermal resistance, that is to say, the additional 150mm thick substrate layer increases the total capacitance and thermal resistance, which makes the total time constant 3.8 times larger than that of the bare roof. The attenuation of the amplitude for sensor A and sensor B is 0.90 and 0.47 respectively. Because of thermal resistance, 150mm substrate layer provided a 42.6% further reduction on the amplitude compared with that of the bare roof. The phase lag for sensor A and sensor B is 0.456 and 1.080, respectively. Due to the thermal capacitance, the 150mm substrate layer provided 0.624rad further phase lag compared with that of the bare roof.

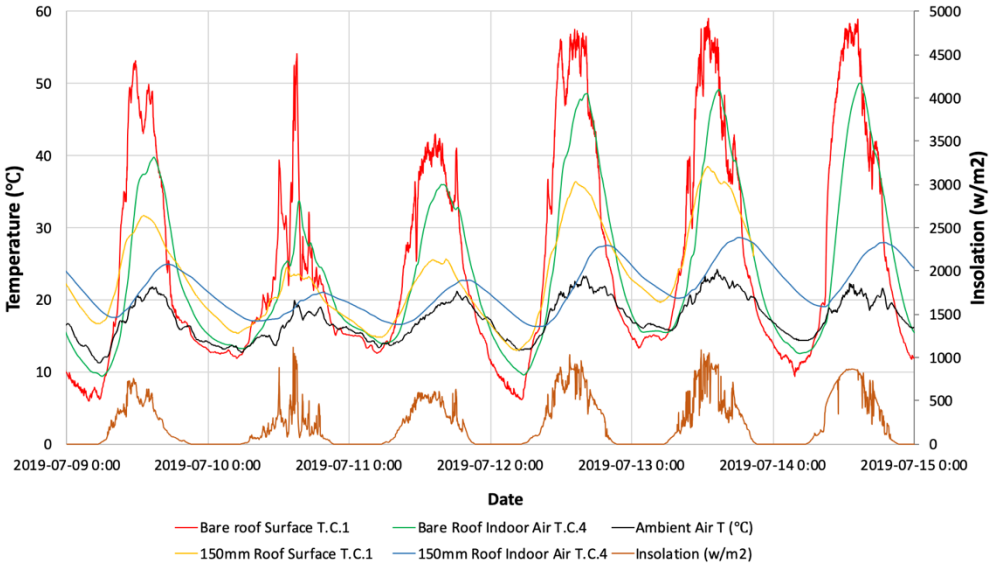

Figure 14 Temperature and insolation results of test cell A and B

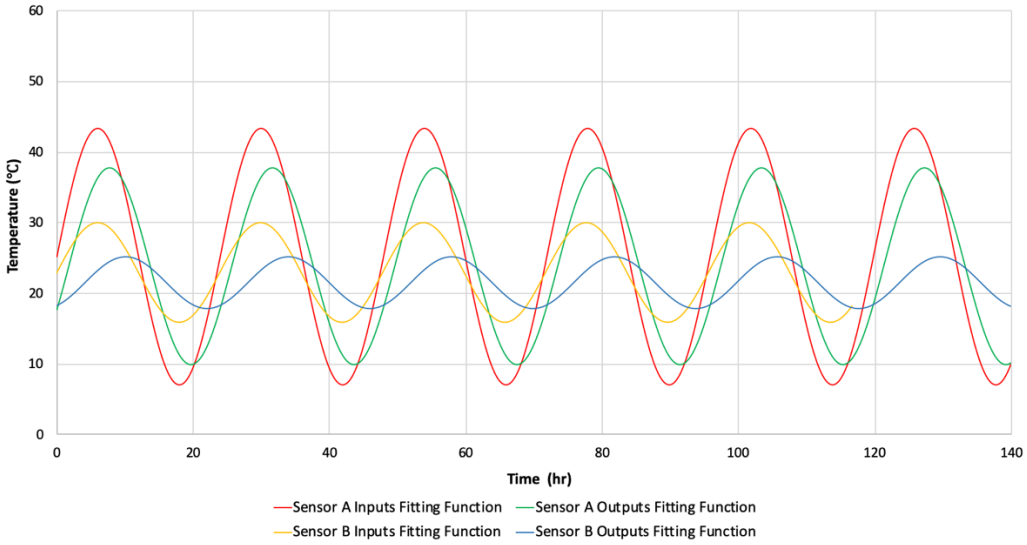

Figure 15 Fitting function plots of temperature inputs and outputs

Table 7 Fitting functions of temperature inputs and outputs

		Fitting function	R^2
Sensor A (Bare Roof)	Input	$T = 18.15sin(0.2623t) + 25.205$	0.77
	Output	$T = 13.93sin(0.2628t - 0.456) + 23.845$	0.80
Sensor B (Roof with 150mm thick substrate)	Input	$T = 5.27sin(0.2630t) + 22.960$	0.61
	Output	$T = 3.66sin(0.2629t - 1.080) + 21.516$	0.58

Table 8 Time constant results of two sensors

	f (cycles per hour)	time constant τ (hour)	$f\,\tau$	Att (-)	φ (rad)
Sensor A	0.042	1.866	0.078	0.898	0.456
Sensor B	0.042	7.110	0.298	0.472	1.080

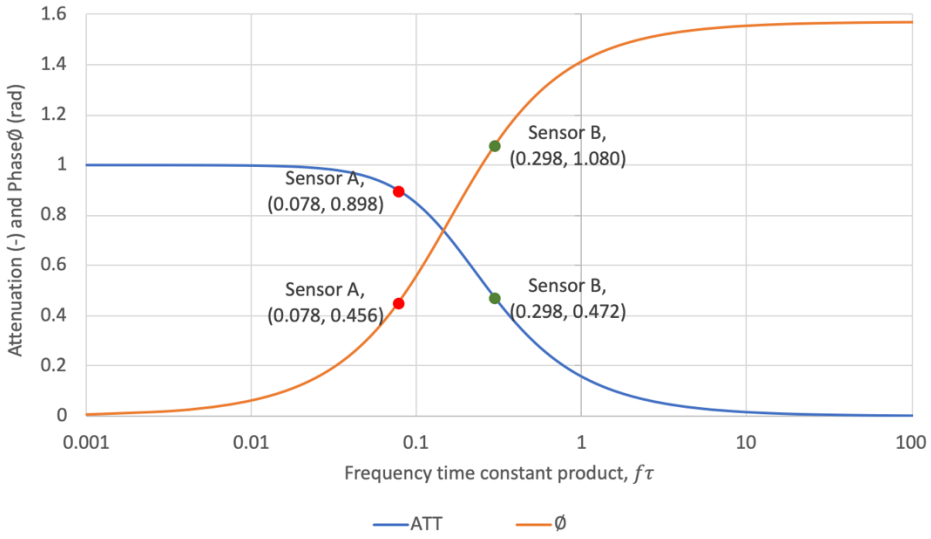

Figure 16 Attenuation and phase angle vs. the product of frequency and the time constant

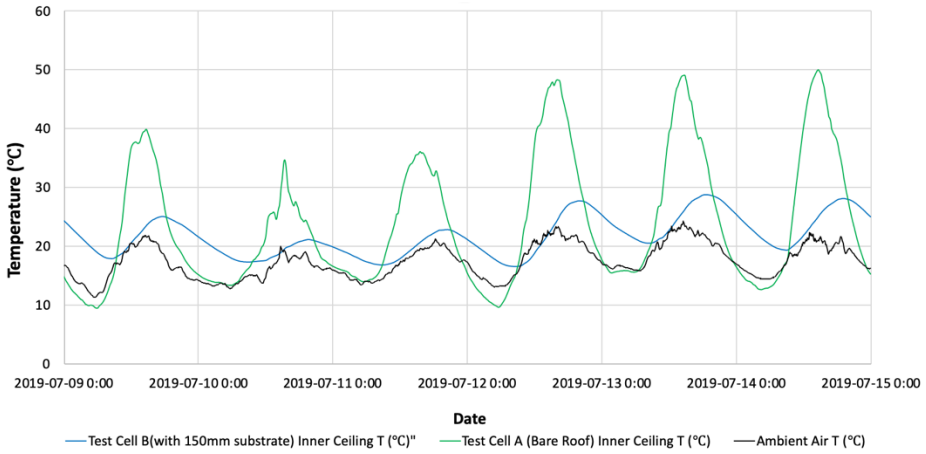

Figure 17 Test cell inner ceiling temperature results of test cell A and B

Figure 17 shows the test cells' inner ceiling temperature from July 09 to July 14. The variation of test cell A inner ceiling temperature is up to 38.7ºC, whereas the variation of test cell B inner ceiling temperature is 12.0ºC. The trendlines of the two test cells' inner ceiling temperature has been analyzed and sine wave trends for each day have been found for both of them. The fitting function of test cell A ceiling temperature T(ºC) vs. time t (hour) is described as:

$$T = A_1 sin(\omega_1 t - \varphi_1) + T_{ave1}$$

and the fitting function of test cell B ceiling temperature T(ºC) vs. Time t (hour) is described as:

$$T = A_2 sin(\omega_2 t - \varphi_2) + T_{ave2}$$

Results of A, ω, φ, T_{ave}, and coefficients of determination R^2 of each day are shown in Table 9. Value A indicates the amplitude of the inner ceiling temperature and as we can see the value of A_1 is much higher than A_2. During the rainy days from July 09 to July 11, the amplitude for both test cells were smaller than on dry days, which is determined by the solar radiation and outdoor temperature. Based on the results, one can see that no matter if the day is rainy or sunny, A_1 is always 4 times larger than A_2. This means the 150mm thick substrate layer provided better thermal protection against outdoor temperature and solar radiation. It had a 75% reduction in the amplitude of the inner ceiling temperature as compared with that of the bare roof test cell and keeps test cell B interior at a relatively

steady state. Examining the results of angular frequency ω, the 150mm thick substrate layer has a tiny positive influence on the value of angular frequency during rainy days, while during sunny days it has a slightly negative influence on the value of angular frequency. From the results of ω_2/ω_1 it can be seen that substrate layer didn't have a large influence on the frequency.

Results of φ shows the phase leg of two cells, which is due to the properties of thermal capacitance. The phase lag φ_1 shows that no matter if on rainy or sunny days, the ceiling temperature delay for each day is always similar for the bare roof test cell, however for cell B with the substrate cover, the phase lag is always larger than test cell A. The delay on rainy days becomes more significant. This is because substrate has a large thermal capacity which stores heat in the daytime and releases it to the ambient environment at night, and as well, substrate thermal capacity increases as moisture content increases. T_{ave} shows the average inner ceiling temperature of the two cells. The bare roof shows a higher average temperature because of its black surface color, and the average temperature difference becomes larger on sunny days as outdoor insolation increases.

Table 9 Two test cells fitting function parameters

	09-Jul	**10-Jul**	**11-Jul**	**12-Jul**	**13-Jul**	**14-Jul**
${R_1}^2$	0.92	0.92	0.97	0.97	0.95	0.95
${R_2}^2$	0.99	0.99	0.98	0.99	0.99	0.99
A_1	14.14	7.85	11.17	19.03	16.04	18.08
A_2	3.47	1.96	2.91	5.58	4.06	4.26
$(A_1 - A_2)/A_1$	0.75	0.75	0.74	0.71	0.75	0.76
ω_1 *(rad/hr)*	0.30	0.28	0.29	0.28	0.30	0.30
ω_2 *(rad/hr)*	0.31	0.30	0.25	0.24	0.27	0.27
ω_2/ω_1	1.03	1.07	0.86	0.86	0.90	0.90
φ_1 *(rad)*	2.89	2.89	2.96	2.86	2.84	2.88

φ_2 *(rad)*	4.02	4.35	3.49	3.28	3.53	3.67
$(\varphi_2 - \varphi_1)$	1.13	1.46	0.53	0.42	0.69	0.79
T_{ave1} (℃)	22.57	19.88	23.21	26.35	28.15	27.5
T_{ave2} (℃)	21.57	19.04	19.61	21.77	24.43	23.67
$(T_{ave1} - T_{ave2})$	1.00	0.84	3.60	4.58	3.72	3.83

4.3.2.2 Extensive roof (Test cell C) vs. Intensive roof (Test cell D)

A test study of extensive and intensive substrate thermal performance was performed from May 30 to June 02. Test cell C is the roof with 150mm thick substrate, which is extensive, and test cell D is the roof with 200mm thick substrate, which is intensive. Figure 18 shows the weather data, including air temperature, wind speed, humidity, and insolation collected from the weather station located on the roof of the University's David Turpin Building. There is no rainfall during those three days and air temperature varied from 10.4ºC (at 06:17 on May 30) to 22.7ºC (at 14:21 on May 31). Humidity varied from 50.8% to 94.1%. The maximum insolation was 918.5W/m^2 (at 13:56 on June 01).

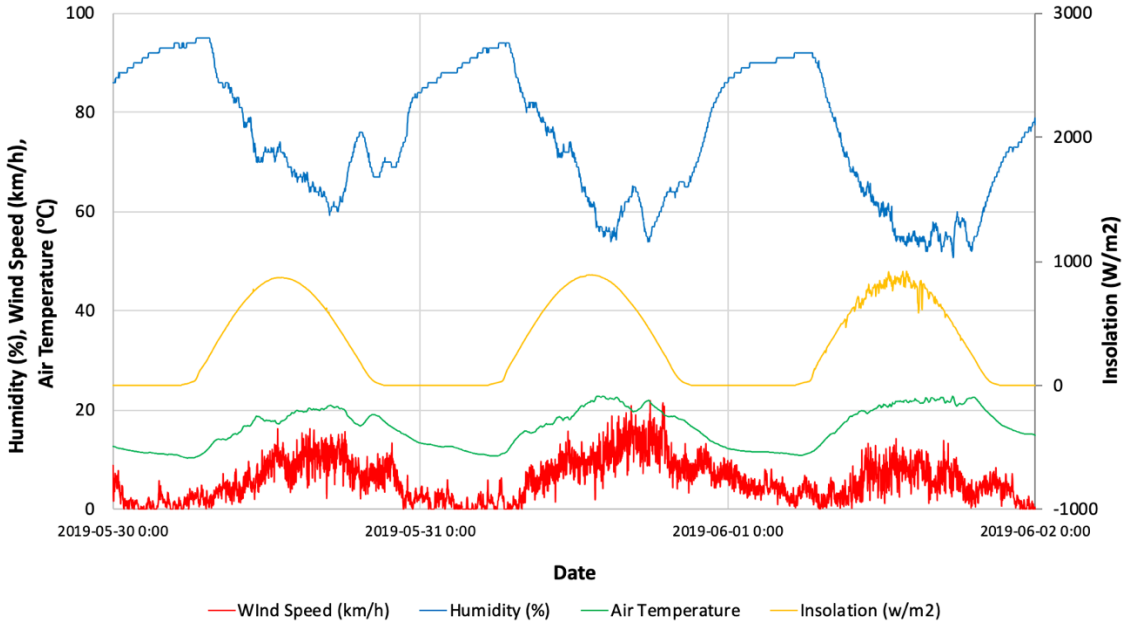

Figure 18 Weather Data (May 30 – June 02, 2019)

Figure 19 shows the test cells surface and inner ceiling temperatures from May 30 to June 01. The surface temperature of the two test cells are always the same all the time due to the same surface color and having the same components. The surface temperature varied from 12.6 ºC to 39.4ºC, with daily peak surface temperature occurring between 13:00 to 16:00 when the insolation was high. As discussed before, because the substrate layer acted as a thermal mass, it released heat to the ambient at night which make the surface temperature of the substrate higher than the ambient air temperature. As for the inner ceiling temperature of the two test cells, similar to previously, a significant reduction in temperature fluctuation and a delay in reaching the peak temperature occurred for both test cells. Ceiling temperature of test cell C varied from 16.8ºC to 30.5ºC, whereas the ceiling temperature of test cell D varied from 18.7ºC to 28.0ºC.

To further compare the thermal performance of two the test cells, the trendline of inner ceiling temperature was been analyzed and sine wave trends for each day were found for both of them. The fitting function of test cell C ceiling temperature T(ºC) vs. time t (hour) is described as:

$$T = A_3 sin(\omega_3 t - \varphi_3) + T_{ave3}$$

and the fitting function of test cell D ceiling temperature T(℃) vs. time t (hour) is described as:

$$T = A_4 sin(\omega_4 t - \varphi_4) + T_{ave4}$$

Results of A, ω, φ, T_{ave}, and coefficients of determination R^2 of each day are shown in Table 10. Results of value A shows a further 40% reduction on the amplitude of ceiling temperature of the cell with 200mm thick substrate compared with that of the cell with 150mm thick substrate, which in turn makes cell D's interior a relatively steady state. Results of ω shows the angular frequency of cell D is a little smaller than that of cell A, and the ratio between ω_3 and ω_4 were all close to 1. This means the thickness of the substrate does not have much of an influence on the angular frequency of the ceiling temperature. Results of phase lag φ indicates a more significant delay for test cell D. This is not surprising because the thermal capacity of substrate increases as the mass of the substrate increases. As for the average inner ceiling temperature T_{ave}, it can be seen that the

difference between those 2 average temperatures is small and can be neglected. This is because those two test cells had the same outer surface temperature, and the thickness of the substrate will not influence the average ceiling temperature.

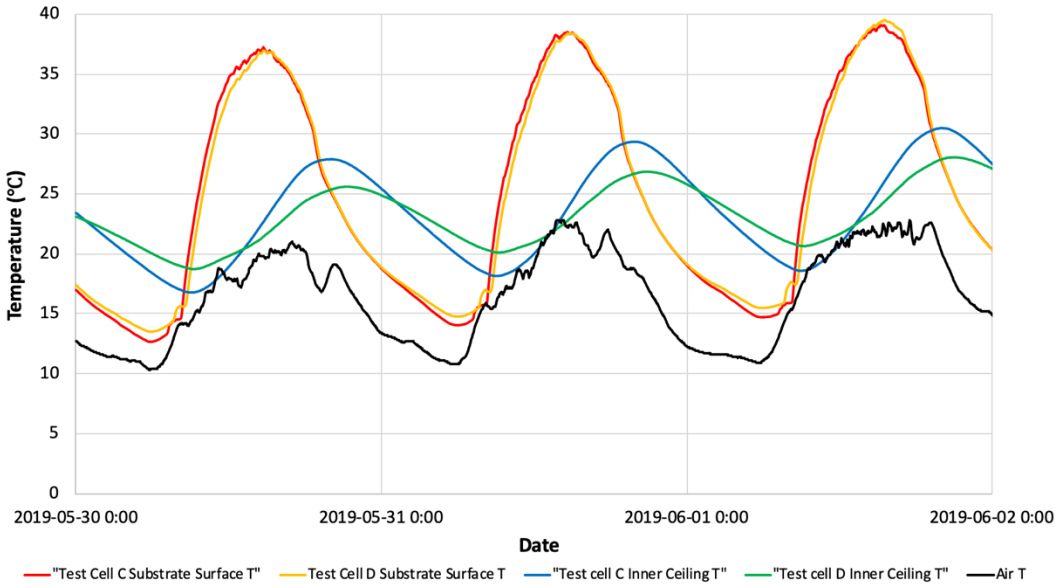

Figure 19 Temperature results of test cell C and D

Table 10 Two test cells fitting function parameters

	30-May	**31-May**	**01-June**
$R_3{}^2$	0.99	0.98	0.99
$R_4{}^2$	0.99	0.99	0.99
A_3	5.36	5.37	5.68
A_4	3.28	3.22	3.55
$(A_3 - A_4)/A_3$	0.39	0.40	0.37
ω_3 *(rad/hr)*	0.25	0.26	0.26
ω_4 *(rad/hr)*	0.24	0.25	0.24
ω_4 / ω_3	0.94	0.96	0.95
φ_3 *(rad)*	3.61	3.74	3.68

φ_4 *(rad)*	3.65	3.84	3.75
$(\varphi_4 - \varphi_3)$	0.04	0.10	0.07
T_{ave3} *(℃)*	22.26	23.57	24.38
T_{ave4} *(℃)*	22.22	23.46	24.35
$(T_{ave3} - T_{ave4})$	0.04	0.11	0.03

4.3.2.3 Roof with irrigation (test cell E) vs. without irrigation (test cell F)

A test study of substrate thermal performance at various moisture contents was performed from July 02 to July 08. Before the study, the two test cells were both covered with 150mm thick substrate and left to rest for two weeks in July to make sure they were both under the same initial conditions, Figure 20 shows the surface temperature, inner temperature, and substrate moisture content of the two test cells before irrigation, and it can be seen that those two cells were under the same conditions prior to the addition of water.

Fifteen liters of water were added to test cell E on June 02, and Figure 21 shows the temperature and moisture content variation of test cell E and F after irrigation. For the substrate moisture content, it can be seen that before irrigation, the two cells had the same moisture content: 17.5%. After irrigation, cell E substrate's moisture content increased from 18% to 49.9% suddenly and dropped gradually until it reached a constant value at around 20% on July 07. For the substrate surface temperature, the surface temperature of the two test cells started to behave differently after 6 hours of irrigation. At night, cell E's surface temperature is 1.5~4ºC lower than that of test cell F. Cell E's maximum surface temperature on June 04 and June 05 is 1.4~1.9ºC lower than cell F.

Table 11 shows the fitting function of the two cells' surface and indoor temperature. It can be seen that for the test cell with irrigation, the amplitude of the inner temperature had a 54% reduction compared with that of the surface temperature, while for the test cell without irrigation, the amplitude of inner temperature had a 46% reduction compared with that of surface temperature. This is because, for the substrate with irrigation, part of the energy absorbed by the substrate was released by evaporation, which decreases the energy

transferred to the inner part. Based on the phase parameter of the fitting function it can be seen that the phase lag of the test cell with irrigation is higher due to the increase of heat capacity when water was added to the substrate.

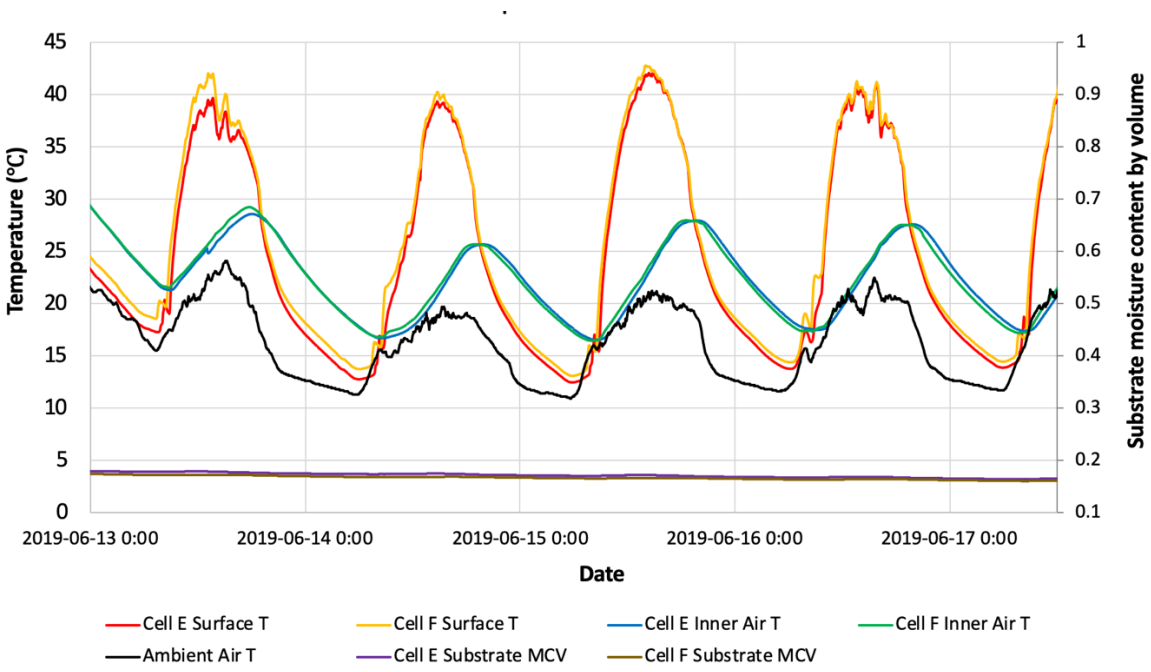

Figure 20 Temperature and moisture content results of test cell E and F before irrigation

Table 11 Fitting functions of surface and indoor air T of test cell E and F

		Fitting function	R^2
Test Cell E (with irrigation)	Surface T	$T = 5.65sin(0.263t) + 19.03$	0.69
	Indoor Air T	$T = 2.60sin(0.265t - 1.256) + 18.84$	0.51
Test Cell F (no irrigation)	Surface T	$T = 4.91sin(0.264t) + 20.64$	0.58
	Indoor Air T	$T = 2.63sin(0.265t - 0.989) + 19.48$	0.45

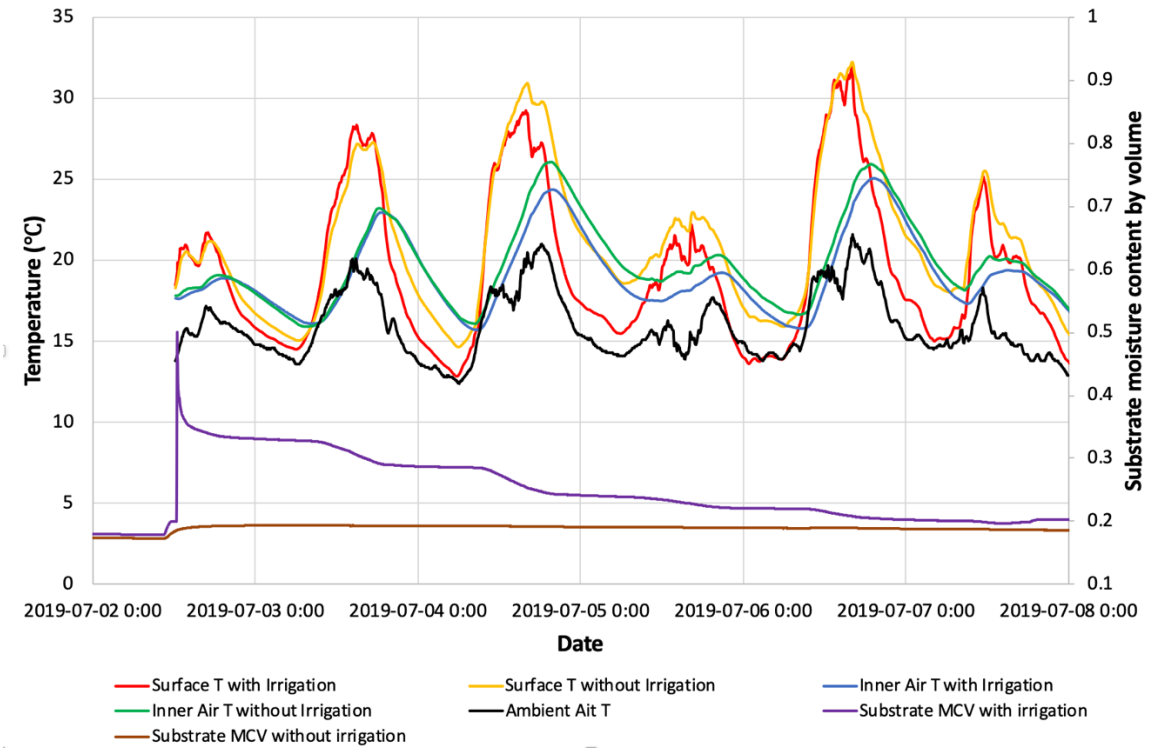

Figure 21 Temperature and moisture content results of test cell E and F after irrigation

4.3.2.4 Roof without vegetation (Test cell G) vs. Roof with vegetation (Test cell H)

A test study of green roof thermal performance with or without a vegetation layer was performed from Aug 07 to Aug 13. Figure 22 shows the weather data, including air temperature, wind speed, humidity, precipitation, and insolation collecting from the weather station located on the roof of the David Turpin Building. Evaporation data were computed based on the collected water mass data every day at 9:00 am using a handmade evaporation pan. There was around 1mm precipitation on August 10. Air temperature varied from 13.6ºC (at 06:45 on Aug 07) to 25.0ºC (at 18:18 on Aug 07). Humidity varied from 48.6% to 97.0%. The maximum insolation was 929.1W/m^2 (at 16:04 on Aug 11). Evaporation results were 5.08kg/(m^2·day) and 4.76kg/(m^2·day) for August 07 and 08 when the insolation was high. For August 09 and 11, when average insolation decreased, evaporation data decreased to 2.70kg/(m^2·day) and 2.42kg/(m^2·day), respectively. As for August 10, there was an increase in water in the pan by 0.14kg/(m^2·day), but the evaporation was zero, due to rainfall on August 10.

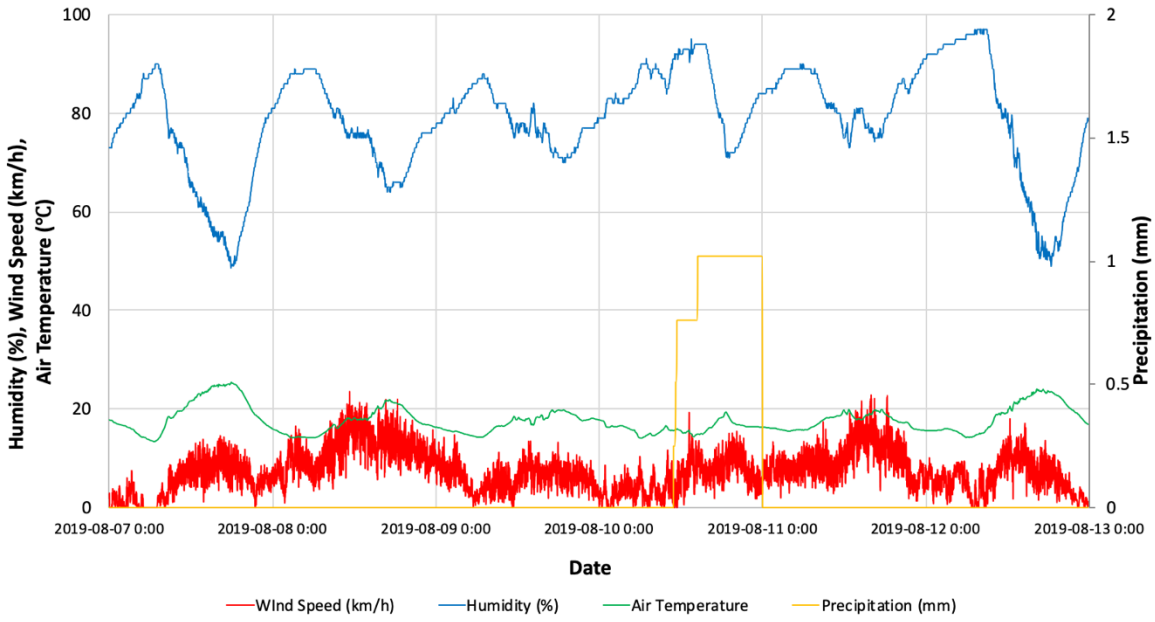

(a)

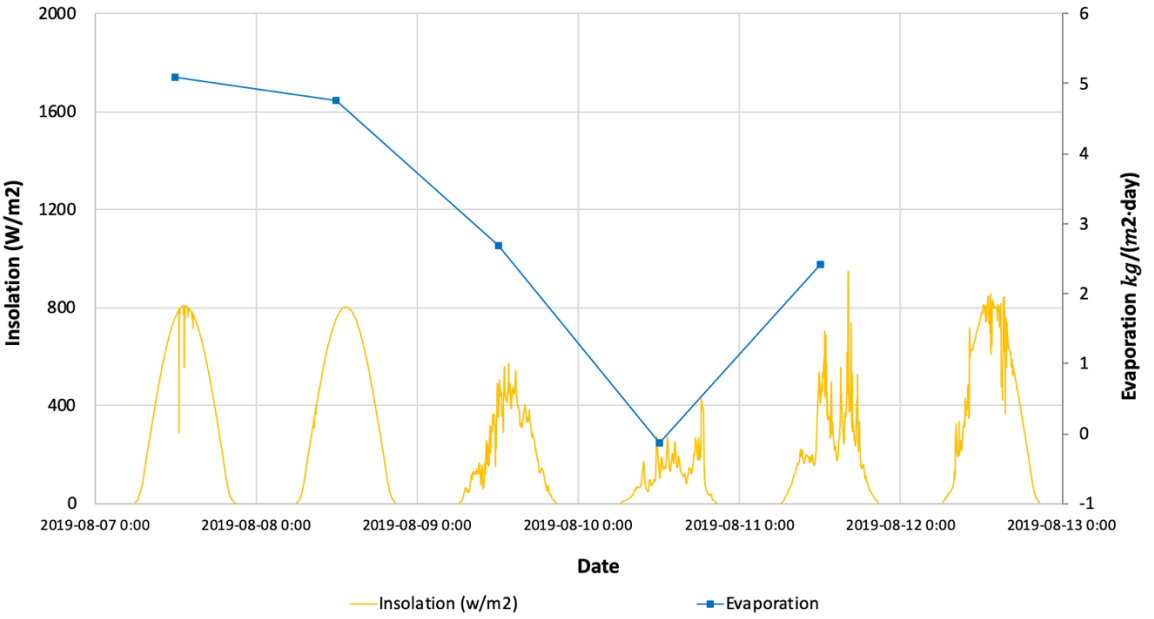

(b)

Figure 22 Weather Data (Aug 07 – Aug 13, 2019) (a) Wind speed, humidity, ait temperature, and precipitation data (b) Insolation and evaporation data

To study the thermal performance of green roof with or without vegetation layer, a layer of sedum mat was placed on the top of test cells H, as shown in Figure 8 (c). The substrate surface and inner air temperature results of the two test cells are shown in Figure 23.

Substrate surface temperature of cell G varied from 14.4 ºC to 49.2 ºC while that of cell H varied from 16.6ºC to 40.9ºC. Temperature variation of the cell with the sedum mat is more stable compared with that of the cell without a sedum mat. When the insolation is high, because of its color and foliage shading effect, the vegetation layer provided more opportunity for transpiration and protection against solar radiation, which decreased the substrate maximum surface temperature by 8.3ºC.

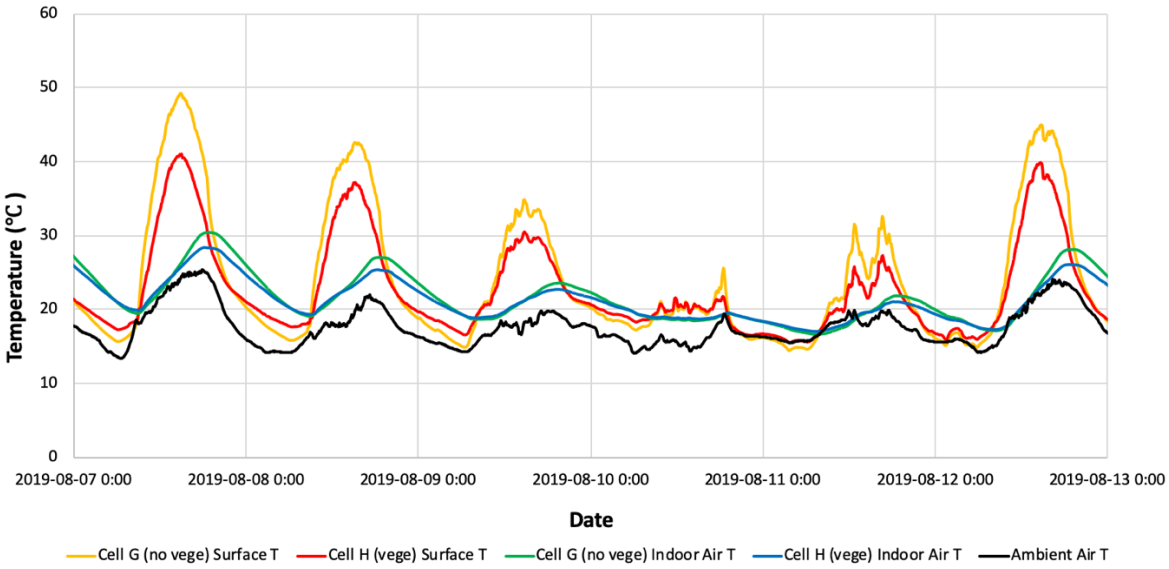

Figure 23 Temperature results of test cell G and H

The trendline of the two test cells inner air temperature has been analyzed and sine wave trends for each day were found. The fitting function of test cell G ceiling temperature T(ºC) vs. time t (hour) is described as:

$$T = A_5 sin(\omega_5 t - \varphi_5) + T_{ave5}$$

and the fitting function of test cell H ceiling temperature T(ºC) vs. time t (hour) is described as:

$$T = A_6 sin(\omega_6 t - \varphi_6) + T_{ave6}$$

Results of A, ω, φ, T_{ave}, and coefficients of determination R^2 of each day are shown in Table 12. Temperature data on August 10 did not following a sine trend. The R^2 value of the two test cells on August 10 are 0.87 and 0.85, which is much lower than the other days, and thus, data of August 10 will be excluded. Based on the results of value A, it can be seen

that on August 07, 08, and 10 when the insolation is high, both cells had high amplitudes compared with the other days. The test cell with sedum mat on had a 25% reduction in the amplitude of inner air temperature as compared to the cell without a sedum mat. From the results of ω_6/ω_5 it can be seen that the vegetation layer didn't have a strong influence on the value of angular frequency. For the phase lag φ of the two cells, phase lag of the test cell without sedum mat was even 0.05 to 0.10 larger than that of the cell with the vegetation layer. This difference is because the delay is mostly determined by the thermal capacity of the substrate layer and both cells had the same amount of substrate, so the phase lag of the two cells inner air temperature is very similar. The average inner air temperature of the cell with sedum mat on was 0.12ºC to 0.72ºC lower than that without sedum mat on.

Table 12 Two test cells fitting function parameters

	07-Aug	**08-Aug**	**09-Aug**	**10-Aug**	**11-Aug**	**12-Aug**
${R_5}^2$	0.99	0.99	0.99	0.87	0.98	0.97
${R_6}^2$	0.99	0.99	0.99	0.85	0.98	0.98
A_5	5.11	3.72	2.48	33.21	2.49	5.4
A_6	3.95	2.78	1.91	30.98	1.9	4.34
$(A_5 - A_6)/A_5$	0.23	0.25	0.23	0.07	0.24	0.20
ω_5 *(rad/hr)*	0.28	0.293	0.285	0.029	0.24	0.235
ω_6 *(rad/hr)*	0.283	0.299	0.285	0.025	0.249	0.234
ω_6/ω_5	1.01	1.02	1.00	0.86	1.04	1.00
φ_5 *(rad)*	3.82	4.02	4.11	2.03	3.17	3.09
φ_6 *(rad)*	3.77	4.01	4	1	3.17	3.01
$(\varphi_6 - \varphi_5)$	-0.05	-0.01	-0.11	-1.03	0.00	-0.08
T_{ave5} *(℃)*	24.81	22.97	21.06	51.7	19	22.05
T_{ave6} *(℃)*	24.18	22.38	20.79	49.69	18.88	21.33
$(T_{ave5} - T_{ave6})$	0.63	0.59	0.27	2.01	0.12	0.72

4.4 Conclusions

4.4.1 Laboratory Experimental Study of Substrate Thermal Conductivity

Results of the experimental study into the thermal conductivity at different temperature and moisture content show that at the same temperature and moisture content, Eagle Lake has the highest thermal conductivity while Sopraflor I has the lowest thermal conductivity. It appears, based on the results available from this study, irrespective of temperature or moisture content, the substrate with higher dry density has higher thermal conductivity. This is consistent with the test performed by Barozzi et al.[33]. Their results showed for sample with density between 100 and 500 kg/m^3, thermal conductivity varied from 0.049 to 0.089 W/m·K. For sample with density between 450 and 650 kg/m^3, thermal conductivity varied from 0.075 to 0.097 W/m·K. For sample with density between 750 and 950 kg/m^3, thermal conductivity varied from 0.102 to 0.128 W/m·K. More research should be performed to further study the relationship between dry density and thermal conductivity for other substrates, as porosity also influences substrate dry density and thermal conductivity.

When temperature changed, in the unfrozen state (T>=5ºC), the Mann-Kendall trend test (M-K test) was used for trend analysis and the results showed there is no significant relationship between thermal conductivity and temperature. The M-K test is a non-parametric test, which means that the data used in the test do not need to meet the assumption of normality. However, there are limitations to the M-K test, particularly for finding a trend with less than four samples. The minimum recommend data number for using this test is at least 8 to 10 data points (https://www.statisticshowto.com/mann-kendall-trend-test/). In this test, 3 sample points were used in the analysis, and thus, the potential for error in the outcomes is large. An ANOVA test was also studied (as shown in Appendix D) and results show that in the unfrozen state the temperature effect is not significant, which is same as the Mann-Kendall trend test results.

In the phase transition zone (between +5ºC and -10ºC), as temperature decreases, thermal conductivity increases sharply during the transition from water to ice because of the

difference in thermal conductivity between the two phases. Results from Zhang et al.[43] also showed that for the thawed substrates, the influence of temperature on the thermal conductivity can be neglected, while in the phase transition zone, thermal conductivity increases significantly as temperature decreases to below zero.

In the unfrozen state (T>=5ºC), when moisture content changed, thermal conductivity increased linearly as moisture content increased. In the frozen state (T=-10ºC), an exponential function exists between thermal conductivity and substrate moisture content prior to freezing. Clarke et al.[34] also showed a simple linear regression fit for the thermal conductivity of three different substrates as a function of moisture content.

To analyze the substrate thermal conductivity as a function of moisture content and temperature in combination, a two-factor ANOVA analysis was conducted. Please see Appendix D for the detailed ANOVA analysis where moisture content by mass is factor 1 and average temperature is factor 2. Results in the unfrozen state show that moisture content is the primary effect on substrate thermal conductivity. Temperature and interaction effects are not significant. While for the results in consideration of frozen substrate, temperature and moisture content together have a significant influence on the substrate thermal conductivity.

4.4.2 Outdoor Experimental Study of Substrate Layer Thermal Performance

Results of the experimental study on the substrate thermal performance show that bare roof and extensive roof were considered as two sensors, the time constant and attenuation of the oscillatory fitting function amplitude are 1.866h, 0.898 for the bare roof sensor, and 7.110h and 0.472 for the extensive roof sensor. Furthermore, sine wave trends of temperature for each day were found and it was found that compared with the bare roof, the extensive roof has 75% reduction on the amplitude of test cell inner ceiling temperature, and a time delay for extensive roof inner ceiling temperature compared with that of the bare roof. Even though the phase lag will not influence the energy consumption, the phase lag indicates the time delay in reaching peak temperature for the indoor environment in this slower manner contributes to indoor thermal comfort. Compared with the extensive roof, there’s a further

40% reduction on the ambient of inner temperature and a further phase lag for the intensive roof. When water was added, test cell inner temperature decreased compared with that of the cell without irrigation, also a significant phase lag can be seen due to the change of heat capacity. The moisture content data collected from the moisture sensor is considered as average moisture content of the substrate, but there is a limitation that in fact the moisture content varies vertically. The moisture content at the bottom of the substrate is higher than that at the top of the substrate. When a sedum mat was added on the top, there's a 20% reduction on the amplitude of inner temperature compared with the cell without sedum mat.

Issa et al.[32] also showed similar results and conclusions. In their research they found that the control roof has the largest daytime and night time indoor temperature fluctuation compared with sand roof and silt clay roof because the substrate layer acted as a thermal mass. Also compared with the non-vegetated roof, the inner temperature of vegetated roof dropped considerably.

Chapter 5 Conclusions and Future Study

5.1 Conclusions

To provide better estimates of the parameters used to model energy and moisture budgets in green roof systems, this research investigated the green roof thermal conductivity as a function of moisture content and temperature. Thermal conductivity of four commercially available green roof substrates (Sopraflor I, ZinCo Blend, Sopraflor X, and Eagle Lake) were tested using the Heat Flow Meter apparatus (NETZSCH HFM 436/3/1E) in the laboratory. Furthermore, to analyze the thermal performance of the green roof substrate layer in isolation, two equally sized, experimental test cells were constructed in Victoria, BC to investigate the thermal performance in an uncontrolled environment with different designs. Comparisons were made for a Bare Roof vs. Extensive(150mm) Roof; Extensive(150mm) Roof vs. Intensive(200mm) Roof; Extensive Roof with varying moisture contents; and Extensive Green Roof with or without vegetation layer. The data were collected during May 2019 to August 2019.

5.1.1 Laboratory Experimental Study of Substrate Thermal Conductivity

The conclusions of the experimental study of substrate thermal conductivity are as follows.

- Among all of four substrates, Sopraflor I has the lowest dry density (856.12kg/m^3) and highest moisture holding capacity while Eagle Lake has the highest dry density (1184.14kg/m^3) and lowest moisture holding capacity due to the high percentage of porous mineral aggregate in Sopraflor I. It appears, based on the results available from this study, irrespective of temperature or moisture content, the substrate with higher dry density has higher thermal conductivity.
- Moist substrate is more conductive compared with dry substrate. In the unfrozen state (T>=5ºC), thermal conductivity increases linearly as moisture content increases and as substrate density increases, the slope of the fitting function increases. In the frozen state (T=-10ºC), an exponential functional relationship exists between thermal conductivity and substrate moisture content prior to freezing.

- In the unfrozen state (T>=5ºC), there is no significant relationship between thermal conductivity and temperature. In the phase transition zone (between +5ºC and -10ºC), as temperature decreases, thermal conductivity increases sharply during the transition from water to ice because of the difference in thermal conductivity between the two phases. Power functions were found between thermal conductivity and temperature when shifted all temperatures to above 0 ºC.

5.1.2 Outdoor Experimental Study of Substrate Layer Thermal Performance

The conclusions from the outdoor experimental study of substrate layer thermal performance are as follows.

- Bare roof and extensive roof test cells were considered as two sensors, roof surface temperatures were considered as inputs of the sensors and interior air temperatures were considered as output. The time constant and attenuation of the oscillatory fitting function amplitude are 1.866h, 0.898 for the bare roof sensor, and 7.110h and 0.472 for the extensive roof sensor. Furthermore, sine wave trends of temperature for each day were found. It was observed that, compared with the bare roof, the extensive roof has 75% reduction on the amplitude of test cell inner ceiling temperature, and a time delay for extensive roof inner ceiling temperature compared with that of bare roof (the phase lag difference between two test cells is from 0.42 to 1.46 rad).
- Compared with the extensive roof, there is a further 40% reduction of the ambient of inner temperature and a further phase lag (0.04 to 0.10 rad) for the intensive roof. When water was added, the inner temperature of the test cell decreased compared with that of the cell without irrigation. This is because part of the energy absorbed by the substrate was released by evaporation, which decreases the energy transferred to the inner part, also a significant phase lag can be seen due to the change of heat capacity. When a sedum mat was added on the top, there is a 20% reduction in the amplitude of inner temperature compared with the cell without the sedum mat.

5.2 Future Study

The recommendations for future research are shown as follows:

(1) Experimental of study of four substrates albedo

According to the energy balance study of green roof in this research, substrate parameters that are critical to green roof energy budget are density, thermal conductivity, specific heat capacity, emissivity, and albedo. As discussed, emissivity is insensitive to substrate moisture content and its composition. Specific heat capacity can be computed based on thermal conductivity and thermal diffusivity, and as thermal conductivity and density were studied in this research, the only left thermal property is albedo, which is also an important input parameter for the green roof numerical study.

(2) Experimental study of green roof substrate layer energy performance

This research studied the green roof substrate layer thermal performance by analysing the temperature and moisture content data, one problem of this research is the substrate layer analysis of energy performance. It is recommended to investigate the energy performance of the substrate, either by using a heat flux sensor to monitor the heat flux through the roof or using the experimental temperature data to perform a numerical energy study.

(3) Comparison between experimental and numerical study of green roof energy performance

After the experimental study of substrate layer energy analysis, a simple numerical study of substrate layer energy performance by using the results in this research as inputs is also recommended to evaluate the conclusions in this research. A comparison between experimental and numerical studies is also recommended to compare the results from each study.

Bibliography

[1] L. Pérez-Lombard, J. Ortiz, and C. Pout, "A review on buildings energy consumption information," *Energy Build.*, vol. 40, no. 3, pp. 394–398, 2008.

[2] L. Yang, H. Yan, and J. C. Lam, "Thermal comfort and building energy consumption implications - A review," *Appl. Energy*, vol. 115, pp. 164–173, 2014.

[3] M. Valipour, "Land use policy and agricultural water management of the previous half of century in Africa," *Appl. Water Sci.*, vol. 5, no. 4, pp. 367–395, 2015.

[4] M. Mahmoodzadeh, P. Mukhopadhyaya, and C. Valeo, "Effects of extensive green roofs on energy performance of school buildings in Four North American climates," *Water (Switzerland)*, vol. 12, no. 1, 2020.

[5] D. Fiaschi, R. Bandinelli, and S. Conti, "A case study for energy issues of public buildings and utilities in a small municipality: Investigation of possible improvements and integration with renewables," *Appl. Energy*, vol. 97, pp. 101–114, 2012.

[6] A. Costa, M. M. Keane, J. I. Torrens, and E. Corry, "Building operation and energy performance: Monitoring, analysis and optimisation toolkit," *Appl. Energy*, vol. 101, pp. 310–316, 2013.

[7] I. Jaffal, S. E. Ouldboukhitine, and R. Belarbi, "A comprehensive study of the impact of green roofs on building energy performance," *Renew. Energy*, vol. 43, pp. 157–164, 2012.

[8] US Department of Energy, "EnergyPlus Engineering Reference: The Reference to EnergyPlus Calculations," *US Dep. Energy*, no. c, pp. 1–847, 2010.

[9] S. Vera *et al.*, "Influence of vegetation, substrate, and thermal insulation of an extensive vegetated roof on the thermal performance of retail stores in semiarid and marine climates," *Energy Build.*, vol. 146, pp. 312–321, 2017.

[10] D. J. Sailor, D. Hutchinson, and L. Bokovoy, "Thermal property measurements for ecoroof soils common in the western U . S .," vol. 40, pp. 1246–1251, 2008.

[11] R. Liu and R. L. Stanford, "The influence of extensive green roofs on rainwater runoff quality : a field-scale study in southwest China," pp. 12932–12941, 2020.

[12] E. Oberndorfer *et al.*, “Green Roofs as Urban Ecosystems: Ecological Structures, Functions, and Services,” *Bioscience*, vol. 57, no. 10, pp. 823–833, 2007.

[13] K. Vijayaraghavan, “Green roofs : A critical review on the role of components , bene fi ts , limitations and trends,” vol. 57, pp. 740–752, 2016.

[14] C. F. Chen, “Performance evaluation and development strategies for green roofs in Taiwan: A review,” *Ecol. Eng.*, vol. 52, pp. 51–58, 2013.

[15] T. van Seters, L. Rocha, D. Smith, and G. MacMillan, “Evaluation of green roofs for runoff retention, runoff quality, and leachability,” *Water Qual. Res. J. Canada*, vol. 44, no. 1, pp. 33–47, 2009.

[16] A. F. Speak, J. J. Rothwell, S. J. Lindley, and C. L. Smith, “Urban particulate pollution reduction by four species of green roof vegetation in a UK city,” *Atmos. Environ.*, vol. 61, pp. 283–293, 2012.

[17] K. L. Getter, D. B. Rowe, J. A. Andresen, and I. S. Wichman, “Seasonal heat flux properties of an extensive green roof in a Midwestern U.S. climate,” *Energy Build.*, vol. 43, no. 12, pp. 3548–3557, 2011.

[18] N. H. Wong, Y. Chen, C. L. Ong, and A. Sia, “Investigation of thermal benefits of rooftop garden in the tropical environment,” *Build. Environ.*, vol. 38, no. 2, pp. 261–270, 2003.

[19] M. Sha, R. Kim, and M. Ra, “Green roof benefits , opportunities and challenges – A review,” *Renew. Sustain. Energy Rev.*, vol. 90, no. April, pp. 757–773, 2018.

[20] T. E. Morakinyo, K. W. D. Kalani, C. Dahanayake, E. Ng, and C. L. Chow, “Temperature and cooling demand reduction by green-roof types in different climates and urban densities: A co-simulation parametric study,” *Energy Build.*, vol. 145, pp. 226–237, 2017.

[21] R. Fioretti, A. Palla, L. G. Lanza, and P. Principi, “Green roof energy and water related performance in the Mediterranean climate,” *Build. Environ.*, vol. 45, no. 8, pp. 1890–1904, 2010.

[22] A. Pianella, R. E. Clarke, N. S. G. Williams, and Z. Chen, “Steady-state and transient thermal measurements of green roof substrates,” *Energy Build.*, vol. 131, pp. 123–131, 2016.

[23] “A Report of the United States General Services Administration The Benefits and

Challenges of Green Roofs on Public and Commercial Buildings," no. May, 2011.

[24] U. Berardi, A. Ghaffarianhoseini, and A. Ghaffarianhoseini, "State-of-the-art analysis of the environmental benefits of green roofs," *Appl. Energy*, vol. 115, pp. 411–428, 2014.

[25] S. C. Cook-patton and T. L. Bauerle, "Potential bene fi ts of plant diversity on vegetated roofs : A literature review," *J. Environ. Manage.*, vol. 106, pp. 85–92, 2012.

[26] M. Gabrych, D. J. Kotze, and S. Lehvävirta, "Substrate depth and roof age strongly affect plant abundances on sedum-moss and meadow green roofs in Helsinki , Finland," vol. 86, pp. 95–104, 2016.

[27] C. Farrell, R. E. Mitchell, C. Szota, J. P. Rayner, and N. S. G. Williams, "Green roofs for hot and dry climates : Interacting effects of plant water use , succulence and substrate," *Ecol. Eng.*, vol. 49, pp. 270–276, 2012.

[28] J. A. Teeri, M. Turner, and J. Gurevitch, "The Response of Leaf Water Potential and Crassulacean Acid Metabolism to Prolonged Drought in Sedum rubrotinctum '," pp. 678–680, 1986.

[29] A. K. Durhman, D. B. Rowe, S. Building, E. Lansing, and C. L. Rugh, "Effect of Substrate Depth on Initial Growth , Coverage , and Survival of 25 Succulent Green Roof Plant Taxa," vol. 42, no. 3, pp. 588–595, 2007.

[30] D. J. Sailor, "A green roof model for building energy simulation programs," vol. 40, pp. 1466–1478, 2008.

[31] S. Ouldboukhitine and R. Belarbi, "Experimental characterization of green roof components," *Energy Procedia*, vol. 78, pp. 1183–1188, 2015.

[32] R. J. Issa, K. Leitch, and B. Chang, "Experimental Heat Transfer Study on Green Roofs in a Semiarid Climate during Summer," vol. 2015, 2015.

[33] B. Barozzi, A. Bellazzi, C. Maffè, and M. Pollastro, "Measurement of Thermal Properties of Growing Media for Green Roofs: Assessment of a Laboratory Procedure and Experimental Results," *Buildings*, vol. 7, no. 4, p. 99, 2017.

[34] R. E. Clarke, A. Pianella, B. Shabani, and G. Rosengarten, "Steady-state thermal measurement of moist granular earthen materials," *J. Build. Phys.*, vol. 41, no. 2, pp. 101–119, 2017.

[35] S. Ouldboukhitine, I. Jaffal, and A. Trabelsi, “Assessment of green roof thermal behavior : A coupled heat and mass transfer model,” vol. 46, pp. 2624–2631, 2011.

[36] Y. Lin and H. Lin, “Thermal performance of different planting substrates and irrigation frequencies in extensive tropical rooftop greeneries,” *Build. Environ.*, vol. 46, no. 2, pp. 345–355, 2011.

[37] Y. Huang, C. Chen, and W. Liu, “Thermal performance of extensive green roofs in a subtropical metropolitan area,” *Energy Build.*, vol. 159, pp. 39–53, 2018.

[38] M. Eksi, D. B. Rowe, I. S. Wichman, and J. A. Andresen, “Effect of substrate depth, vegetation type, and season on green roof thermal properties,” *Energy Build.*, vol. 145, pp. 174–187, 2017.

[39] L. Jiang and M. Tang, “Thermal analysis of extensive green roofs combined with night ventilation for space cooling,” *Energy Build.*, vol. 156, pp. 238–249, 2017.

[40] P. C. Tabares-velasco and J. Srebric, “A heat transfer model for assessment of plant based roo fi ng systems in summer conditions,” vol. 49, pp. 310–323, 2012.

[41] G. A. Narsilio, J. Kress, and T. Sup, “Computers and Geotechnics Characterisation of conduction phenomena in soils at the particle-scale : Finite element analyses in conjunction with synthetic 3D imaging,” vol. 37, pp. 828–836, 2010.

[42] T. S. Y. J. C. Santamarina, “Fundamental study of thermal conduction in dry soils,” vol. i, no. June 2006, pp. 197–207, 2008.

[43] M. Zhang, J. Lu, Y. Lai, and X. Zhang, “Variation of the thermal conductivity of a silty clay during a freezing-thawing process,” *Int. J. Heat Mass Transf.*, vol. 124, pp. 1059–1067, 2018.

[44] “E2399-05 Standard Test Method for Maximum Media Density for Dead Load Analysis of Green Roof Systems,” *ASTM*, no. 8.4.2017, pp. 1–4, 2017.

[45] G. Apparatus, H. Flow, and M. Apparatus, “Standard Practice for Determination of Thermal Resistance of Loose-Fill Building,” *Significance*, vol. 04, pp. 1–11, 2003.

[46] T. Denner, “Operating Instructions Heat Flow Meter HFM 436/3 Lambda,” *NETZSCH*, 2014.

[47] “D698-07 Standard Test Methods for Laboratory Compaction Characteristics of Soil Using Standard Effort (12 , 400 ft-lbf / ft 3 (600 kN-m / m 3)),” *ASTM Int.*, vol. 3, pp. 1–13, 2016.

[48] R. E. Clarke, “Flexible Buffer Materials to Reduce Contact Resistance in Thermal Insulation Measurements,” 2014.

[49] M. Kottek, J. Grieser, C. Beck, B. Rudolf, and F. Rubel, “World map of the Köppen-Geiger climate classification updated,” *Meteorol. Zeitschrift*, vol. 15, no. 3, pp. 259–263, 2006.

[50] M. Akther, J. He, A. Chu, C. Valeo, U. T. Khan, and B. Van Duin, “Response of green roof performance to multiple hydrologic and design variables: a laboratory investigation,” *Water Sci. Technol.* |, no. July, pp. 1–7, 2018.

[51] G. Nellis and S. Klein, *Heat Transfer*. 2009.

[52] C518-98, “Standard Test Method for Steady-State Thermal Transmission Properties by Means of the Heat Flow Meter Apparatus,” vol. 04, pp. 1–10, 2011.

Appendix A Detailed Preparation and Measurement of Substrate Thermal Conductivity Using Heat Flow Meter

1. Preparation of dry substrate

Preparation of dry substrates has the following procedure:

- Substrate was dried in oven at 104℃ according to Standard ASTM E2399-05, until the mass difference between last two measurement over the mass of final substrate is less than 1%.
- The dry substrate was then poured into the holding frame, a 14kg cylindrical mold with diameter of *150mm* was applied at different positions of substrate top surface, as shown in Figure A1. Each position was applied for 2 minutes and a 2.5kg manual rammer was dropped from a height of 150mm five times at each position for more compression. Cylindrical mold and rammer are shown in Figure A2. This compaction method was based on Standard ASTM D698-07. A metal ruler was then used to level off substrate to the top of holding frame.

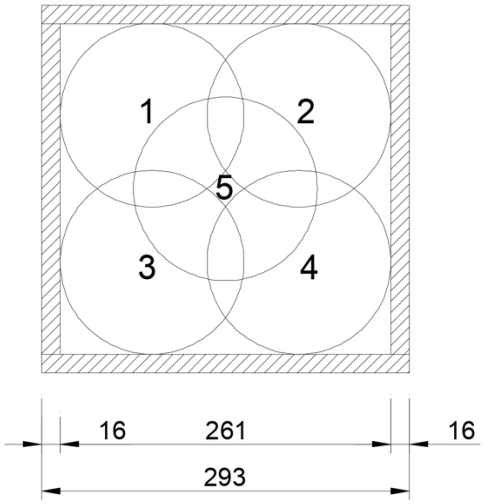

Figure A1 Mold Pattern for Compaction


Figure A2 Cylindrical Mold and Compaction Rammer

- The substrate together with holding frame was sealed with cling wrap to prevent the change in moisture content.
- Mass of whole sample M_t, holding frame M_{hf} and cling wrap M_{cr} were measured, volume of holding frame V_{hf}, mass of dry substrate M_{ds} and density of dry substrate ρ_{ds} were computed basing on the following equation.

$$\rho_{ds} = \frac{M_{ds}}{V_{hf}} = \frac{M_t - M_{hf} - M_{cr}}{V_{hf}} \quad \text{(A1)}$$

- Two buffer sheets were put on the top and bottom of sample and the whole sample was ready for the experiment.

2. Preparation of wet substrate

Preparation of wet substrates has the following procedure:

- Dry samples with mass of M_{ds} were poured into a big container, to obtain a specific moisture content θ by mass, following equations are used to determine the mass of water M_w to be added to the substrate.

$$M_w = M_{ds}\theta \quad \text{(A2)}$$

- Water with mass of M_w was added into dry substrate and was well mixed with substrate using a hand shovel.

- Wet substrate was then poured into holding frame and was compacted using the same compaction method as described in dry substrate preparation.
- The substrate together with holding frame was sealed with cling wrap to prevent the change in moisture content.
- Mass of whole sample M_t, holding frame M_{hf} and cling wrap M_{cr} were measured, volume of holding frame V_{hf}, mass of wet substrate M_{ws} and density of wet substrate ρ_{ws} were computed basing on the following equation.

$$\rho_{ws} = \frac{M_{ws}}{V_{hf}} = \frac{M_t - M_{hf} - M_{cr}}{V_{hf}} \quad \text{(A3)}$$

- The substrate together with holding frame were left for 12 hours to get a uniform moisture distribution and also to verify the sealing of holding frame.
- If mass of sample doesn't change much after 12 hours, then it is ready for the experiment.
- After the test, mass of total test sample was measured again to check moisture losses.

3. Substrate thermal conductivity measurement

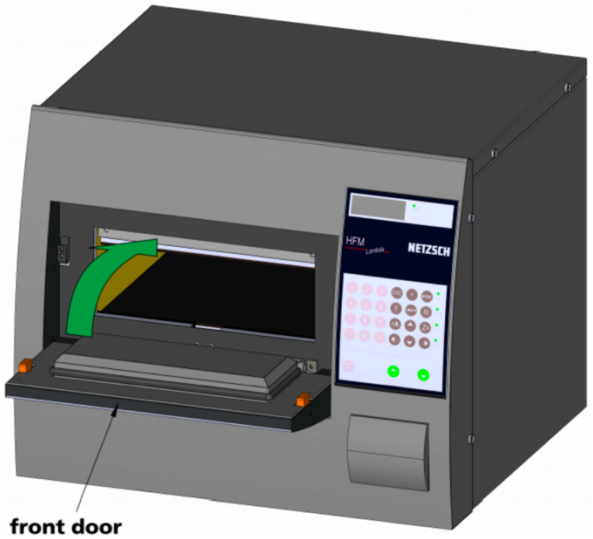

Figure A3 Heat Flow Meter

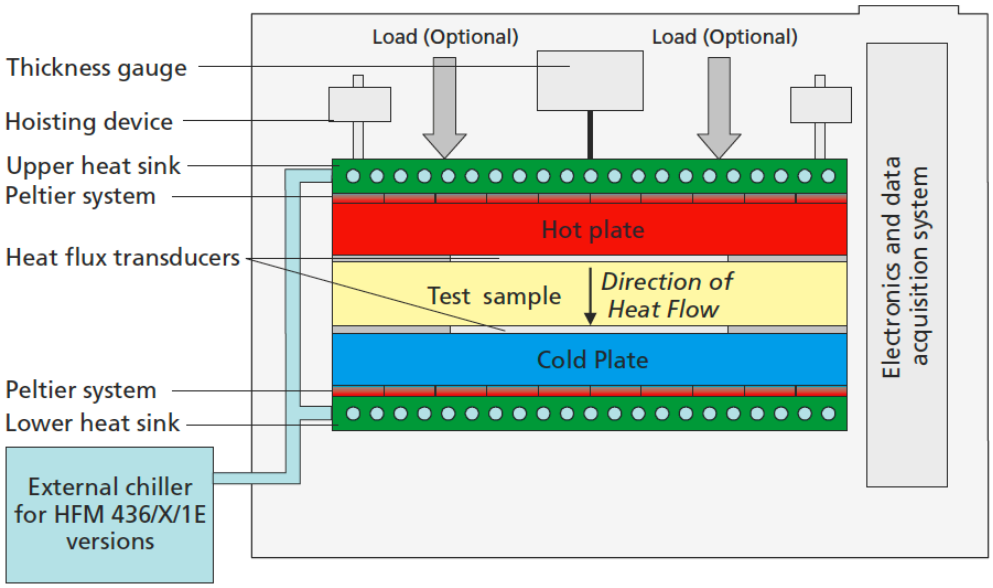

Figure A4 Measuring principle of Heat Flow Meter

Substrates thermal conductivity were measured through a steady-state measurement using Heat Flow Meter, as shown in Figure A3. Heat Flow Meter is an apparatus to determine thermal conductivity through a process of steady-state measurement. Measuring principle of HFM is shown in Figure A4, the test sample with size of $300 \times 300mm$ and thickness of 5-100mm is contacted with hot and cold plates which have two different stable temperature. Heat flows vertically from hot plate to cold plate through the test sample because of the temperature gradient. During the test progress, sensors from upper and lower plates will take readings of temperature and heat flux once per minute until all reading get stabilized. Thermal conductivity of test sample under steady-state condition are then calculated. The heat flux transducers (as shown in Figure A4) just sense the metering area of samples, which is 100x100mm in the center part. A voltage V which is proportional to the metering area heat flux q (W/m^2) is produced. Heat flux q is defined as the rate of heat flow Q (W) through area A (m^2), it is influenced by the following for factors.:

- Test sample thermal conductivity K;
- Thickness of test sample Δx;
- Temperature difference through the test sample ΔT;
- Areas of heat flows A.

As the test arrives at equilibrium, relations between those factors is shown in the following Fourier heat flow equation:

$$q = \frac{Q}{A} = K\frac{\Delta T}{\Delta x} \tag{A4}$$

Since voltage V is proportional to the metering area heat flux q, voltage signal can be converted to heat flux using proportionality N:

$$q = N \cdot V \tag{A5}$$

Where factor N is determined by a calibration test using a reference standard specimen which value of thermal conductivity can be traced in National Metrology Laboratory. Thermal conductivity of the test sample can be calculated using the following equation.

$$K = NV\frac{\Delta \mathrm{x}}{\Delta \mathrm{T}} \tag{A6}$$

In this experimental study, HFM 436/3/1E was used to test the thermal conductivity of three substrates.

Since lateral heat gains or losses could not be controlled or calculated automatically, but just neglected by increasing the guard area size and decreasing thermal conductivity of edge materials, there is no guarantee that this is suitable under all testing conditions[52]. It is necessary to do a calibration test under testing temperature. Calibration test is to calculate the calibration factor N under different temperature. In this test, calibration sample shown in Figure A5 was used, Sample ID is 1450D494 and chose 1450D as the reference type. Calibration test was performed under -10, 5, 20 and 35ºC. Results of calibration factor is shown in Table A1.

Figure A5 Calibration sample

Table A1 Calibration factor

Mean Temperature (℃)	−10	5	20	35
N Value	0.00656	0.00651	0.00652	0.00657

After calibration test, measurements of test sample thermal conductivity were performed, Figure A6 shows the test sample in heat flow meter, upper plate was moved down and stopped automatically until it touched the sample top surface with a little pressure. Mean test sample temperature was set to -10ºC, 5ºC, 20ºC, and 35ºC with delta temperature between the upper and lower plate of 20ºC. Figure A7 shows the inputs of equilibrium parameters, which determined when the system has reached steady state. Rough block size and fine block size are both 10 points, update rate is 1 minute. The status of measurement includes rough, fine and done. Test started with “Rough” status, when the max rough error (1% in this research) is achieved, status changed to “Fine”, and when the max fine error is reached, the status changed to “Done” which means it reaches a steady state and results were recorded (0.2% in this research). The most important parameters in the measurement are fine block size and max fine error.

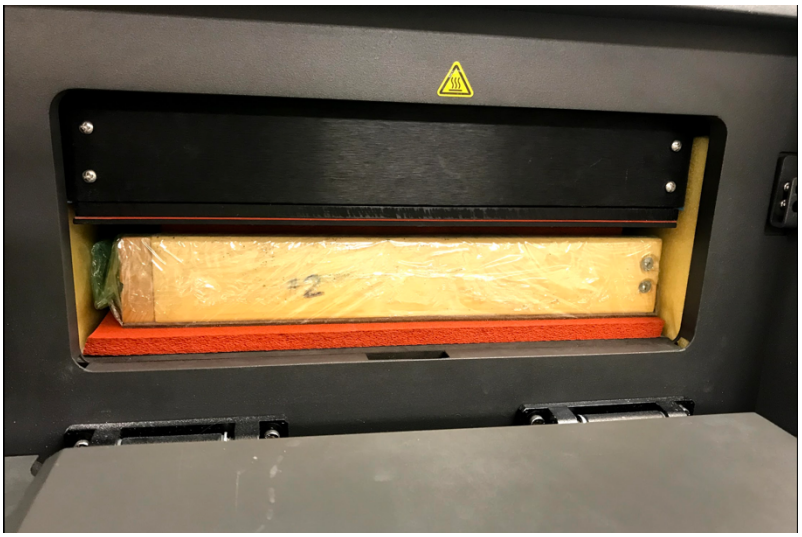

Figure A6 Test sample in HFM

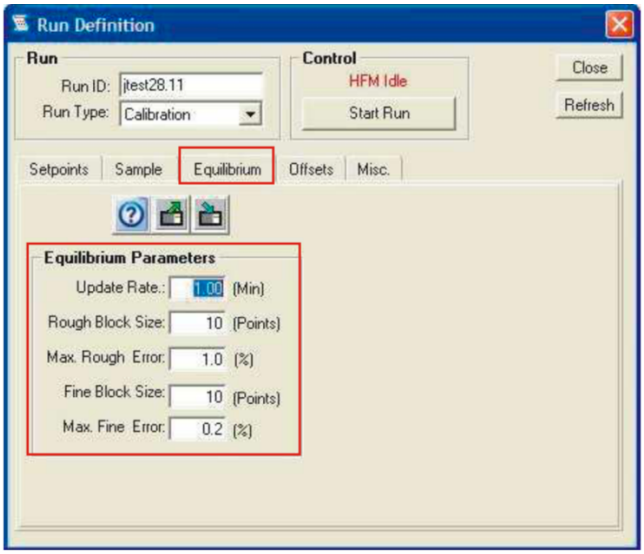

Figure A7 Equilibrium Parameters

Figure A8 shows the data reading window when the heat flow meter is running, pk/ave (peak/average) is the ratio of maximum deviation of every thermal conductivity value to the average thermal conductivity of the data in the block (latest 10 points for both rough and fine block size), when pk/ave was smaller than 1%, fine status reached, when pk/ave is smaller than 0.2%, the measurement was done. N(t) is the calibration value at time t, according to Table A1. K(t) is the instantaneous thermal conductivity of test sample at time t. K(ave) is the average thermal conductivity for the block at time t.

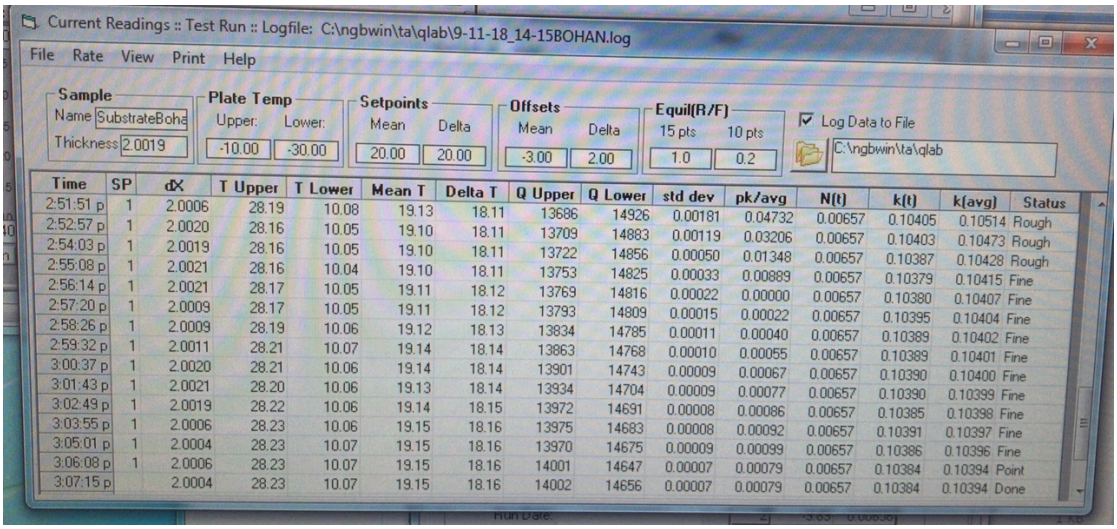

Time	SP	dX	T Upper	T Lower	Mean T	Delta T	Q Upper	Q Lower	std dev	pk/avg	N(t)	k(t)	k(avg)	Status
2:51:51 p	1	2.0006	28.19	10.08	19.13	18.11	13686	14926	0.00181	0.04732	0.00657	0.10405	0.10514	Rough
2:52:57 p	1	2.0020	28.16	10.05	19.10	18.11	13709	14883	0.00119	0.03206	0.00657	0.10403	0.10473	Rough
2:54:03 p	1	2.0019	28.16	10.05	19.10	18.11	13722	14856	0.00050	0.01348	0.00657	0.10387	0.10428	Rough
2:55:08 p	1	2.0021	28.16	10.04	19.10	18.11	13753	14825	0.00033	0.00889	0.00657	0.10379	0.10415	Fine
2:56:14 p	1	2.0021	28.17	10.05	19.11	18.12	13769	14816	0.00022	0.00000	0.00657	0.10380	0.10407	Fine
2:57:20 p	1	2.0009	28.17	10.05	19.11	18.12	13793	14809	0.00015	0.00022	0.00657	0.10395	0.10404	Fine
2:58:26 p	1	2.0009	28.19	10.06	19.12	18.13	13834	14785	0.00011	0.00040	0.00657	0.10389	0.10402	Fine
2:59:32 p	1	2.0011	28.21	10.07	19.14	18.14	13863	14768	0.00010	0.00055	0.00657	0.10389	0.10401	Fine
3:00:37 p	1	2.0020	28.21	10.06	19.14	18.14	13901	14743	0.00009	0.00067	0.00657	0.10390	0.10400	Fine
3:01:43 p	1	2.0021	28.20	10.06	19.13	18.14	13934	14704	0.00009	0.00077	0.00657	0.10390	0.10399	Fine
3:02:49 p	1	2.0019	28.22	10.06	19.14	18.15	13972	14691	0.00008	0.00086	0.00657	0.10385	0.10398	Fine
3:03:55 p	1	2.0006	28.23	10.06	19.15	18.16	13975	14683	0.00008	0.00092	0.00657	0.10391	0.10397	Fine
3:05:01 p	1	2.0004	28.23	10.07	19.15	18.16	13970	14675	0.00009	0.00099	0.00657	0.10386	0.10396	Fine
3:06:08 p	1	2.0006	28.23	10.07	19.15	18.16	14001	14647	0.00007	0.00079	0.00657	0.10384	0.10394	Point
3:07:15 p		2.0004	28.23	10.07	19.15	18.16	14002	14656	0.00007	0.00079	0.00657	0.10384	0.10394	Done

Figure A8 Data reading window

Appendix B Thermal Conductivity Results of Four Substrates

Table B1 Sopraflor I Thermal Conductivity (W/m·K)

Sopraflor I		**Mean Temperature (℃)**			
		-10	5	20	35
Moisture content by mass	0%	0.127	0.138	0.149	0.148
	10%	0.286	0.204	0.233	0.250
	20%	0.578	0.258	0.297	0.345
	30%	1.010	0.346	0.414	0.4
	40%	2.412	0.465	0.522	0.492
	50%	8.760	0.724	0.761	0.790

Table B2 ZinCo Blend Thermal Conductivity (W/m·K)

ZinCo Blend SI		**Mean Temperature (℃)**			
		-10	5	20	35
Moisture content by mass	0%	0.140	0.149	0.154	0.134
	10%	0.423	0.224	0.251	0.312
	20%	0.835	0.344	0.419	0.487
	30%	2.306	0.481	0.537	0.513
	40%	10.138	0.658	0.659	0.732

Table B3 Sopraflor X Thermal Conductivity (W/m·K)

Sopraflor X		**Mean Temperature (℃)**			
		-10	5	20	35
Moisture content by mass	0%	0.197	0.202	0.197	0.208
	10%	0.549	0.313	0.367	0.389
	20%	2.183	0.622	0.693	0.618
	30%	13.540	0.874	1.102	1.020

Table B4 Eagle Lake Thermal Conductivity (W/m·K)

Eagle Lake		**Mean Temperature (°C)**			
		-10	5	20	35
Moisture content by mass	0%	0.197	0.202	0.197	0.208
	10%	0.549	0.313	0.367	0.389
	20%	2.183	0.622	0.693	0.618
	30%	13.540	0.874	1.102	1.020

Appendix C Mann-Kendall Trend Test Results

1. ZinCo Blend trend test results

XLSTAT 2019.2.1.58716 - Mann-Kendall trend tests - Start time: 5/22/2019 at 2:07:39 PM / End time: 5/22/2019 at 2:07:39 PM
Time series: Workbook = new new K.xlsx / Sheet = Sheet2 / Range = 'Sheet2'!$H$1:$L$4 / 3 rows and 5 columns
Date data: Workbook = new new K.xlsx / Sheet = Sheet2 / Range = 'Sheet2'!$G$1:$G$4 / 3 rows and 1 column
Significance level (%): 5
Continuity correction: Yes
Confidence interval (%)(Sen's slope): 95

Summary statistics:

Variable	Observations	Obs. with missing data	Obs. without missing data	Minimum	Maximum	Mean	Std. deviation
K0	3	0	3	0.134	0.154	0.146	0.010
K0.1	3	0	3	0.224	0.312	0.262	0.045
K0.2	3	0	3	0.344	0.487	0.417	0.071
K0.3	3	0	3	0.481	0.537	0.510	0.028
K0.4	3	0	3	0.657	0.732	0.682	0.043

Mann-Kendall trend test / Upper-tailed test (K0):

p-value (one-tailed)	0.500
alpha	0.05

Test interpretation:
H0:
Ha:
As the computed p-value is greater than the significance level alpha=0.05, one cannot reject the null hypothesis H0.

The continuity correction has been applied.

Sen's slope:

	Value	Lower bound (95%)	Upper bound (95%)
Slope	-0.007	-0.007	-0.019
Intercept	0.156	0.193	0.156

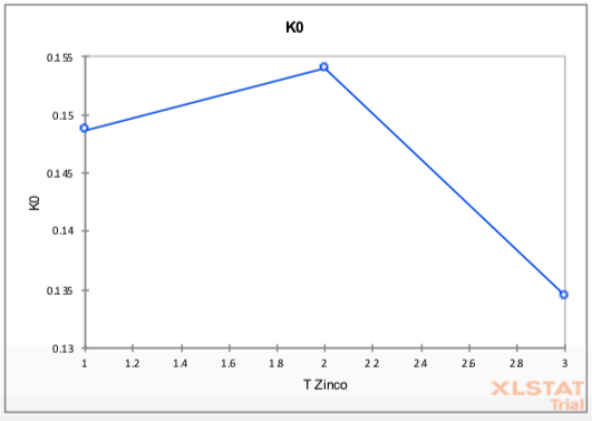

Mann-Kendall trend test / Upper-tailed test (K0.1):

p-value (one-tailed)	0.148
alpha	0.05

Test interpretation:
H0:
Ha:
As the computed p-value is greater than the significance level alpha=0.05, one cannot reject the null hypothesis H0.

The continuity correction has been applied.

Sen's slope:

	Value	Lower bound (95%)	Upper bound (95%)
Slope	0.044	0.044	0.026
Intercept	0.181	0.198	0.181

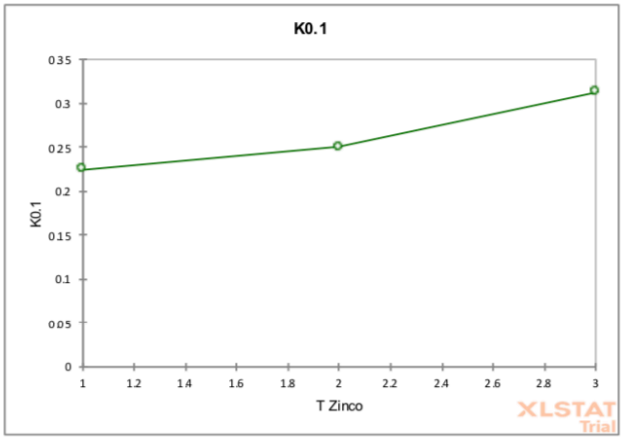

Mann-Kendall trend test / Upper-tailed test (K0.2):

p-value (one-tailed)	0.148
alpha	0.05

Test interpretation:
H0:
Ha:
As the computed p-value is greater than the significance level alpha=0.05, one cannot reject the null hypothesis H0.

The continuity correction has been applied.

Sen's slope:

	Value	Lower bound (95%)	Upper bound (95%)
Slope	0.071	0.071	0.068
Intercept	0.273	0.284	0.273

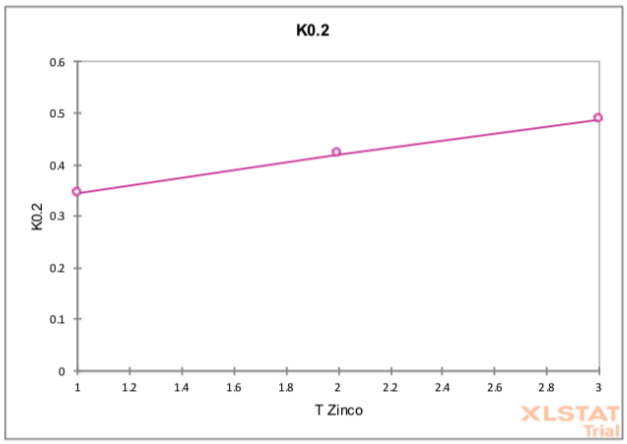

Mann-Kendall trend test / Upper-tailed test (K0.3):

p-value (one-tailed)	0.500
alpha	0.05

Test interpretation:
H0:
Ha:
As the computed p-value is greater than the significance level alpha=0.05, one cannot reject the null hypothesis H0.

The continuity correction has been applied.

Sen's slope:

	Value	Lower bound (95%)	Upper bound (95%)
Slope	0.016	0.016	-0.024
Intercept	0.465	0.585	0.465

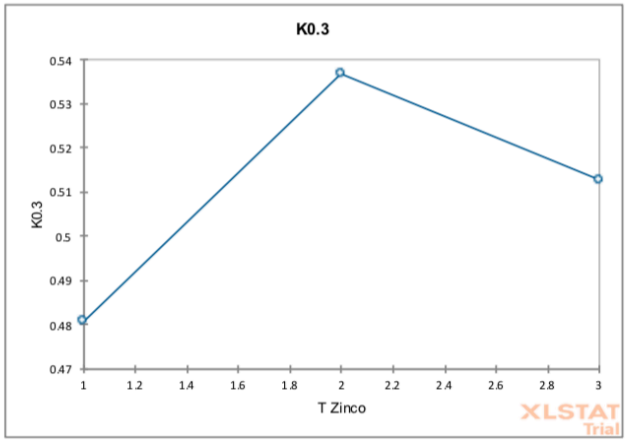

Mann-Kendall trend test / Upper-tailed test (K0.4):

p-value (one-tailed)	0.148
alpha	0.05

Test interpretation:
H0:
Ha:
As the computed p-value is greater than the significance level alpha=0.05, one cannot reject the null hypothesis H0.

The continuity correction has been applied.

Sen's slope:

	Value	Lower bound (95%)	Upper bound (95%)
Slope	0.037	0.037	0.002
Intercept	0.619	0.655	0.619

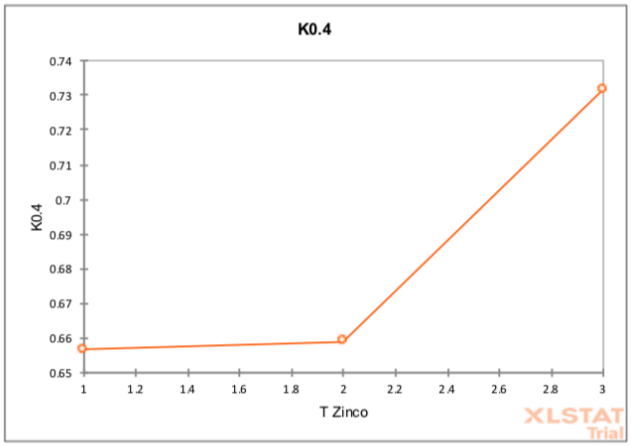

2. Sopraflor I trend test results

XLSTAT 2019.2.1.58716 - Mann-Kendall trend tests - Start time: 5/22/2019 at 2:07:55 PM / End time: 5/22/2019 at 2:07:55 PM
Time series: Workbook = new new K.xlsx / Sheet = Sheet2 / Range = Sheet2!$H$8:$M$11 / 3 rows and 6 columns
Date data: Workbook = new new K.xlsx / Sheet = Sheet2 / Range = Sheet2!$G$8:$G$11 / 3 rows and 1 column
Significance level (%): 5
Continuity correction: Yes
Confidence interval (%)(Sen's slope): 95

Summary statistics:

Variable	Observations	Obs. with missing data	Obs. without missing data	Minimum	Maximum	Mean	td. deviation
K0	3	0	3	0.138	0.149	0.145	0.006
K0.1	3	0	3	0.204	0.250	0.229	0.023
K0.2	3	0	3	0.258	0.345	0.300	0.044
K0.3	3	0	3	0.346	0.441	0.400	0.049
K0.4	3	0	3	0.465	0.522	0.493	0.029
K0.5	3	0	3	0.724	0.789	0.758	0.032

Mann-Kendall trend test / Upper-tailed test (K0):

p-value (one-tailed)	0.500
alpha	0.05

Test interpretation:
H0:
Ha:
As the computed p-value is greater than the significance level alpha=0.05, one cannot reject the null hypothesis H0.

The continuity correction has been applied.

Sen's slope:

	Value	Lower bound (95%)	Upper bound (95%)
Slope	0.005	0.005	-0.001
Intercept	0.133	0.152	0.133

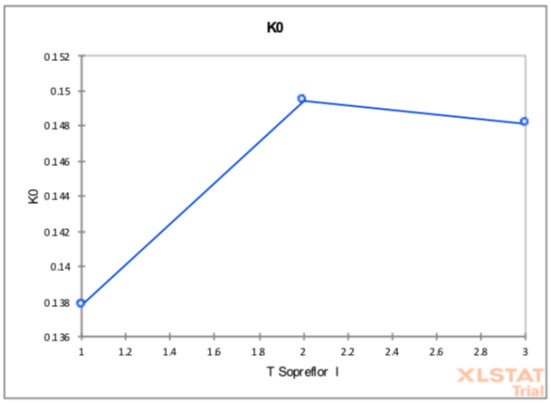

Mann-Kendall trend test / Upper-tailed test (K0.1):

p-value (one-tailed)	0.148
alpha	0.05

Test interpretation:
H0:
Ha:
As the computed p-value is greater than the significance level alpha=0.05, one cannot reject the null hypothesis H0.

The continuity correction has been applied.

Sen's slope:

	Value	Lower bound (95%)	Upper bound (95%)
Slope	0.023	0.023	0.017
Intercept	0.182	0.200	0.182

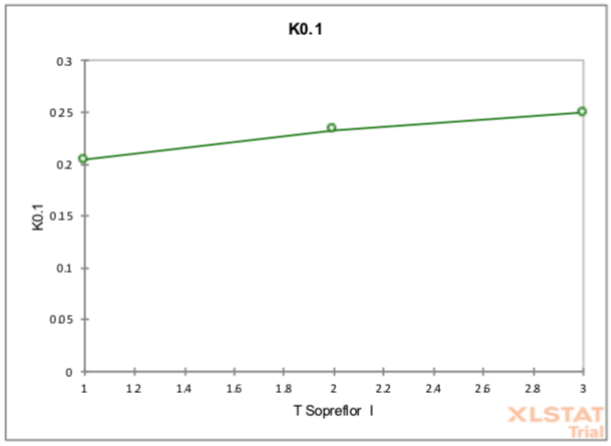

Mann-Kendall trend test / Upper-tailed test (K0.2):

p-value (one-tailed)	0.148
alpha	0.05

Test interpretation:
H0:
Ha:
As the computed p-value is greater than the significance level alpha=0.05, one cannot reject the null hypothesis H0.

The continuity correction has been applied.

Sen's slope:

	Value	Lower bound (95%)	Upper bound (95%)
Slope	0.044	0.044	0.039
Intercept	0.214	0.219	0.214

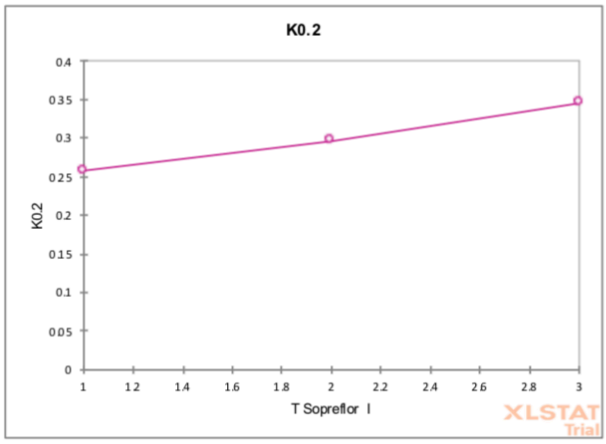

Mann-Kendall trend test / Upper-tailed test (K0.3):

p-value (one-tailed)	0.148
alpha	0.05

Test interpretation:
H0:
Ha:
As the computed p-value is greater than the significance level alpha=0.05, one cannot reject the null hypothesis H0.

The continuity correction has been applied.

Sen's slope:

	Value	Lower bound (95%)	Upper bound (95%)
Slope	0.047	0.047	0.026
Intercept	0.299	0.362	0.299

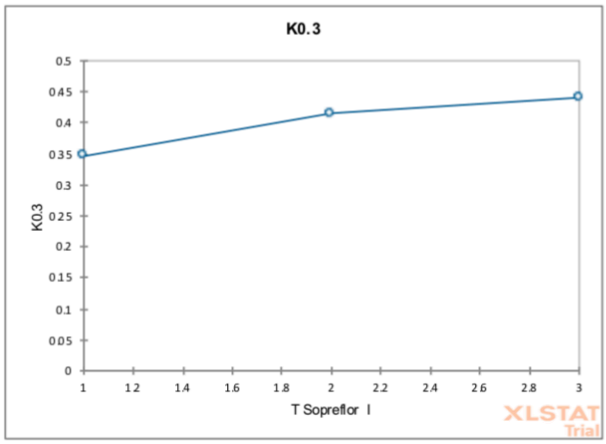

Mann-Kendall trend test / Upper-tailed test (K0.4):

p-value (one-tailed)	0.500
alpha	0.05

Test interpretation:
H0:
Ha:
As the computed p-value is greater than the significance level alpha=0.05, one cannot reject the null hypothesis H0.

The continuity correction has been applied.

Sen's slope:

	Value	Lower bound (95%)	Upper bound (95%)
Slope	0.013	0.013	-0.031
Intercept	0.452	0.584	0.452

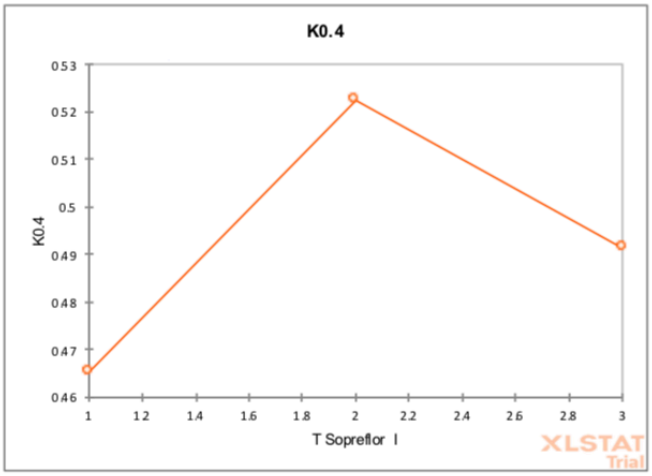

Mann-Kendall trend test / Upper-tailed test (K0.5):

p-value (one-tailed)	0.148
alpha	0.05

Test interpretation:
H0:
Ha:
As the computed p-value is greater than the significance level alpha=0.05, one cannot reject the null hypothesis H0.

The continuity correction has been applied.

Sen's slope:

	Value	Lower bound (95%)	Upper bound (95%)
Slope	0.032	0.032	0.029
Intercept	0.692	0.704	0.692

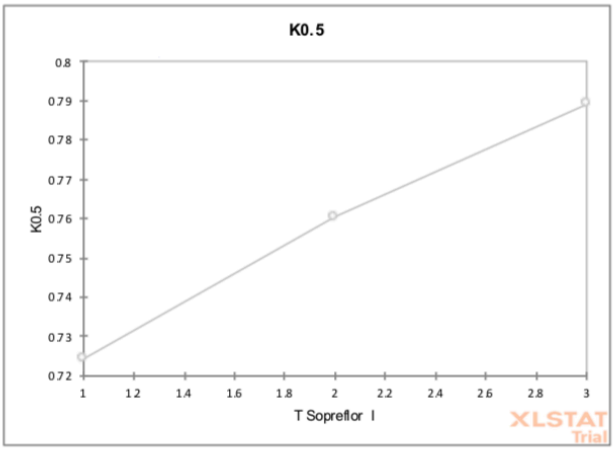
K0.5
0.8
0.79
0.78
0.77
0.76
0.75
0.74
0.73
0.72
K0.5
1
1.2
1.4
1.6
1.8
2
2.2
2.4
2.6
2.8
3
T Sopreflor I
XLSTAT
Trial

3. Sopraflor X trend test results

XLSTAT 2019.2.1.58716 - Mann-Kendall trend tests - Start time: 5/22/2019 at 2:08:28 PM / End time: 5/22/2019 at 2:08:28 PM
Time series: Workbook = new new K.xlsx / Sheet = Sheet2 / Range = Sheet2!$H$14:$K$17 / 3 rows and 4 columns
Date data: Workbook = new new K.xlsx / Sheet = Sheet2 / Range = Sheet2!$G$14:$G$17 / 3 rows and 1 column
Significance level (%): 5
Continuity correction: Yes
Confidence interval (%)(Sen's slope): 95

Summary statistics:

Variable	Observations	Obs. with missing data	Obs. without missing data	Minimum	Maximum	Mean	Std. deviation
K0	3	0	3	0.162	0.181	0.173	0.010
K0.1	3	0	3	0.289	0.369	0.327	0.040
K0.2	3	0	3	0.465	0.578	0.528	0.057
K0.3	3	0	3	0.665	0.718	0.685	0.029

Mann-Kendall trend test / Upper-tailed test (K0):

p-value (one-tailed)	0.500
alpha	0.05

Test interpretation:
H0:
Ha:
As the computed p-value is greater than the significance level alpha=0.05, one cannot reject the null hypothesis H0.

The continuity correction has been applied.

Sen's slope:

	Value	Lower bound (95%)	Upper bound (95%)
Slope	0.003	0.003	-0.014
Intercept	0.174	0.190	0.174

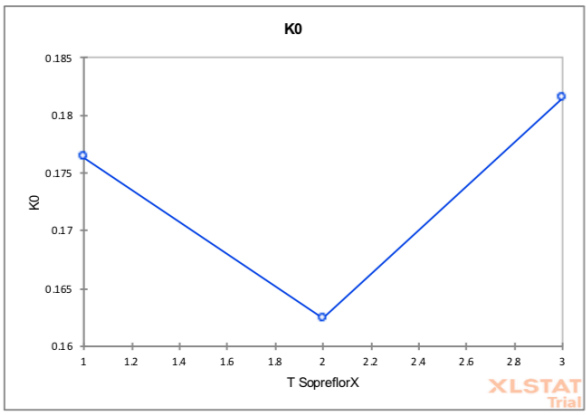

Mann-Kendall trend test / Upper-tailed test (K0.1):

p-value (one-tailed)	0.148
alpha	0.05

Test interpretation:
H0:
Ha:
As the computed p-value is greater than the significance level alpha=0.05, one cannot reject the null hypothesis H0.

The continuity correction has been applied.

Sen's slope:

	Value	Lower bound (95%)	Upper bound (95%)
Slope	0.040	0.040	0.035
Intercept	0.250	0.254	0.250

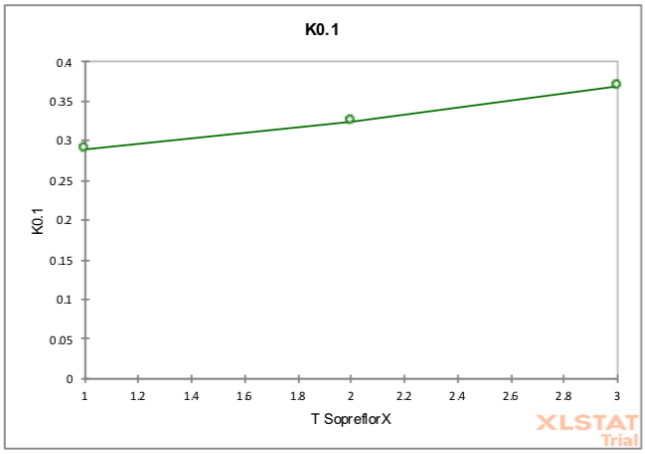

Mann-Kendall trend test / Upper-tailed test (K0.2):

p-value (one-tailed)	0.148
alpha	0.05

Test interpretation:
H0:
Ha:
As the computed p-value is greater than the significance level alpha=0.05, one cannot reject the null hypothesis H0.

The continuity correction has been applied.

Sen's slope:

	Value	Lower bound (95%)	Upper bound (95%)
Slope	0.056	0.056	0.037
Intercept	0.409	0.466	0.409

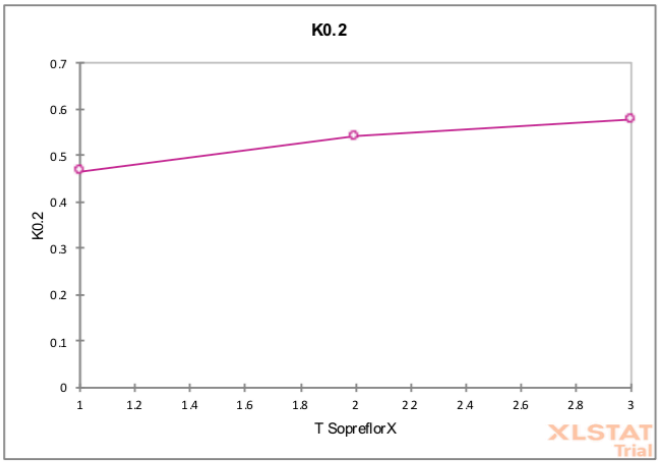

Mann-Kendall trend test / Upper-tailed test (K0.3):

p-value (one-tailed)	0.148
alpha	0.05

Test interpretation:
H0:
Ha:
As the computed p-value is greater than the significance level alpha=0.05, one cannot reject the null hypothesis H0.

The continuity correction has been applied.

Sen's slope:

	Value	Lower bound (95%)	Upper bound (95%)
Slope	0.026	0.026	0.005
Intercept	0.639	0.660	0.639

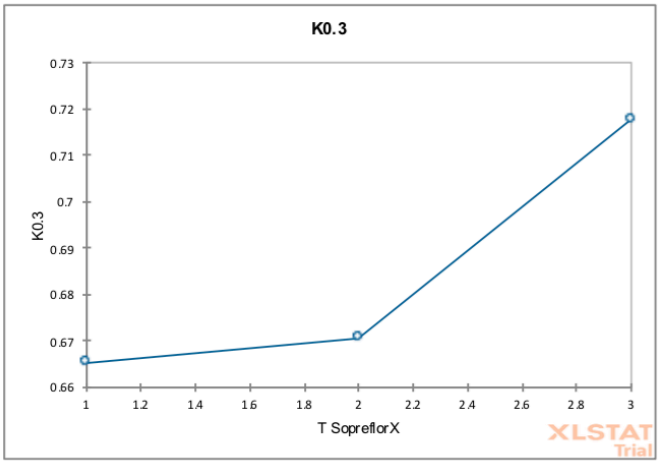

4. Eagle Lake trend test results

XLSTAT 2019.2.1.58716 - Mann-Kendall trend tests - Start time: 5/22/2019 at 2:08:51 PM / End time: 5/22/2019 at 2:08:51 PM
Time series: Workbook = new new K.xlsx / Sheet = Sheet2 / Range = Sheet2!$H$20:$K$23 / 3 rows and 4 columns
Date data: Workbook = new new K.xlsx / Sheet = Sheet2 / Range = Sheet2!$G$20:$G$23 / 3 rows and 1 column
Significance level (%): 5
Continuity correction: Yes
Confidence interval (%)(Sen's slope): 95

Summary statistics:

Variable	Observations	Obs. with missing data	Obs. without missing data	Minimum	Maximum	Mean	Std. deviation
K0	3	0	3	0.197	0.208	0.202	0.006
K0.1	3	0	3	0.313	0.389	0.356	0.039
K0.2	3	0	3	0.618	0.693	0.644	0.042
K0.3	3	0	3	0.874	1.102	0.999	0.115

Mann-Kendall trend test / Upper-tailed test (K0):

p-value (one-tailed)	0.500
alpha	0.05

Test interpretation:
H0:
Ha:
As the computed p-value is greater than the significance level alpha=0.05, one cannot reject the null hypothesis H0.

The continuity correction has been applied.

Sen's slope:

	Value	Lower bound (95%)	Upper bound (95%)
Slope	0.003	0.003	-0.006
Intercept	0.199	0.208	0.199

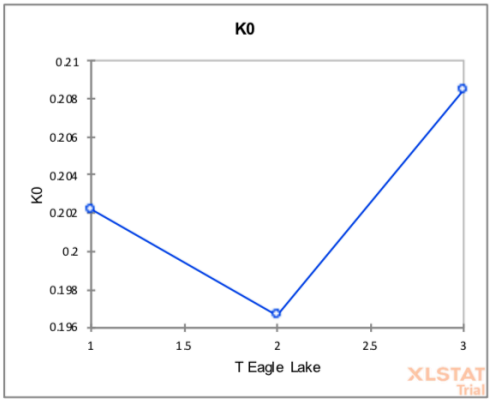

Mann-Kendall trend test / Upper-tailed test (K0.1):

p-value (one-tailed)	0.148
alpha	0.05

Test interpretation:
H0:
Ha:
As the computed p-value is greater than the significance level alpha=0.05, one cannot reject the null hypothesis H0.

The continuity correction has been applied.

Sen's slope:

	Value	Lower bound (95%)	Upper bound (95%)
Slope	0.038	0.038	0.022
Intercept	0.275	0.322	0.275

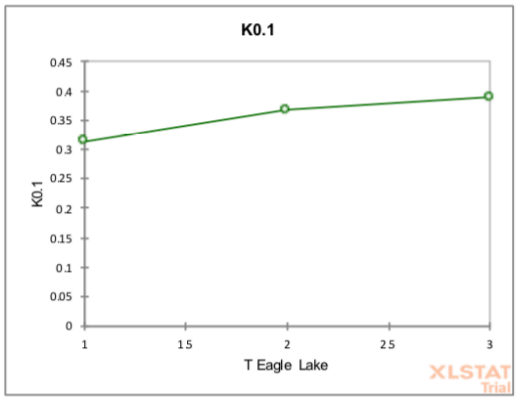

Mann-Kendall trend test / Upper-tailed test (K0.2):

p-value (one-tailed)	0.500
alpha	0.05

Test interpretation:
H0:
Ha:
As the computed p-value is greater than the significance level alpha=0.05, one cannot reject the null hypothesis H0.

The continuity correction has been applied.

Sen's slope:

	Value	Lower bound (95%)	Upper bound (95%)
Slope	-0.002	-0.002	-0.075
Intercept	0.624	0.844	0.624

Appendix D Two-factor ANOVA Analysis of Substrate Thermal Conductivity

To analysis the substrate thermal conductivity as a function of moisture content and temperature, two-factor ANOVA analysis method was used. Moisture content by mass is factor 1 and average temperature is factor 2. Four substrates thermal conductivity data under different average temperature and moisture content is shown in Table D1.

Table D1 Four Substrates thermal conductivity date under different average temperature and moisture content

		Factor 1 - Moisture Content by Mass			
		0%	10%	20%	30%
Factor 2 – Average Temperature (°C)	-10	0.197	0.549	2.183	13.540
	-10	0.140	0.423	0.835	2.306
	-10	0.127	0.286	0.578	1.010
	-10	0.179	0.501	1.856	8.414
	5	0.202	0.313	0.622	0.874
	5	0.149	0.224	0.344	0.481
	5	0.138	0.204	0.258	0.346
	5	0.176	0.289	0.465	0.665
	20	0.197	0.367	0.693	1.102
	20	0.154	0.251	0.419	0.537
	20	0.149	0.233	0.297	0.414
	20	0.162	0.324	0.541	0.671
	35	0.208	0.389	0.618	1.020
	35	0.134	0.312	0.487	0.513
	35	0.148	0.250	0.345	0.441
	35	0.181	0.369	0.578	0.718

ANOVA results in the unfrozen state is shown in Table D2. It can be seen from the results that sample, which is factor 2 temperature $\boldsymbol{\rho}$-value 0.524 is greater than the significance level, which means in the unfrozen state the temperature effect is not significant, which is same as the Mann-Kendall trend test results. As for the columns, which is factor 1 moisture

content, ρ-value is much less than the significance level. The interaction effect is also not significant because ρ-value 0.997 is much greater. In conclusion in the unfrozen state, moisture content is the main effect of substrate thermal conductivity.

Table D2 ANOVA results in the unfrozen state

Anova: Two-Factor With Replication

SUMMARY	0.0000001	0.1	0.2	0.3	Total
5					
Count	4	4	4	4	16
Sum	0.665	1.031	1.689	2.367	5.752
Average	0.166	0.258	0.422	0.592	0.360
Variance	0.001	0.003	0.025	0.053	0.044
20					
Count	4	4	4	4	16
Sum	0.662	1.174	1.950	2.724	6.511
Average	0.166	0.294	0.487	0.681	0.407
Variance	0.000	0.004	0.029	0.090	0.065
35					
Count	4	4	4	4	16
Sum	0.673	1.320	2.027	2.691	6.710
Average	0.168	0.330	0.507	0.673	0.419
Variance	0.001	0.004	0.015	0.067	0.055
Total					
Count	12	12	12	12	
Sum	2.000	3.525	5.667	7.781	
Average	0.167	0.294	0.472	0.648	
Variance	0.001	0.004	0.020	0.059	

ANOVA

ırce of Variat	*SS*	*df*	*MS*	*F*	*P-value*	*F crit*
Sample	0.03194621	2	0.0159731	0.65896404	0.52351556	3.25944631
Columns	1.59078819	3	0.53026273	21.8757779	3.0719E-08	2.86626555
Interaction	0.0136357	6	0.00227262	0.09375589	0.99658729	2.36375096
Within	0.87262992	36	0.02423972			
Total	2.50900002	47				

ANOVA results under all temperature is shown in Table D3. It can be seen from the results that factor 1, factor 2, as well as inaction all have significant influence on the substrate thermal conductivity.

Table D3 ANOVA results in consideration of frozen and unfrozen state

Anova: Two-Factor With Replication

SUMMARY	0.0000001	0.1	0.2	0.3	Total
-10					
Count	4	4	4	4	16
Sum	0.643	1.759	5.453	25.269	33.124
Average	0.161	0.440	1.363	6.317	2.070
Variance	0.001	0.013	0.603	33.606	13.469
5					
Count	4	4	4	4	16
Sum	0.665	1.031	1.689	2.367	5.752
Average	0.166	0.258	0.422	0.592	0.360
Variance	0.001	0.003	0.025	0.053	0.044
20					
Count	4	4	4	4	16
Sum	0.662	1.174	1.950	2.724	6.511
Average	0.166	0.294	0.487	0.681	0.407
Variance	0.000	0.004	0.029	0.090	0.065
35					
Count	4	4	4	4	16
Sum	0.673	1.320	2.027	2.691	6.710
Average	0.168	0.330	0.507	0.673	0.419
Variance	0.001	0.004	0.015	0.067	0.055
Total					
Count	16	16	16	16	
Sum	2.643	5.284	11.119	33.050	
Average	0.165	0.330	0.695	2.066	
Variance	0.001	0.010	0.294	13.191	

ANOVA

ırce of Variat	*SS*	*df*	*MS*	*F*	*P-value*	*F crit*
Sample	33.6984431	3	11.2328144	5.20728705	0.0034054	2.79806064
Columns	35.7709761	3	11.9236587	5.52754739	0.00242282	2.79806064
Interaction	65.1997227	9	7.24441364	3.35835171	0.0029139	2.08173039
Within	103.542417	48	2.1571337			
Total	238.211559	63				